

Instituto Tecnológico y de Estudios Superiores de Monterrey

Campus Monterrey

School of Engineering and Sciences



Effect of the electromagnetic fields in the process of arc extinction in molded case
circuit breakers

A thesis presented by

David Alejandro Chávez Campos

Submitted to the
School of Engineering and Sciences
in partial fulfillment of the requirements for the degree of

Master of Science

In

Energy Engineering

Monterrey, Nuevo León

May 15th, 2018

Instituto Tecnológico y de Estudios Superiores de Monterrey

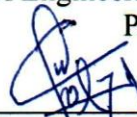
Campus Monterrey

School of Engineering and Sciences

The committee members, hereby, certify that have read the thesis presented by David Alejandro Chávez Campos and that it is fully adequate in scope and quality as a partial requirement for the degree of Master of Science in Energy Engineering,



Federico Ángel Viramontes Brown, Ph.D.
Tecnológico de Monterrey
School of Engineering and Sciences
Principal Advisor



Efraín Gutiérrez Villanueva, M.Sc.
Schneider Electric México
Co-advisor



José de Jesús Valerio Leija, M.Sc.
Schneider Electric México
Committee Member



Ruben Morales Menéndez, Ph.D.
Associate Dean of Graduate Studies
School of Engineering and Sciences

Monterrey Nuevo León, May 15th, 2018

Declaration of Authorship

I, David Alejandro Chávez Campos, declare that this thesis titled, “Electromagnetic Characterization of Arc Extinction in Molded Case Circuit Breakers” and the work presented in it are my own. I confirm that:

- This work was done wholly or mainly while in candidature for a research degree at this University.
- Where any part of this thesis has previously been submitted for a degree or any other qualification at this University or any other institution, this has been clearly stated.
- Where I have consulted the published work of others, this is always clearly attributed.
- Where I have quoted from the work of others, the source is always given. With the exception of such quotations, this thesis is entirely my own work.
- I have acknowledged all main sources of help.
- Where the thesis is based on work done by myself jointly with others, I have made clear exactly what was done by others and what I have contributed myself.

David Alejandro Chávez Campos
Monterrey Nuevo León, May 15th, 2018

Dedicatoria

A Dios, por su presencia constante en mi vida, por brindarme su guía en este reto.

A mis padres, Armando y María Elena, por su apoyo incondicional y su infinito amor.

A mis hermanos Armando, Marielena y Angélica, mis sobrinitos Oscarito y Armandito, que me llenan de alegría y me motivan siempre.

A mis amigos, cada uno contribuyó bastante y estuvieron conmigo en todas las etapas de este ciclo.

Gracias a todos por mostrarme que los retos se pueden enfrentar con la mejor de las sonrisas y que las cosas difíciles tienen grandes recompensas.

Acknowledgments

I would first like to thank my thesis advisor Ph.D. Federico Ángel Viramontes Brown of the School of Engineering & Sciences at Instituto Tecnológico y de Estudios Superiores de Monterrey, Campus Monterrey, for his constant support, to give the right direction to all the research at this work that represented a huge challenge.

I would also like to thank the experts from Schneider Electric, who were involved deeply in the validation survey for this research project: Ms.C. Efraín Gutiérrez Villanueva, Ms. C. José de Jesús Valerio Leija. Without their passionate participation and input, the validation survey could not have been successfully conducted, I would also like to thank to Mauricio Díaz Salas, to include me in the Schneider Electric team with my fellows: Julio César Bautista Cruz, with whom I worked and learned a lot about the Circuit Breakers; Carlos Alberto Gutiérrez Andrews, who supported unconditionally me on many issues of every kind of topics; Jorge Armando Orozco Martínez who gave me support of electric industrial systems.

I am grateful to my colleagues from the "Industrial Consortium for the Promotion of Applied Research in Mexico", they made this challenge more fun and with their motivation I have reached the goal.

I must express my very profound gratitude to Ph.D. Osvaldo Micheloud Vernack for giving me the opportunity to be part of this great family, I would like to thank for his support not only limited to the research area also in the personal and professional areas.

Finally, I thank to Tecnológico de Monterrey support on tuition and CONACyT with the support for living, there was an awesome opportunity and I am very happy with the results.

Effect of the electromagnetic fields in the process of arc extinction in molded case circuit breakers

by

David Alejandro Chávez Campos

Abstract

The new computational tools developed in the last decade are a great contribution to solve complex problems related to the design of circuit breakers. In the past, the experimental research was almost the unique way to improve this kind of technology, a lot of tests were made at laboratories and it was so expensive. Finite Element Analysis made possible to simulate scenarios and develop new technology supporting experimental test and decreasing the number of experimental essays. This thesis proposes the analysis of a module of arc extinction of a Molded Case Circuit Breaker (MCCB) by using Finite Element Method (FEM) software. In this work, the Lorentz force that moves the arc to the arc chutes and lets the elimination of the electric arc is calculated and a model is proposed that determines the contribution of each element of the MCCB to increase or align this magnetic force at the arc. The characteristics of the arc chute are reviewed too, the features analyzed were: the shape of plates, the material used in their fabrication, the influence of the number of plates in the Lorentz forces, and the variation of the distance between plates. The contribution to the Lorentz forces at the arc of the main elements of the module of arc extinction is shown in this work. It is also determined the configurations that allow a better design in the construction of arc chutes. As results, we obtain that the main purpose of the cheeks in the MCCB arc module extinction is to align the magnetic field in the arc. All other steel components increase the Lorentz force in it, accelerating the process of extinction. The best material to increase the magnetic forces is the AFK1 due to its high level of magnetic saturation but this material is so expensive. As a conclusion of this work, we obtain a methodology to design and calculate the effects of the magnetic fields in the arc produced in the chamber extinction of the MCCB.

Keywords— Circuit Breaker, Lorentz force, electric arc, MCCB.

Resumen

Las nuevas herramientas computacionales desarrolladas en la última década son una gran contribución para resolver problemas complejos relacionados con el diseño de interruptores. En el pasado, la investigación experimental era casi la única forma de mejorar este tipo de tecnología, se realizaban muchas pruebas en laboratorios y esto era muy costoso. El Análisis de Elementos Finitos hizo posible simular escenarios y desarrollar nuevas tecnologías que respalden los ensayos experimentales y disminuyan el número de ensayos experimentales. Esta tesis propone el análisis de un módulo de extinción de arco de un disyuntor de caja moldeada (MCCB) utilizando el software del método de elementos finitos (FEM). En este

trabajo, se calcula la fuerza de Lorentz que mueve el arco hacia la cámara de extinción y permite su eliminación y se propone un modelo que determine la contribución de cada elemento del MCCB para aumentar esta fuerza magnética en el arco. También se revisaron las características del conducto de arco, las características analizadas fueron: la forma de las placas, el material utilizado en su fabricación, la influencia del número de placas en las fuerzas de Lorentz y la variación de la distancia entre las placas. La contribución a las fuerzas de Lorentz en el arco de los elementos principales del módulo de extinción de arco se muestra en este trabajo. También se determinan las configuraciones que permiten un mejor diseño en la construcción de rampas de arco. Como resultados, obtenemos que el objetivo principal de las mejillas en la extinción del módulo de arco MCCB es alinear el campo magnético en el arco. Todos los demás componentes de acero aumentan la fuerza de Lorentz en él, acelerando el proceso de extinción. El mejor material para aumentar las fuerzas magnéticas es el AFK1 debido a su alto nivel de saturación magnética, pero este material es muy costoso. Como conclusión de este trabajo obtenemos una metodología para diseñar y calcular los efectos de los campos magnéticos en el arco producido en la extinción de la cámara del MCCB.

Contents

Abstract.....	i
Resumen	i
List of Figures.....	v
List of Tables	vii
Lexicon	ix
CHAPTER I: Introduction.....	1
I.I Problem Statement	3
I.II Objectives	3
I.III Justification	3
I.IV Scope and Limitations.....	4
I.V Thesis organization.....	4
CHAPTER II: Background.....	5
II.I Electric arc: thermal plasma.	5
II.I.I Formation and characteristics of the electric arc.....	7
II.I.II Arc interruption.....	9
II.II Theoretical models	10
II.II.I Magneto-hydrodynamic model.....	11
II.III Low Voltage Circuit Breakers	13
II.III.I Trip units	13
II.III.II Molded Case Circuit Breakers	14
II.III.III Arc chutes	16
II.III.IV Magnetic materials.....	16
CHAPTER III: Simulations and models	21
III.I Introduction	21
III.I.I Methodology using Altair Flux®	21
III.II Parameters	21
III.III Simulations with FEM software	21
CHAPTER IV: Qualitative study of MCCB electric arc.....	25
IV.I Materials and characteristics of the MCCB modeled.	27
IV.II Evaluated cases	29
IV.II.I Case I: Flat geometry, 35 kA excluding the steel components	29
IV.II.II Case II: Original geometry 35 kA excluding the steel components	29

IV.II.III Case III: Original geometry 35 kA including the arc chutes	30
IV.II.IV Case IV: Flat geometry 35 kA including the arc chutes.....	30
IV.II.V Case V: Original geometry 35 kA including the arc chutes and shields	31
IV.II.VI Case VI: Original geometry 35 kA including the arc chutes and the cheeks .	32
IV.II.VII Case VII: Original geometry 35 kA including all steel components: arc chutes, shields, cheeks and arc runners	32
IV.II.VIII Case VIII: Original geometry 5 kA excluding the steel components	33
IV.II.VIII Case IX: Original geometry 5 kA including the arc chutes.....	33
IV.III Results of the qualitative study of the electric arc in an MCCB	34
CHAPTER V: Analysis of arc chutes	45
IV.I Plates shape	45
IV.II Plates material.....	50
IV.III Number of plates in the arc chute.....	56
IV.IV Distance between plates	57
CHAPTER VI: Conclusions.....	61
CHAPTER VII: Future work.....	63
Appendix B: Mesh data of the models	73
Analysis of the MCCB module extinction	73
Cases I – IX	73
Analysis of the arc chutes:.....	73
Shape analysis	73
Material analysis.....	73
Number of plates analysis	74
Distance between plate analysis	75
Appendix C: Features of the MCCB analyzed.....	77
Bibliography	81

List of Figures

Figure 1. Image of an electron trajectory in a homogeneous electric field. The trajectory is interrupted by elastic collisions with neutral atoms.[5].....	6
Figure 2. Comparison of electrical conductivity data of air plasma at atmospheric.....	8
Figure 3. Electric arc structure.....	8
Figure 4. Scheme of the grid and the arc black box.	9
Figure 5. Picture of a Molded Case Circuit Breaker. (Courtesy of Schneider Electric®).	16
Figure 6. Classification of magnetic materials according to their behavior before external magnetic fields.	18
Figure 7. Magnetic curve of ferromagnetic and paramagnetic materials. (The effect of the H field in the air is amplified to note the linear behavior of the paramagnetic material)	19
Figure 8. Diagram of Transient Magnetic application algorithm of Altair Flux®.	22
Figure 9. MCCB Extinction Module. (Ampule) from Schneider Electric®.....	26
Figure 10. 3D Model of an extinction module of an MCCB in Altair Flux®.....	26
Figure 11. Model simplified versus Model with all steel components.	28
Figure 12. Geometry of the Case I.	29
Figure 13. Geometry of the case II.	30
Figure 14. Geometry of the case III.	30
Figure 15. Geometry of the case IV.	31
Figure 16. Geometry of the case V.	31
Figure 17. Geometry of the case VI.	32
Figure 18. Geometry of the case VII.	33
Figure 19. Isovalues of the magnetic field at the electric arc module of extinction.	35
Figure 20. Isovalues of the magnetic flux density at the cheeks.	36
Figure 21. Alignment of magnetic fields at the arc 1.	36
Figure 22. Current density vectors in the electric arc 1.....	37
Figure 23. Paths to calculate current density and magnetic fields into and between the arc.	38
Figure 24. X & Y components from the magnetic flux density at the arc 1.....	40
Figure 25. Z component of the magnetic flux density at the arc 1.	41
Figure 26. X & Z components of current density at the arc 1.	42
Figure 27. Y component of current density at the arc 1.....	42
Figure 28. Lorentz force of cases analyzed.	44
Figure 29. Models of plates with different shapes.	45
Figure 30. Model to compare shapes in plates.	47
Figure 31. Graph of Magnetic flux density at X direction through the path of Figure 23.	48
Figure 32. Current densities at the arc.	49
Figure 33. Lorentz force acting in the arc through a straight trajectory in Y direction from 10 mm of distance to 0.5 mm from the origin defined in figure 12	50
Figure 34. Contours of magnetic flux density at the plate made of AFK1.	52
Figure 35. Magnetic fields of the arc varying the material of the plate.	52
Figure 36. Current density at the arc varying the materials of the plate.....	53
Figure 37. Vectors and contours of eddy currents in the plate.	54
Figure 38. Eddy current density of the materials.....	55
Figure 39. Y component of the Lorentz force of the arc varying with the distance.	56
Figure 40. Lorentz force vs number of plates.	57
Figure 41. Model proposed to analyze the distance between plates.....	58

Figure 42. Lorentz forces vs distance between plates.	59
Figure 43. Magnetic fields of an arc chute of five plates.	60
Figure A- 1. Import geometry from modeler context in Altair Flux®	65
Figure A- 2. Geometry imported from the model with air surrounded the MCCB	66
Figure A- 3. Mesh of model of the MCCB extinction module.	66
Figure A- 4. Configuration of the formulation model in Transient Magnetic 3D application.....	67
Figure A- 5. Current applied to the model in the circuit dedicated context.	68
Figure A- 6. Importing material from material manager.....	68
Figure A- 7. Material manager from Altair Flux®	69
Figure A- 8 Volume regions of the MCCB extinction module.	69
Figure A- 9. Assignment terminals to solid conductors.	70
Figure A- 10. Face assigned to the input current.	70
Figure A- 11. Scenario to solve the MCCB extinction module model.	71
Figure A- 12. Post-processing analysis in Altair Flux. (Isovalues, arrows vectors and paths).....	72
Figure-C 1.L-frame assembly [36].	77
Figure-C 2. L-frame model with the trip unit annexed[36].	78
Figure-C 3. Example of L-frame 300-450 A Thermal Unit Trip curves time vs I/I _r . [36].....	79
Figure-C 4 Example of L-frame 900-1200 A Thermal Unit Trip curves time vs I/I _r [36].	79
Figure-C 5. Short time trip curve of a L-frame MCCB [36].	80

List of Tables

Table 1. Materials used in main components of an L-frame MCCB extinction module.	27
Table 2. Properties of the material used in simulations.	28
Table 3. Results of the qualitative study of MCCB design.	34
Table 4. Nomenclature of graph cases.	39
Table 5. Lorentz forces of studied cases with a quick description.	43
Table 6. Current source parameters.	46
Table 7. Properties of magnetic materials for new designs of plates.	51
Table-C 1. Interrupting Rating of the Schneider Electric MCCBs [36].	77
Table-C 2. Code and Standards accomplished by Circuit Breakers of Schneider Electric [36].	78

Lexicon

Arc chute. Series of plates in the path of that arc that split it up into smaller segments

Arc column. Region where the ions and electrons circulate through a column of ionized gases and metallic vapors, in this zone the plasma could be considered as quasi-neutral fluid

Arc root. Short segment of the electric arc, where the arc surges from the cathode or the anode.

Arc runner. Component of the MCCB responsible for facilitating the movement of the arc of the contacts to the extinction chamber.

Blade. Element that is part of the MCCB, its main function is to rotate and with this movement separate the contacts in the arc extinction module.

CB. Circuit Breaker.

CFD analysis. Computerized Fluid Dynamics is a branch of fluid mechanics that uses numerical analysis and data structures to solve and analyze problems that involve fluid flows.

Cheek. Metallic component of the MCCB that reorient the arc towards the chamber extinction.

Contact. Metallic elements, allow current when touching and break the current when moved apart.

Drift velocity. Average velocity that a particle, such as an electron, attains in a material due to an electric field.

Extinction Module. Unit of an MCCB responsible for the extinction of the arc.

FEM. Finite Element Method refers to a numerical method to solve differential equations using bordering conditions.

HVCB. High Voltage Circuit Breaker.

Ionization. Process by which an atom or a molecule acquires a negative or positive charge by gaining or losing electrons to form ions.

Isovalues graph. It is referred to a graph where contours are drawn in the faces of the model

Lorentz force. Combination of electric and magnetic force on a point charge due to electromagnetic fields.

LVCB. Low Voltage Circuit Breaker.

MCCB. Molded Case Circuit Breaker.

Mesh. Represent (a geometric object) as a set of finite elements for computational analysis or modeling.

MVCB. Medium Voltage Circuit Breaker

Plasma. Fourth state of the matter, created by the ionization of a gas.

Terminals. Extreme of the current path in the circuit breaker.

Trip units. Module of a circuit breaker that sends a signal to interrupt the current through the circuit.

VEM. Volume Element Method.

Volume Region. Volume where the properties of material and border conditions are well defined in a model simulated in Altair Flux[®].

Wave velocity. Speed of an electromagnetic wave travels through the space.

CHAPTER I:

Introduction

The human development in the last century has allowed urban centers expansion, let them be more and more complex, the reliability of electricity networks is essential to these centers do not collapse in their daily activities, currently, most commercial processes involve constant use of electrical networks, high, medium and low voltage. The appearance of failures in electrical systems is inevitable, so it is sought minimal damages and the failures that arise do not have lethal repercussions and also that the equipment does not receive permanent damage, it is for this reason that the coordinated use of electrical protections has gained great relevance since the last century. In the field of design, operation, and maintenance of electrical systems, the greatest concern should be the safety of the workers who operate and maintain the electrical system. The designers of this kind of systems should not only take the necessary precautions to protect systems and equipment. The operation, maintenance, and protection of electrical networks have led builders to pay particular attention to the production of breaking equipment. The integrity of devices on the power grid and the people security in their locality are guaranteed by the circuit breakers (CB). Also, is promoted the continuity of service by restricting the interruption of the current to the defective circuit branch.

The circuit breakers are divided mainly into three different types according to the voltage level: High Voltage Circuit Breakers (HVCB), Medium Voltage Circuit Breakers (MVCB) and Low Voltage Circuit Breakers (LVCB). LVCBs are understood as circuit breakers for voltage levels lower than 1000 V that use air as switching medium. The operation of most LVCBs is based on the interruption of the electric current, establishing a long enough separation distance between the electrodes through a switching medium[1], [2], [3]. During the process of contacts opening, this switching medium, generally gaseous, becomes conductive due to the high temperatures involved in the process, allowing the conduction of the electrical current through it. This process is known as an electric arc. Thus, the basic technology for the current interruption in most LVCBs is characterized by the electric arc elimination, which is a complex phenomenon where lots of physic interactions take place in a very short time.

The circuit breaker has become an essential control and safety device by ensuring the interruption of the current when it is needed or when a fault occurs. To achieve this, it must open the circuit and evacuate the electromagnetic energy stored in the circuit. In the case of low-voltage limiting circuit-breakers, it forces a rapid return to zero current by taking advantage of the remarkable properties of the electric arc to dissipate electromagnetic energy and to oppose the current rise (limiter effect)[4]. There exist two main types of currents that trip the circuit breaker[3]:

- A short-circuit, that is, a current peak, typically very highly exceeding nominal working conditions and possibly very limited in time, as prescribed by the standards;
- An over-current, that is, a current slightly exceeding nominal working conditions, but for possibly a long time, as prescribed by the standards.

This thesis is focused on the electric arc phenomenon in molded case circuit breakers which operate into AC systems, this phenomenon appears when high values of current are reached which happens when short-circuit currents appear, which are in order of thousands of amperes for LV grids. The contribution of this research is on the behavior of the electric arc during the elimination of the short circuit current at the module of arc extinction. Special attention is on the Lorentz force at the electric arc.

I.I Problem Statement

It is considered important to study the behavior of the short-circuit current that becomes an electric arc, during the process of eliminating a short circuit. To carry out this study, simulation tools based on the finite element technique will be used. This novitiare approach will evaluate the modifications that need to be made in the modern circuit breakers to make them more efficient and competitive.

I.II Objectives

The objective of this research is focused on evaluating the impact of the magnetic field produced by short-circuit currents in the process of extinction of the electric arc that is generated when the switch contacts are separated. Especially when this arc forms and starts its journey towards the extinction chamber.

To explain this process three scenarios are studied:

- To make a qualitative survey of the electrical parameters to understand the function of each component in an MCCB
- To optimize a model of arc chutes, verifying materials, geometry, number of plates and distance between them

I.III Justification

This thesis proposal is made to develop a project raised by Schneider Electric Company, it is expected to explain the interaction of the physics of the phenomena to extinguish the electric arc, understand the electromagnetic interactions into the internal components of the MCCB model. This requires the application of specialized software that allows characterizing such phenomena, this would be the first step to redesign and optimize a new generation of circuit breakers.

I.IV Scope and Limitations

The scope of this thesis proposal is to characterize the conditions that are presented in the electric arc phenomenon in MCCBs, this implies that the voltages and currents used in the simulations are in the range of LVCBs. The models described in this thesis consider only the effects of the electromagnetic fields and electric variables in the process of the arc interruption; the erosion of the contacts, the effect of the gravity, the kinetic energies, effects of pressure, enthalpy, entropy and other variables of MHD models are not considered in the simulations and surveys. Altair Flux[®] is designed to simulate electromagnetic phenomena in solid structures, thus the arc is modeled in all cases with fixed dimensions not as a fluid. The previous conditions of the arc initiation are not considered in this thesis, this work considerate only the lapse when plasma is stabilized, the deionization process is neither considered in this thesis proposal.

I.V Thesis organization

In the present chapter, a brief introduction to the work of this thesis is given and objectives are set, as well is enunciated the justification of the project. In the same section, its scope is proposed and the study problem is defined.

In chapter two is explained the characteristics of the plasma, its properties and is discussed various ways of studying it through proposed mathematical models. It is also explained about low voltage circuit breakers, with an emphasis on molded case models. The importance of ferromagnetic materials and their properties is also explained in a concise way.

The scope of the software used is defined, a little information is explained about its operation and the parameters that will be measured in each simulation are defined in chapter three.

Nine scenarios are defined, these simulations are performed with FEM software to review how the magnetic fields in the arc extinction module in the MCCB are modified, all of these is shown and explained in chapter four. This analysis helps to determine how the modification in the magnetic field allows the increase of the Lorentz forces in the arc, the contribution of each component of the circuit breaker to the total sum of forces perceived in the electric arc is also determined.

In chapter five of this thesis a complete analysis is made about arc chutes, shapes, materials, number of plates and distance between plates are reviewed and how each of these characteristics affects the magnetic fields in the arc chute and modify the Lorentz forces perceived in the electric arc.

In chapter six are written the conclusions of each chapter and the final chapter of this thesis is about the future work, suggestions for new researches are described in this chapter.

CHAPTER II:

Background

II.I Electric arc: thermal plasma.

The plasma state is a gaseous mixture of positive ions and electrons [5][6]. Plasmas can be fully ionized, as the plasma in the Sun, or partially ionized, as in fluorescent lamps, which contain a large number of neutral atoms. In this section, is discussed the defining qualities of the plasma state, which result from the fact that we have a huge number of charged particles that interact with electric forces. In particular, we see that the plasma state is able to react in a collective manner. Therefore, the plasma medium is more than the sum of its constituents. Before going deeper into definitions of the plasma state, let us recall the characteristic properties of a neutral gas. A gas is characterized by the number of particles per unit volume, which we call the number density n . The unit of n is m^{-3} . The motion of the particles (in thermodynamic equilibrium) is determined by the temperature T of the gas. In an ideal gas, the product of number density and temperature gives the pressure, $p = nk_B T$, in which k_B is Boltzmann's constant. We will use the same terminology for plasmas, but in the plasma state, we have a mixture of two different gases, light electrons, and heavy ions. Therefore, we have to distinguish the electron and ion gas by individual densities, n_e and n_i . Moreover, plasmas are often in a non-equilibrium state with different temperatures, T_e and T_i of electrons and ions. Such two-temperature plasmas are typically found in gas discharges. The solar plasma (in the interior and photosphere), on the other hand, is a good example of an isothermal plasma with $T_e = T_i$. Plasmas exist in an environment that provides for a large number of ionization processes of atoms. These can be photoionization by an intense source of ultraviolet radiation or collisional ionization by energetic electrons. Impact ionization is the dominant process in gas discharges because of the ample supply of energetic electrons.

The difference between a neutral gas and a plasma are listened as we follow, in a neutral gas, particles interact only during a collision [5], i.e. when two gas atoms "feel" the short-range van der Waals force, which decays with the interparticle distance as r^{-6} . For most of the time, the gas atoms fly on a straight path independent of the other atoms. This is quite different in a plasma. The Coulomb force that describes the electrostatic interaction decays only slowly as r^{-2} , which makes it a long-range force. This means that each plasma particle interacts with a large number of other particles. Therefore, plasmas show a simultaneous response of many particles to an external stimulus.

In this sense, plasmas show collective behavior, which means that the macroscopic result to an external stimulus is the cooperative response of many plasma particles. Mutual shielding of plasma particles or wave processes are examples of collective behavior. The use of an electric discharge is one of the most common ways to create and maintain a plasma [6]. Here, the energy from the electric field is accumulated between collisions by the electron that subsequently transfers a portion of this energy to the heavy neutral particles through collisions. Even with a high collision frequency, the electron temperature and heavy particle

temperature normally will be different. Because the collision frequency is pressure dependent, high pressures will increase this frequency and the electron's mean free path between collisions will decrease. One can show that the temperature difference between electrons and heavy neutral particles is proportional to the square of the ratio of the energy an electron receives from the electric field (\vec{E}) to the pressure (p). Only in the case of small values of E/p do the temperatures of electrons and heavy particles approach each other; thus, this is a basic requirement for local thermodynamic equilibrium (LTE) in a plasma. Additionally, LTE conditions require chemical equilibrium as well as restrictions on the gradients. When these conditions are met, the plasma is termed a thermal plasma. Conversely, when there are large departures from these conditions, $T_e > T_n$, the plasma is termed a nonequilibrium plasma or nonthermal plasma.

In a gas discharge (as an electric arc) with a low degree of ionization, the motion of electrons and ions is governed by the applied electric field and collisions with the atoms [2], [5]–[9] of the background gas. Most of the electron collisions are elastic. Therefore, we will neglect ionizing collisions in the calculation of friction forces. Because of the equal mass of positive ions and atoms of the parent gas, the momentum exchange between the heavy particles is very efficient. Besides elastic scattering, the process of charge exchange plays an important role, in which a moving ion captures an electron and leaves a slow ion behind. In the momentum balance, this process is equivalent to a head-on collision in a billiards game. The figure 1, shows the electron movement in a homogeneous electric field.

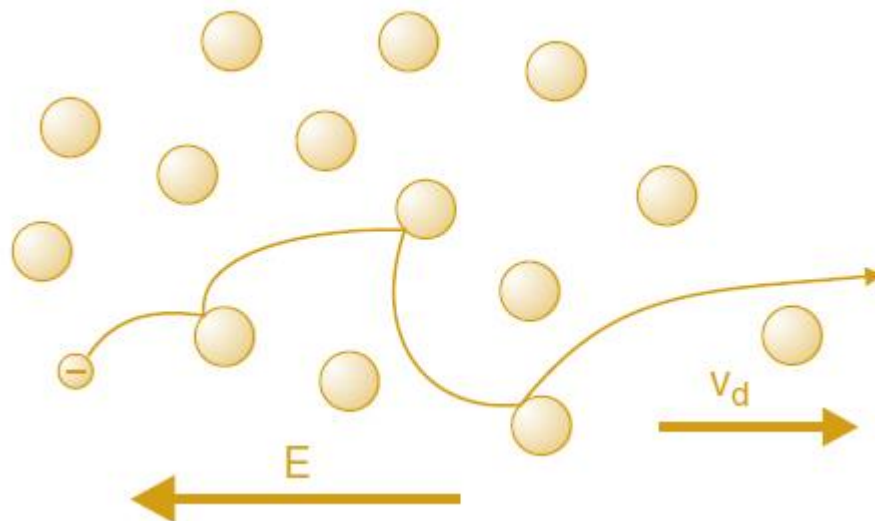


Figure 1. Image of an electron trajectory in a homogeneous electric field. The trajectory is interrupted by elastic collisions with neutral atoms.[5]

When we talk about electromagnetism, there are two types of velocity, the speed of electromagnetic waves and the speed of the electrons, the last is called the drift velocity v_d , which is established when the electric field force is balanced by the friction force. To calculate the value of this velocity is required to know the electron mobility μ_e .

$$v_d = -\mu_e \vec{E} \quad (2.1) \text{ Draft velocity}$$

The electron mobility is defined as we follow:

$$\mu_e = \frac{e}{v_m} \quad (2.2) \text{ Electron mobility}$$

Where v_m is called as the effective collision frequency for momentum transfer. This quantity is inherent to the material. These quantities describes the electric arc discharge, these could be calculated only as a single particles, to be calculated as a set of electrons there exist several fluid models. These equations are very important when we analyze a complete model of the electric gas discharge, but to find the electron mobility and calculate the most probable trajectories of the particles is a very difficult task so simpler models are proposed to evade the most fundamental equations

II.I.I Formation and characteristics of the electric arc

The formation of the electric arc depends mainly on the separation of the circuit breaker contacts [5], [6], [10], the magnitude of the applied current and the ionization of the medium. When the separation of the contacts starts, the electric arc appears and continues if the temperature in the circuit breaker chamber is high enough to ionize the isolating medium and if the current is enough to melt and volatilize the metal. The value of the current is important at the beginning of the circuit breaker contacts' separation [10]. If the current is low, the rise in temperature is not enough to provoke the melting and volatilization of the metal and only a spark is originated. With the beginning of the arc between electrodes, sufficient electrons are released from the cathode. The movement of these electrons from the cathode to the anode causes the ionization of the medium (air and metal vapors). This ionization causes a quick appearance of additional electrons that enables the arc maintenance. The arc behaves as a conductor, being the electrical conductivity of the plasma column in the range of 1000-10000 S/m, depending on the temperature [1], [6], [11], [12]. The influence of the temperature in the conductivity is shown in Figure 2.

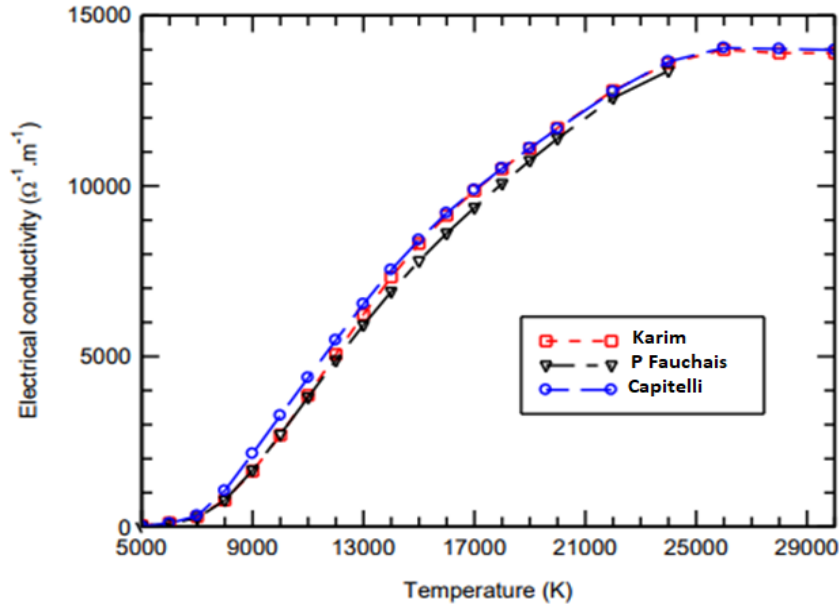


Figure 2. Comparison of electrical conductivity data of air plasma at atmospheric pressure [11].

Physically, the arc appears as an incandescent gas column with an approximately rectilinear trajectory between electrodes, whose core reaches temperatures between 6000 to 20,000 K [1], [3], [10], [13]. Three different regions may be distinguished in the electric arc as we can see in Figure 3: the central arc column, the anode, and cathode regions, both located in the extreme of the contacts. The regions adjacent to the contacts are transition areas between the gaseous conductor constituted by the arc column, which has a variable conductivity and the solid conductor with an essentially constant conductivity.

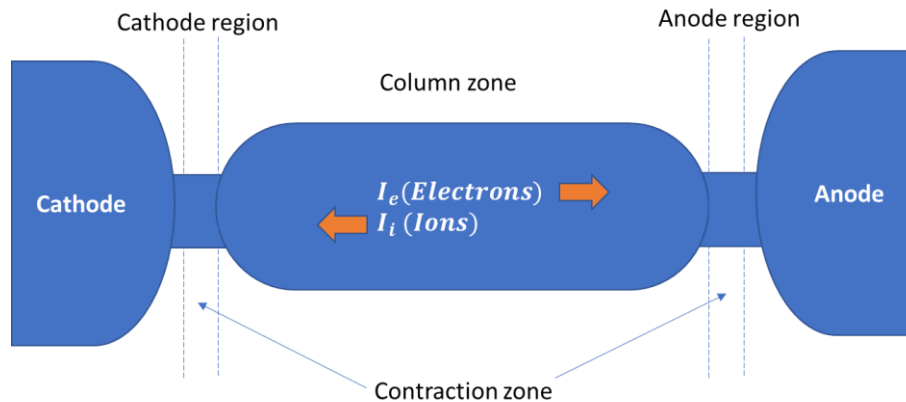


Figure 3. Electric arc structure.

The plasma is considered to be very close to thermal equilibrium [7], [12], [14]–[16] when the speed of energy transmission from the environment to the plasma is reduced, compared to the energy exchange that takes place between the particles themselves. Then, all molecules, ions, and electrons have the same temperature. By contrast, at the beginning of the arc and when it is about to extinguish, the energy exchange between the arc and the environment becomes comparable to the internal energy exchange. Thus, the thermal equilibrium is broken for those instants [3], [10].

The arc voltage is another important characteristic of the electric arc. The distribution of the voltage drop along the arc is not linear, but in the proximity of the electrodes there is a significant voltage drop (8 to 20 V at the cathode and 1 to 12 V at the anode) [6], [8], [10], [15], [17]–[19], being considerably smaller and proportional to the length in the central area, corresponding to the arc column. The magnitude of the electric fields presented in the cathode regions is near to 108 – 109 V/m. Current density is one of the most important electrical variables to calculate, as we have mentioned the great currents leads the electric arc, the typical values in contacts of metallic materials as copper, are close to $10^6 - 10^8 \frac{A}{cm^2}$. The increase in the arc current leads generally to an increase in the diameter so that the section of the arc tends to be automatically adjusted.

II.I.II Arc interruption

The main purpose of the MCCB is to interrupt as fast as can be possible, to do this provokes a less deployment of energy and less erosion of the contacts material. When we are working with AC models we have a natural cross through zero of the current. The event in LVCB lasts less than half a cycle (~ 0.007 s) [20], a reignition could be possible if the voltage is not enough to close definitively the circuit, the magnitude of the transient recovery voltage determinates if will exist a restrike or not.

To model the arc interruption several models are proposed, as an example, we have the Cassie and Mayr black box model [10], [21]. These arc models are usually written as a formula for the arc conductance g , as a function of circuit parameters such as current i , arc voltage U_0 , the period T and the power losses P . Cassie and Mayr models are given by the next two equations:

$$\frac{dg}{dt} = \frac{1}{T} \left(\frac{iu}{U_0^2} - g \right) \quad (2.3) \quad \text{Cassie's model}$$

$$\frac{dg}{dt} = \frac{1}{T} \frac{(P-g)}{i^2} \quad (2.4) \quad \text{Mayr's model}$$

These equations have been modified by adding different electric terms to approximate in a better way to the experimental results. In Figure 4 is shown a scheme of the arc black box model.

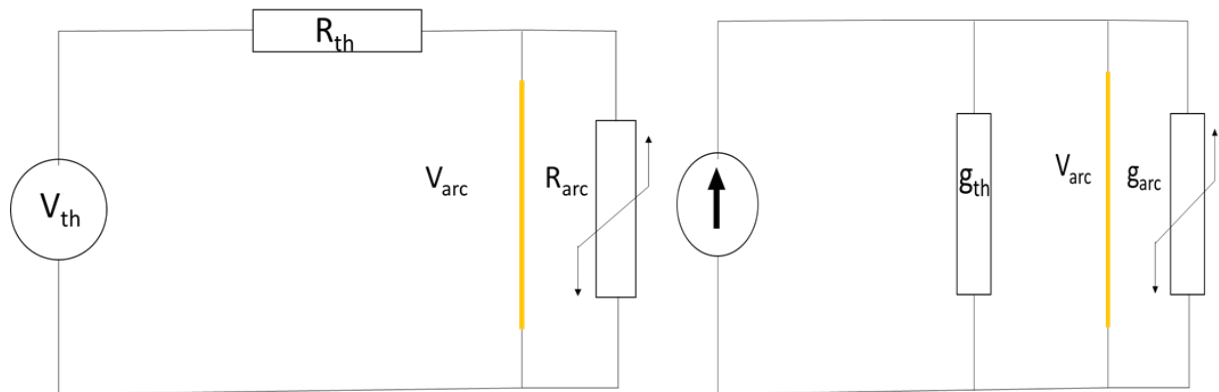


Figure 4. Scheme of the grid and the arc black box.

These simplistic schemes are useful for determining the most basic configurations for selecting an appropriate circuit breaker but not describe the phenomenon effectively, the physics of the arc are ignored and the parameters are obtained by experimental tests.

Another kind of model is the graph-diagram model, this neither describes the physics on the electric arc phenomenon but is useful to calculate times and voltages in the arc interruption process. The data used in this model is obtained by experimental tests similar to the black box model.

Finally, the most descriptive method to simulate the electric arc is by using the fluids theory, physical models are used to describe the phenomenon, especially the magnetohydrodynamics model (MHD model), the method is the most complete, involves the electromagnetic and thermal parameters in the arc interruption process.

II.II Theoretical models

The huge number of particles makes it impossible to solve Newton's equation for each of these particles [5]. Consequently, we will seek a description similar to hydrodynamics, in which the motion of fluid elements is studied instead of tracing the individual molecules. In particular, to make the plasma model accurate, a self-consistent description for the plasma motion and the electromagnetic fields will be used.

The starting point for the fluid model is a correct combination of Maxwell's equations with the particle currents and space charges. Maxwell's equations are given in a form that uses the electric field \vec{E} and the magnetic field \vec{B} . For \vec{B} , we will use the names magnetic induction, magnetic field and magnetic flux density synonymously. Because they appear in the equation of motion \vec{E} and \vec{B} are the natural field quantities. Below are presented the Maxwell Equations in its differential form:

$$\nabla \cdot \vec{E} = \frac{\rho}{\epsilon_0} \quad (2.5) \quad \textit{Gauss's Law}$$

$$\nabla \cdot \vec{B} = 0 \quad (2.6) \quad \textit{Gauss's Law for magnetism}$$

$$\nabla \times \vec{E} = -\frac{\partial \vec{B}}{\partial t} \quad (2.7) \quad \textit{Faraday's Law of Induction}$$

$$\nabla \times \vec{B} = \mu_0 \left(\vec{J} + \epsilon_0 \frac{\partial \vec{E}}{\partial t} \right) \quad (2.8) \quad \textit{Ampere's circuital law}$$

Table 1. Maxwell Equations Differential form.

Where ρ is the total charge density and \vec{J} is the current density carried by particles. These two quantities contain the action of the plasma motion on the fields. Let us shortly recall the physical implications of the set of Maxwell's equations:

The first equation (2.5) is related to the Poisson's equation, which links the electric field to the space charge. This will be our workhorse for electrostatic problems in plasmas. Often, we will also use the electric potential Φ , which is linked to the electric field by $\vec{E} = -\nabla\Phi$.

The vanishing of the divergence of the magnetic flux density \vec{B} in equation (2.6) is an experimental fact that there are no magnetic monopoles in ordinary matter.

When we integrate the electric field along a loop of area $A\hat{n}$ that encircles a magnetic flux $\Phi_m = \int \vec{B} \cdot dA\hat{n}$, we obtain the integral form of the induction law from (2.7) equation, $U_{ind} = -\frac{d\Phi_m}{dt}$, which states that the voltage induced in the loop is the (negative) change of the magnetic flux through this loop. The induced voltage can depend on three factors: the change in magnetic flux density \vec{B} , the change of area $|\vec{A}|$ and a changing angle between magnetic field direction and the area normal, which is contained in the dot product $\vec{B} \cdot d\vec{A}$.

The Ampere's circuital law from de equation (2.8) states that the curl of the magnetic flux density \vec{B} is determined by the conduction current \vec{J} and the displacement current $\epsilon_0 \frac{\partial \vec{E}}{\partial t}$. calculating the stationary magnetic field of a straight wire, we will use the integral form of Ampere's law, $\oint \vec{B} \cdot d\vec{s} = \mu_0 I$.

We need to discuss why we do not use the magnetic field strength \vec{H} [5], or the dielectric displacement \vec{D} . The single particle model had the important result that a gyrating particle has a magnetic moment, which is antiparallel to the direction of \vec{B} . Therefore, a plasma is a diamagnetic medium. Moreover, the magnetic moment is either a conserved quantity, when we try to change the magnetic flux density, or it scales as $\propto 1/B$, when we prescribe the particle energy. Therefore, we cannot expect any proportionality $\vec{B} = \mu_r \mu_0 \vec{H}$ that is typical of ferromagnetic materials. Therefore, introducing H would not help simplifying our models.

There is one crucial difference between hydrodynamics and plasma fluid models. In hydrodynamics, the molecules of the liquid are strongly coupled. This means that the molecules are continuously colliding with their neighbors. A pair of particles will only slowly drift apart by diffusion. Hence, it is meaningful to partition the liquid into macroscopic fluid elements, which contain many molecules that stay close together for a long time. These fluid elements move along streamlines of the flow pattern [5], [6], [18]. An immediate application of the two-fluid model can be derived into magnetohydrostatic. This part does not consider the forces implied in the movement but there is another model that implies other variables and it is called magnetohydrodynamics (MHD).

II.II.I Magneto-hydrodynamic model

The magneto-hydrodynamic approach is most useful in the case of highly ionized or completely ionized plasma. Initially, this was especially important in problems relating to controlled thermonuclear fusion; it is important now for low-temperature plasma applications, such as the plasma centrifuges, and specialized propulsion systems [22]. An electric arc is a form of thermic plasma and this model is considered valid in our research

work, to analyze electric arc is strictly necessary to consider the macroscopic properties of the plasma. To understand the derivation of the MHD model from the two-fluid model is straightforward although several steps are required. First, clear statements of the length and time scales of interest are required, which establish the basis for comparing the sizes of various terms in the two-fluid model. Second, since MHD focuses on macroscopic scales, there are several obvious simplifications that can be made related to the small mass of the electrons, the non-relativistic velocity of the plasma, and the shortness of the Debye length. Finally, the transition from the two-fluid model to the MHD model is made by introducing single-fluid variables and neglecting those terms that are small, because of the narrowing focus on the length and time scales associated with MHD. The Navier-Stokes equation is modified as follows:

$$\rho \frac{\partial \vec{v}}{\partial t} + \rho(\vec{v}\nabla)\vec{v} = -\nabla p + \frac{4}{3}\nabla\mu(\nabla \cdot \vec{v}) - \nabla \times \mu(\nabla \times \vec{v}) + \vec{J} \times \vec{B} + \rho\vec{g} \quad (2.9) \text{ Navier-Stokes equation of conservation of momentum modified}$$

The first term is the change of momentum in the volume control, the second one is the momentum difference in the incoming and outgoing flow, the third one is the pressure gradient, the fourth and fifth terms are the surface forces on the control volume, the fourth one is the Lorentz force, which is related to the magnetic field. The last one is the accelerating gravity force and usually is neglected.

$$\frac{\partial \rho}{\partial t} + \nabla(\rho\vec{v}) = 0 \quad (2.10) \text{ Navier-Stokes equation of conservation of mass}$$

The change rate of density in the control volume is represented with the first term, the second one denotes the flow mass outgoing in the control volume.

$$\rho \frac{\partial H}{\partial t} + \rho(\vec{v} \cdot \nabla)H - \frac{\partial p}{\partial t} - (\vec{v} \cdot \nabla p) = \nabla \cdot \frac{\lambda}{c_p} \nabla H - \nabla \cdot \vec{q}_R + \vec{J} \cdot \vec{E} \quad (2.11) \text{ Navier-Stokes equation of conservation of energy}$$

The equation of conservation of energy defines, in the first term the local change rate of the energy in the control volume; the second term is the enthalpy difference of fluid circulating in the control volume; the third and the fourth terms are the work produced by the changing pressure, usually small compared to the enthalpy exchange. The fourth term shows the heat loss by conduction, the fifth one is the heat loss by radiation (highly important in electric arc formulation). the sixth one is the viscous dissipation term and the last one is the electric energy dissipation in the control volume due to ohmic heating, this term is added to display the relationship between the fluid dynamics with the electric field.

To considerate all variables will be extremely complicated, for this reason, several simplifications are made in the MHD models[10]:

- There is a thermodynamic equation of state for each component of the plasma (electrons, ions, atoms and molecular species), but it is usually neglected in the macroscopic scale analysis.

- Arc plasma is electrically neutral and is represented as a mixture of gases at high temperature.
- Physical properties of plasma (thermal conductivity, viscosity, density, specific heat, electrical conductivity) depend on its temperature and pressure conditions.
- The behavior of the gaseous mass is described by applying the Navier Stokes (conservation of mass, momentum, and energy) and Maxwell's equations.
- The magnetic field is calculated by applying Biot-Savart or by calculating the magnetic vector potential once the current distribution is known.
- The energy conservation equation is modified by considering additional terms that represent the generation of heat by Joule effect and the heat dissipation by radiation.

These considerations are valid to simulate the electric arc in an LVCB but only in the arc interruption process, the deionization of the arc and the glow discharge at the extinction are not easy to explain with the considerations explained before.

II.III Low Voltage Circuit Breakers

Low-voltage circuit breakers include Molded Case Circuit Breakers, (MCCB), Low Voltage Power Circuit Breakers (LVPCB) and Isolated Circuit Breakers (ICCB) and Mini Circuit Breakers (MCB). A circuit breaker is a device designed to protect the load and cables. All circuit breakers protect the circuit conductors mainly by detecting and interrupting the overcurrent [1]–[4], [23]. The opening of the circuit breaker is a reaction to situations of transient current, such as short circuits or faults in the electrical system. The circuit breakers are classified according to the available interruption capacity and the nominal direct current. The interrupting capacity of a circuit breaker is the maximum short-circuit current that the circuit breaker can safely interrupt at a defined voltage. This short-circuit current described by the current magnitude and its value is in symmetrical amperes RMS. The amount of current that a circuit breaker can transmit until it reaches the overload conditions and opens the circuit is defined as the DC classification [19], [24],[25].

II.III.I Trip units

Two types of trip units are used in low voltage circuit breakers:

- thermal magnetic
- electronic

The thermal-magnetic trip unit consists of two fundamental parts, the magnetic trip unit and the thermal trip unit. For overload protection is designed the magnetic trip unit, made up of an electromagnetic device, with a fixed threshold, which starts the instantaneous trip of the circuit breaker on a pre-determined overcurrent value with a constant trip time (~ 10 ms) for short circuit protection [23]. The magnetic trip element is often referred to as the instantaneous trip time and responds quickly in reaction to a high level short-circuit currents. The thermal element is usually a type of bimetallic which is enlarged in a period of time in a range of 10 – 500 s as a result of the heat in a circuit triggered by the overload current that

is less than the magnetic pick-up threshold. Then, the element triggers the molded case switch MCCB after a delay time [3], [10], [23].

The electronic trip units instead use a microprocessor to process the current signal and opening in case of a fault. By digital processing of the signal, they provide protection functions, it is used typically in Medium Voltage Circuit Breakers, High Voltage Circuit Breakers and less used in Low Voltage Power Circuit Breakers.

II.III.II Molded Case Circuit Breakers

A molded case circuit breaker (MCCB) as we have denoted before, is a type of electrical protection device that can be used for a wide range of voltages (120 V – 600 V). The main distinctions between molded-case and miniature circuit breaker are that the MCCB can have current ratings of up to 2,500 amperes, and its trip settings are normally adjustable. MCCBs tend to be much larger than MCBs. As all the other types of circuit breakers, an MCCB has three main purposes:

- Protection against overload. An overload occurs when the system is affected by an overcurrent, this current is a little greater than the nominal one for a considerably long time. this will activate the bimetallic component (thermal trip unit).
- Protection against electrical faults. As we have mentioned, these type of fails in the systems must be limited and the MCCB must open in a very short time period, in the order of less than $\frac{1}{2}$ of a cycle of 60 or 50 Hz.
- Switching a circuit on and off. This function is adequate only when we do not have an appropriate manual switch.

The wide range of current ratings available from molded-case circuit breakers allows them to be used in a wide variety of applications. MCCBs are available with current ratings that range from low values such as 15 amperes to industrial ratings such as 2,500 amperes. This allows them to be used in both low-power and high-power applications. Many companies classify the MCCBs according to the current which they can be operated in normal conditions, this current is called “rated current”, they also classified by their capacities to interrupt the short circuit currents. This classification is useful to find the appropriate MCCB for the required application. In order to explain the possible applications of an MCCB Lily Chan, an expert of MCB and MCCB for Guangzhou Shilin Electrical Company, made an MCCB classification according to its application [26]:

- Main electric feeder protection – The electric feeder circuits that supply power to large distribution boards normally have very high currents, of hundreds of amperes. In addition, if more circuits are added to the system in the future, it may be necessary to adjust the circuit breaker trip settings. Therefore, a molded-case circuit breaker is required.
- Capacitor bank protection – Capacitor banks are a very important component of commercial and industrial electrical systems since they allow power factor correction – reducing line currents and preventing fees from the electric utility company. Large capacitor banks may draw high currents and will require MCCB protection.

- Generator protection – Large electrical generators may provide an output of hundreds of amperes. In addition, gen-sets are normally very expensive. The high current ratings of molded case circuit breakers allow them to provide reliable protection in this application.
- Welding applications – Some welding machines may draw very high currents that exceed the capabilities of miniature circuit breakers, requiring the use of an MCCB.
- Low current applications that require adjustable trip settings – MCCBs are not only for high current applications. There are models rated below 100 amperes for when low current equipment requires the adjustable trip settings provided by MCCBs.
- Motor protection – The reliable protection capabilities of MCCBs make them an adequate choice for motor protection. A molded case circuit breaker can be adjusted to provide overload protection without tripping during the inrush current of an electric motor.

In summary, an MCCB offers adequate protection whenever an application requires a high current rating, adjustable trip settings, or a combination of both factors.

The MCCB is composed of several components that are studied in this work, the most important are shown in Figure 5. The terminals are the paths where the currents travel, usually, are made of copper; the contacts are made of a different material, the most common material used to design contacts is an alloy of silver and carbon [1], [18], [27], [28]. Another alloy used in MCCBs are tungsten and silver [6]. The silver contributes to increasing the conductivity of the contacts, the carbon and tungsten increase the mechanical resistivity and reduces the erosion [1], [10]. The blade is a rotative device made of copper, under normal conditions of the system the blade is fixed and the current travels through it, but when a fault appears, it rotates and separates the contacts, deviating through the arc runners to the arc to the extinction chamber and interrupting the fault current. Others important elements are the shields, they are compact pieces of steel that enhance the magnetic flux in its interior. One of the most important elements of the circuit breakers are the arc chutes, they are designed to attract the arc, elongate it and finally deionize the plasma, thus interrupting the failure completely.

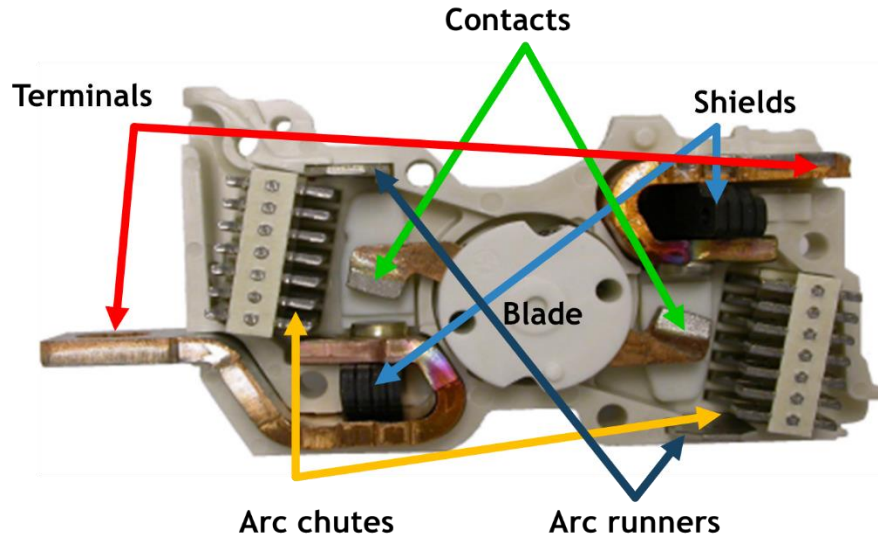


Figure 5. Picture of a Molded Case Circuit Breaker. (Courtesy of Schneider Electric®).

II.III.III Arc chutes

The arc chute is a series of plates ordered and fixed one over one in the path of that arc, they split it up into smaller segments, lowering the energy in each arc segment to that it needs less dielectric strength (of air) to extinguish it, or really, to not allow it to sustain itself any longer. The arc chute also serves to cool the thermal energy in the arc. Without arc chutes, the breaker would need to be larger and the heat energy of the arcs would deteriorate it considerably faster.

The arc chamber is where the arc chutes and the other components, as the shields or arc runners are located. The geometry and materials of the arc chamber determinate the capacity of extinction of the LVCB. The arrangement of the plates that conform the arc chute must be well designed, the distance between the contacts and the plates is suggested to be around 3.2 to 4.7 mm [27], the thickness of the plates cannot be very small to avoid melting, as a result of heat generated by the arc (1.4 to 2.4mm). The number of plates used in the geometry varies with the space available and depends on the application. For circuit breakers with voltages up to 600V it is recommended to use at least 10 to 12 plates (for a contact separation of 25.4mm)[10], [27], [29], while for circuit breakers with interruption capacity of 20 kA at 4800V, around 50 to 60 plates should be used. The metal coating used in the plates has to be considered, being nickel the most effective according to the literature [27]–[29]. The typical material used in the manufacturing of the metal plates (also called splitters) are ferromagnetic materials, as different types of iron alloys, cladding of common base metals (as steel or copper) with other metals (as nickel) is a technique used to reduce the corrosion effects in the plates [30].

II.III.IV Magnetic materials

In this proposal we treat three types of magnetic materials, plasma is classified as diamagnetic material, the air that surrounds the MCCB acts as a paramagnet and the steel components

have a ferromagnetic behavior, thus is convenient to explain the definitions and what implies this classification in the properties of each material. The magnetic fields affect materials differently, some materials are highly influenced by small magnetic field and others need to be exposed to a huge amount of magnetic flux to present notable effects in their internal composition. There exists a classification according to the effect of the core material on the flux density. The main magnetic materials are:

- **Diamagnetic:** A magnetic field acting on any atom induces a magnetic dipole for the entire atom by influencing the magnetic moment caused by the orbiting electrons. These dipoles oppose the magnetic field, causing the magnetization to be less than zero. This behavior, called diamagnetism, gives a relative permeability of about 0.99995 [31] (or a negative susceptibility approximately -10^{-6} , note the negative sign). Materials such as pure copper, silver, silicon, gold, and alumina are diamagnetic at room temperature. Superconductors are perfect diamagnets; they lose their superconductivity at higher temperatures or in the presence of a magnetic field. In a diamagnetic material, the magnetization \vec{M} direction is opposite to the direction of the applied field \vec{H} (Magnetization term is explained in next paragraph and now we only need to know that is related with the alignment of the spins).
- **Paramagnetic:** When materials have unpaired electrons, a net magnetic moment due to electron spin is associated with each atom. When a magnetic field is applied, the dipoles align with the field, causing a positive magnetization. Because the dipoles do not interact, extremely large magnetic fields are required to align all of the dipoles. In addition, the effect is lost as soon as the magnetic field is removed. This effect, called paramagnetism, is found in metals such as aluminum, titanium, and alloys of copper. The magnetic susceptibility (χ_m) of paramagnetic materials is positive and lies between 10^{-4} and 10^{-5} [31]. Ferromagnetic and ferrimagnetic materials above the Curie temperature also exhibit paramagnetic behavior.
- **Ferromagnetic:** Ferromagnetic behavior is caused by the unfilled energy levels in the 3d level of iron, nickel, and cobalt. Similar behavior is found in a few other materials, including gadolinium (Gd). In ferromagnetic materials, the permanent unpaired dipoles easily line up with the imposed magnetic field due to the exchange interaction, or mutual reinforcement of the dipoles. Large magnetizations are obtained even for small magnetic fields, giving large susceptibilities approaching 10^6 [31]. The susceptibility of ferromagnetic materials depends upon the intensity of the applied magnetic field.

In Figure 6 is shown the behavior of the magnetic materials according with the external magnetic field applied, in the circles are represented the alignment of the spins, we suppose that we apply an external magnetic field H with the same magnitude to all magnetic materials, the alignment varies according to their intrinsic properties, another brief analysis is using the lines with colors, they represent the amount of field H applied to achieve the same quantity of magnetic flux density B . We note that the electrons of the ferromagnetic materials react strongly to external magnetic flux, they align their spins in the same direction that the applied external field easily, the ferrimagnetic materials need

more quantity of magnetic field to order their atoms in a preferred direction. The paramagnetic materials need a huge amount of field H to reach that levels of alignment. Finally, we note that the diamagnetic materials show a different behavior, if we apply a huge amount of field H , the diamagnetic materials (as the plasma of the electric arc) avoid the formation of the magnetic fields in their interior, and they order its atom in the opposite direction to the external magnetic field.

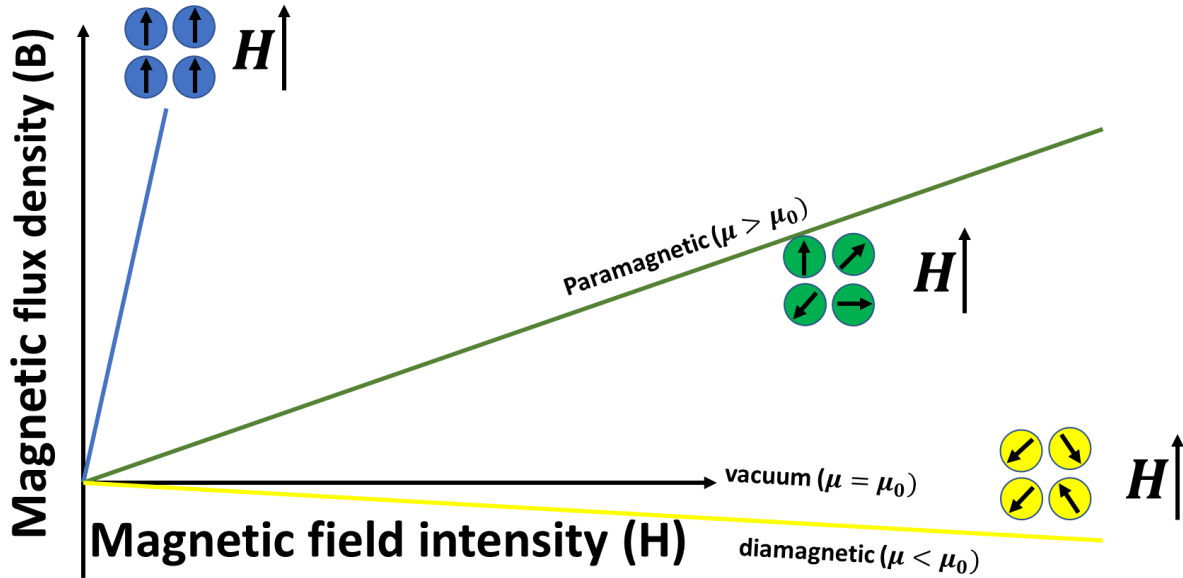


Figure 6. Classification of magnetic materials according to their behavior before external magnetic fields.

In this thesis proposal, there are two main types of magnetic materials analyzed, the plasma, which is a diamagnetic material and the components of steel (arc chutes, cheeks, and shields), that are pieces with ferromagnetic properties. This last part is so important because the arc is affected by the Lorentz forces, which depends on magnetic properties of the splitters (generally made of ferromagnetic materials). We can see in the following sections of this work that the magnetic properties of the steel are very important to us, in next paragraphs is described the typical BH curves also called *Magnetization curves of ferromagnetic materials*. To understand deeply the curves is important to know the magnetization concept, denoted as M , this represents the increase in the inductance due to the core material, so we can rewrite the equation for inductance as [31]:

$$\vec{B} = \mu_0 \vec{M} + \mu_0 \vec{H} \quad (2.12) \text{ Magnetic flux density}$$

The first part of this equation is simply the effect of the applied magnetic field. The second part is the effect of the magnetic material that is present. This is similar to our discussion on dielectric polarization and the mechanical behavior of materials. In materials, stress causes strain, the electric field \vec{E} induces dielectric polarization \vec{P} , and a magnetic field \vec{H} causes magnetization \vec{M} that contributes to the total flux density \vec{B} . The magnetic susceptibility m ,

which is the ratio between magnetization and the applied field, gives the amplification produced by the material:

$$\chi_m = \frac{\vec{M}}{\vec{H}} \quad (2.13) \text{ Magnetic susceptibility}$$

Both μ_r and χ_m refer to the degree to which the material enhances the magnetic field and are therefore related by

$$\mu_r = \chi_m + 1 \quad (2.14) \text{ Relative permeability}$$

Ferromagnetic materials depend on the applied field (\vec{H}). For ferromagnetic and ferrimagnetic materials, the term $\mu_0 \vec{H} \ll \mu_0 \vec{M}$. Thus, for these materials, $\vec{B} \cong \mu_0 \vec{M}$. Figure 7 shows this effect in the ferromagnetic materials. After we exceed the saturation point of the ferromagnetic materials its permeability decreases and their behavior is the same as a paramagnetic material ($\mu_r \cong 1$). Then, if we apply huge quantities of magnetic field \vec{H} the term $\mu_0 \vec{M}$ is less significant than the $\mu_0 \vec{H}$.

Magnetization curve of ferromagnetic and paramagnetic materials

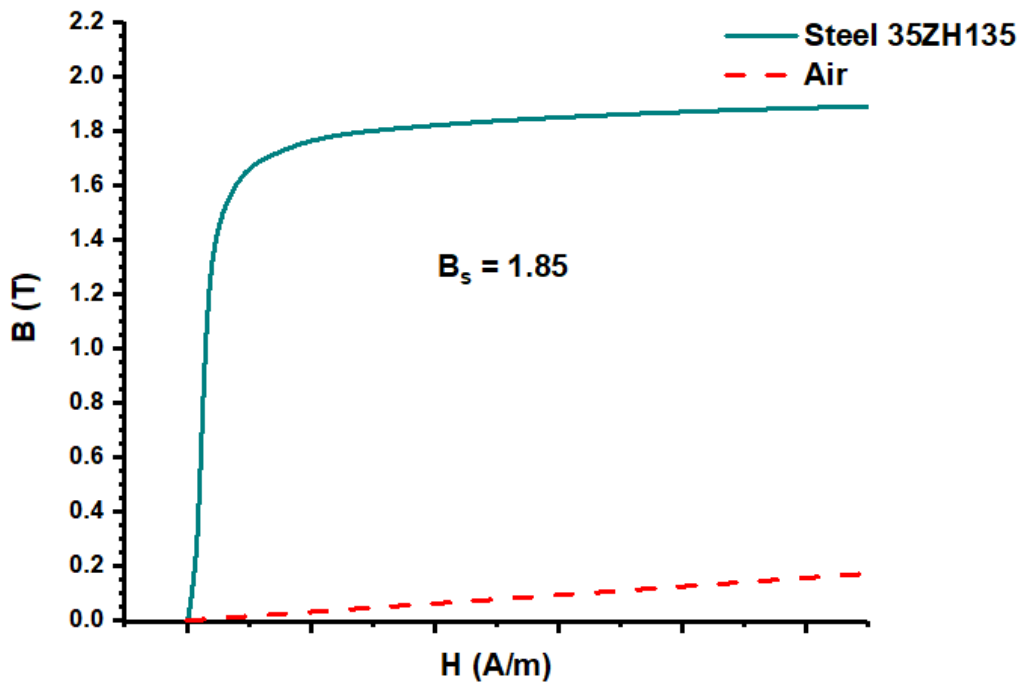


Figure 7. Magnetic curve of ferromagnetic and paramagnetic materials. (The effect of the H field in the air is amplified to note the linear behavior of the paramagnetic material)

It is important to mention that ferromagnetic materials could change their behavior when the Curie temperature is reached, also called Curie point, this is the temperature at which certain magnetic materials undergo a sharp change in their magnetic properties. In the case of rocks and minerals, remanent magnetism appears below the Curie point—about 570 °C for the common magnetic mineral magnetite.

CHAPTER III:

Simulations and models

III.I Introduction

In this chapter is described the methodology using the FEM software to create the studied cases, the Altair® Flux functioning and its limitations are described.

III.I.I Methodology using Altair Flux®

All models were simulated in Altair Flux® software, the methodology is shown in appendix A of this thesis proposal. The thesis is divided into three main topics:

- A qualitative study of MCCB electric arc.
- Analysis of arc chutes

In the first survey, the geometries were obtained from Schneider Electric Company and used to simulate the electromagnetic parameters. The main purposes of this investigation were to evaluate the effect of the geometry and each component from the Extinction Module of the L-frame MCCBs. This is treated deeply in chapter IV of this investigation.

The second topic the design was simpler and it was built and parametrized using the geometric tools of Altair Flux®. The shape of the first models taken to this study was obtained from Iturregui and Slade investigations [10], [30]. All materials properties were consulted from the internal database of Flux and the missing information that was not found in this database was obtained from *MatWeb: Online Materials Information Resource* [32]. The characteristics of the arc chutes studied were: the plates shape, the plates material, the influence of the number of plates in the Lorentz forces, and how the distance affects the Lorentz force in the arc extinction process.

III.II Parameters

At this point, we have mentioned the most important physical quantities that describe the electric arc phenomenon, such as electric field \vec{E} , the magnetic flux density \vec{B} , current density \vec{J} and the Lorentz force \vec{F}_L , this analysis will be centered in the last three quantities.

III.III Simulations with FEM software

To solve the Maxwell equations involved in the electric arc phenomenon is *Altair Flux*®, this software uses the Finite Element Method techniques to solve the electromagnetic equations in the model of the MCCB.

Flux has a module where we can simulate transient magnetic and steady-state AC phenomena, in its user's guide documents, Altair present the *Transient Magnetic Application* as follows:

“The Transient Magnetic application allows the study of the phenomena created by a time variable magnetic field. The magnetic field is related to the presence of variable

currents (and possibly permanent magnets). This application allows the consideration of induced currents in conducting regions (Eddy currents). It allows the consideration of skin effects and proximity effects in the conducting regions, too". [33]

A typical example of a problem treated as a Transient Magnetic application is presented in the figure below. This is an example with coupling with an external circuit.

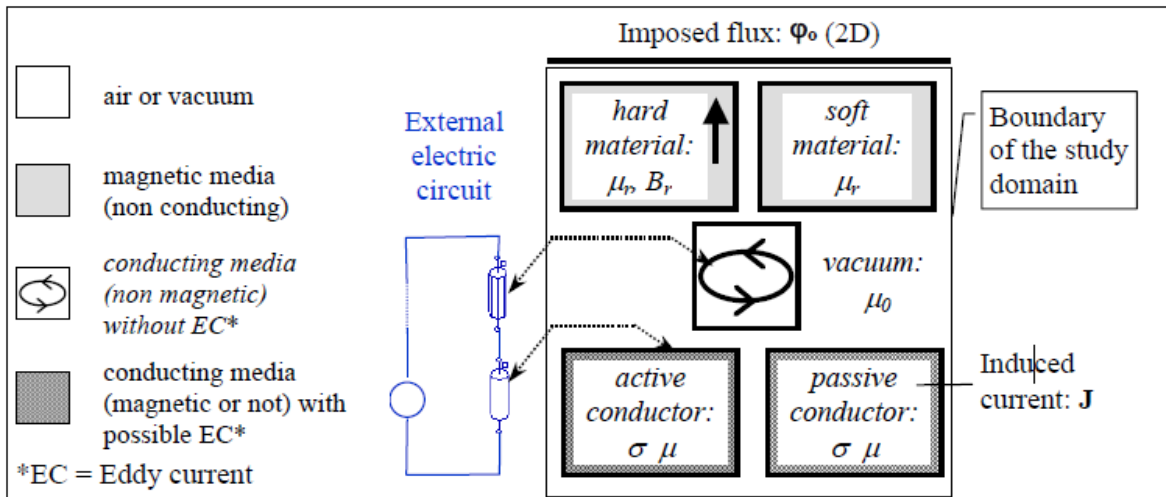


Figure 8. Diagram of Transient Magnetic application algorithm of Altair Flux®.

Active conductor definition [33]:

In the previous Figure 8, the conducting media could be an active (■) media: the conductor is supplied by an external current or voltage source.

The equations used for the solving are:

- Maxwell's equations (for a magnetic system)
- The constitutive equations of the matter, (relation between two physical quantities (especially kinetic quantities as related to kinematic quantities) that is specific to a material or substance, and approximates the response of that material to external stimuli, usually as applied fields or forces).

The computation conditions for a Transient Magnetic application are the following: the state variables are time dependent: $\frac{d}{dt} \neq 0$ (transient or variable state: current sources vary with time) the computation concerns only the \vec{B} and \vec{E} fields (the \vec{D} field is not computed).

The equations of the electric fields \vec{E} and \vec{D} and of the magnetic fields \vec{B} , \vec{H} can't be decoupled.

To solve these equations, two models are used:

- the vector model, which uses the magnetic vector potential (written \vec{A}) derived from the equation: $\vec{B} = \nabla \times \vec{A}$. This function A is given the name "vector potential" but it

is not directly associated with work the way that scalar potential is. The vector potential is defined to be consistent with Ampere's Law and can be expressed in terms of either current I or current density \vec{J} (the sources of the magnetic field).

- the scalar model, which uses: magnetic scalar potentials (written Φ_{tot}). It is an important mathematician tool that surges when the condition $\nabla \times \vec{B} = 0$ is assumed, the result of solve these differential equations give us a special function called magnetic scalar potential, denoted with the Φ symbol.

This thesis, as we have mentioned is focused on explaining the process of the extinction of an electric arc, they are proposed three cases of study. The first one is a qualitative study that explains how the geometry of the arc modifies the magnetic fields and this contributes to a faster extinction of the arc so the module used in Altair Flux[®] is the *Transient Magnetic Application* but applying special macros to annulate the eddy currents effects in the solid conductors. The second case treats about the characteristics of the plates in the arc chute of the chamber extinction, thus the *Transient Magnetic Application* is used again, but this time without the use of any kind of macro.

CHAPTER IV:

Qualitative study of MCCB electric arc

From the outside, an MCCB looks like a very simple piece of an electric equipment, but the role of this circuit breakers is complex and it has a very important function. They are designed to connect and disconnect the equipment linked to their terminals. Also, they provide protection against overload and short-circuit faults. At the inside of the circuit breaker is located a module of extinction, these modules operate mainly in short-circuit faults. The most important parts of this module are contacts, terminals, shields, arc chutes and cheeks, these last three elements mentioned are located in the chamber of extinction. In some models, the protective devices are housed separately. Usually, in an MCCB the electric arc extinction module and the tripping module are in the same place (in a plastic case). The emphasis of this research project in the electric arc extinction module. The determination of the Lorentz force at the birth of the electric arc is cover in this chapter.

For the simulation models, the electric arc is represented by a DC current that flows through a cylinder with the dimensions of the arc. The radius of the arc is approximated to 2.5 mm, a reasonable estimation according to [34], [35]. Because this goal is to determine the maximum value of the Lorentz force applied to the arc, a DC current was used.

The design of the components take into consideration the working duties that are submitted. By norm, they have to perform according to the design specifications.

In this research work, the aim is focused to the short-circuit elimination. This is done with through the arc extinction module, during this process the magnetic field is very important because it leads the electric arc to the arc chutes at the arc extinction chamber. For that reason, the objectives of this thesis are:

- To evaluate the effect of the main components of the MCCB extinction module in the magnetic field generated by the arc .
- To evaluate the Lorentz forces that redirect the electric arc toward the arc chute.

In this chapter, the evaluation of the circuit breaker components according to the variations in the Lorentz force at the electric arc, is discussed. The electromagnetic simulations were done using, as an example, the circuit breaker shown below.

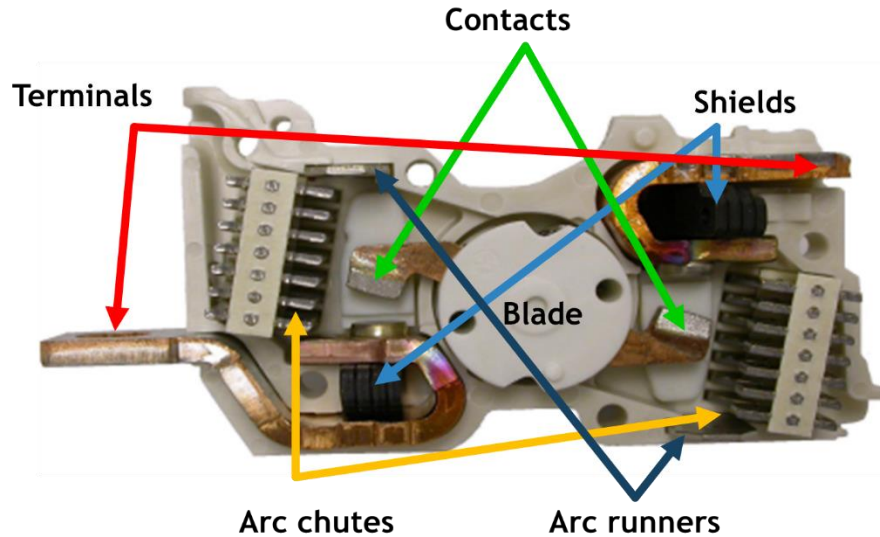


Figure 9. MCCB Extinction Module. (Ampule) from Schneider Electric ®.

This is a module of extinction of a typical MCCB L-frame model from Schneider Electric. These models operate with rated currents from 70 to 600 A. They have an interrupting capacity according to the voltage of the network where they are located, if the circuit breaker is located at 240 V the maximum value of peak current that is possible to interrupt is 125 kA but if it operates in 600 V this value drops to 50 kA. Several models of this frame have a capacity to interrupt failures from DC systems by adding other components to the original set [36], but they are not studied in this work.

A preliminary test was done to verify and understand the function and reaction to the magnetic fields of all steel components. Probably, the results of these tests are not corresponding with the real MCCB models because we are simplifying the models, excluding important effects as the thermal variables. Our main intention was to know how are related the magnetic field and the current density with the Lorentz force in a qualitative form. To find out this, we simulated a 3D model of an MCCB, it is showed in Figure 10:

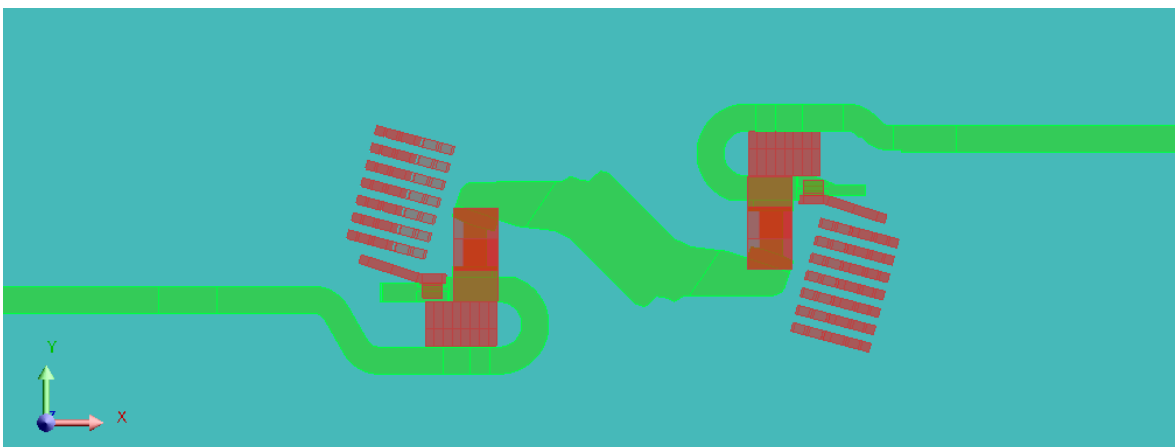


Figure 10. 3D Model of an extinction module of an MCCB in Altair Flux®.

In Figure 10 is appreciated the 3D model in Altair Flux® of the extinction module of the MCCB. In red are shown the steel components, in green the copper elements, the blue zone represents the air surrounding the MCCB extinction module. The selection of materials for a correct simulation is very important, as we will see in later studies the material and the geometrical shape of the device, play a great role in its operation and functionality. That is why in the next section a brief analysis of the properties of the materials that compose the devices is made.

IV.I Materials and characteristics of the MCCB modeled.

The components of the module of extinction of an MCCB are listed in Table 1, in this table is shown the content of each material used in the design of all components modeled in the simulation. We can divide these materials into two main categories: ferromagnetic and paramagnetic materials, as we can see each component have specific materials to give them the desired properties and fulfill their function. The materials that play a very important role are two: Copper which is a material with great electrical conductivity and poor magnetic properties, (it is classified as a paramagnetic material). and the mild steel known as SAE1010 under the standards of the Society of Automotive Engineers (abbreviated for our analysis as Steel 1010) is a material with very remarkable magnetic properties and electrical properties that are not the best (approximately 10 times less than those of the copper) are typical of an electrical conductor.

Component	Material	Content	Component	Material	Content
Pastille contact mobile + (sublayer)	Silver, Ag	79 ± 0.5	Arc runners	SAE1010	
	Tungsten carbide, WC	20 ± 0.5		Carbon, C	0.080 - 0.13 %
	Carbon fiber, Cf	1 ± 0.5		Iron, Fe	99.18 - 99.62 %
	Cu	28 ± 0.5		Manganese, Mn	0.30 - 0.60 %
	Ag	72 ± 0.5		Phosphorous, P	≤ 0.040 %
Shield (Cale Blindage)	SAE1010			Sulfur, S	≤ 0.050 %
	Carbon, C	0.080 - 0.13 %		Cheeks	SAE1010
	Iron, Fe	99.18 - 99.62 %	Carbon, C		0.080 - 0.13 %
	Manganese, Mn	0.30 - 0.60 %	Iron, Fe		99.18 - 99.62 %
	Phosphorous, P	≤ 0.040 %	Manganese, Mn		0.30 - 0.60 %
	Sulfur, S	≤ 0.050 %	Phosphorous, P		≤ 0.040 %
Blade	Cooper, Cu + Oxygen, O	99.9999%	Sulfur, S		≤ 0.050 %
Terminals	Cooper, Cu + Oxygen, O	99.9999%			

Table 1. Materials used in main components of an L-frame MCCB extinction module.

The materials chose to simulate the model were only two, the SAE 1010 steel and the copper. Silver and plasma properties were omitted in this first approximation.

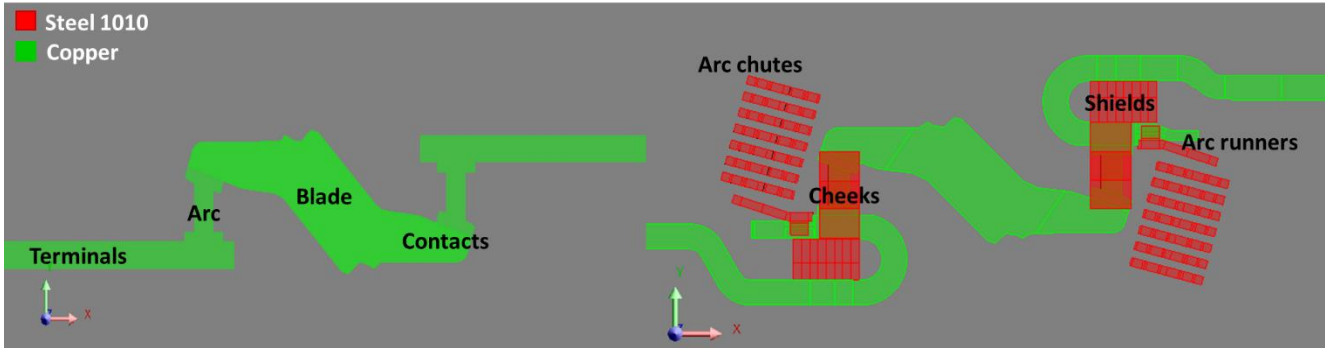


Figure 11. Model simplified versus Model with all steel components.

The copper is presented in green in Figure 11, and it is modeled for the current path (including the terminals), the contacts and the blade, the electric arcs are modeled with the properties of the copper, the magnetic properties of the silver and plasma are similar to the copper, because both are paramagnets so this simplification is valid to begin analyzing the phenomenon. The components in red are the shields, the arc chutes, and the cheeks, they were modeled with the properties of the steel 1010, as we mentioned before.

The properties of all mentioned materials are listed in Table 2, they were obtained from the materials database of Altair Flux®.

Material	Magnetic properties	Electric properties	Thermal conductivity
Copper	Linear isotropic with $\mu_r = 1$	Isotropic resistivity, linear function of temperature: $\rho(T) = \rho_0(1 + aT_0)$ $\rho_0 = 1.564 \times 10^{-8} \Omega m$ $a = 0.00427$	Isotropic constant Thermal conductivity $\kappa_c = 394 \frac{W}{mK}$
Steel 1010	Isotropic spline saturation with an initial permeability $\mu_r = 2022.6835$ Saturation magnetization = 1.9 T Knee adjusting coefficient = 0.9636	Isotropic resistivity $\rho_0 = 1.43 \times 10^7 \Omega m$	Isotropic constant Thermal conductivity $\kappa_c = 60 \frac{W}{mK}$

Table 2. Properties of the material used in simulations.

The study consisted of circulating a current of 35 kA through the current paths, several cases were considered, the geometry was varied by modifying the steel components and the loop, the most simplified model is shown at the left of this same figure and is explained in the next

section as Case I. The arcs are named as “arc 1” to the arc at the left of the geometry and the arc at the right is named as “arc 2.

IV.II Evaluated cases

For the determination of the magnetic flux effect on the electric arc, nine design cases were evaluated. In the next section the models, with the research questions are illustrated.

IV.II.I Case I: Flat geometry, 35 kA excluding the steel components

This model is the simplest one, the steel components that are outside of the current path are neglected. The loop of the geometry at the terminals is replaced with a flat copper component. The MCCB model is surrounded by only air. The current applied is 35 kA of direct current. This value of 35 kA is selected because it is a typical value in short-circuit currents, the type of current is taken as DC because in this general analysis it is sought to determine the maximum values reached in the densities of magnetic flux, density of currents and in the Lorentz forces, for simplicity the function corresponding to a short circuit current is not taken into account and only the case where the current values are maximum is analyzed.

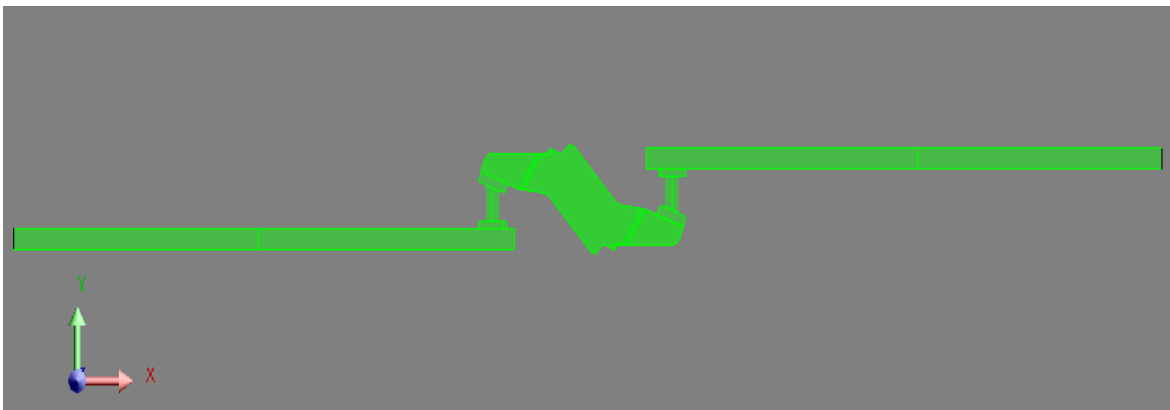


Figure 12. Geometry of the Case I.

One of the main interests of this case is to know the influence of this loop on the Lorentz forces. The steel components are also discarded, in order to make a comparison of results easier. In this simulation we will obtain directly the magnetic force that arises due to the fact of making current flow through a conductor. The effect of the geometry of the blade is perceived in this experiment. This case is the basis for the future comparison of results.

IV.II.II Case II: Original geometry 35 kA excluding the steel components

In this second case, the original geometry of the current path is taken into account, the loop effect is added. As in the previous case, components composed of steel are omitted, it is considered that the model is surrounded only by air. Through this case it is expected to compare and determine the effect that this loop has on the magnetic flux density in the arc and the Lorentz force perceived in the electric arc. This geometry is particular to this type of breakers, so it is interesting to know the function and effect of the geometry in the process of arc extinction.

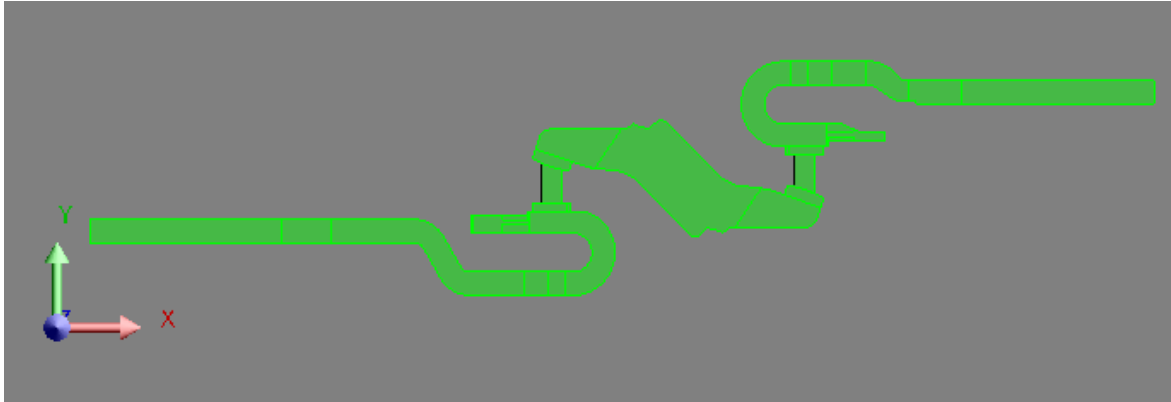


Figure 13. Geometry of the case II.

The current path is shown in green. All green elements were simulated with copper properties as the other simulations of the anterior cases.

IV.II.III Case III: Original geometry 35 kA including the arc chutes

In this case, the arc chutes are added to the original model of the path, in this simulation is verified the effect of the arc chute on the magnetic fields and consequently in the Lorentz forces. In this case it is expected to perceive the effect of the arc chutes and the loop. The assigned current is the same as in the previous cases.

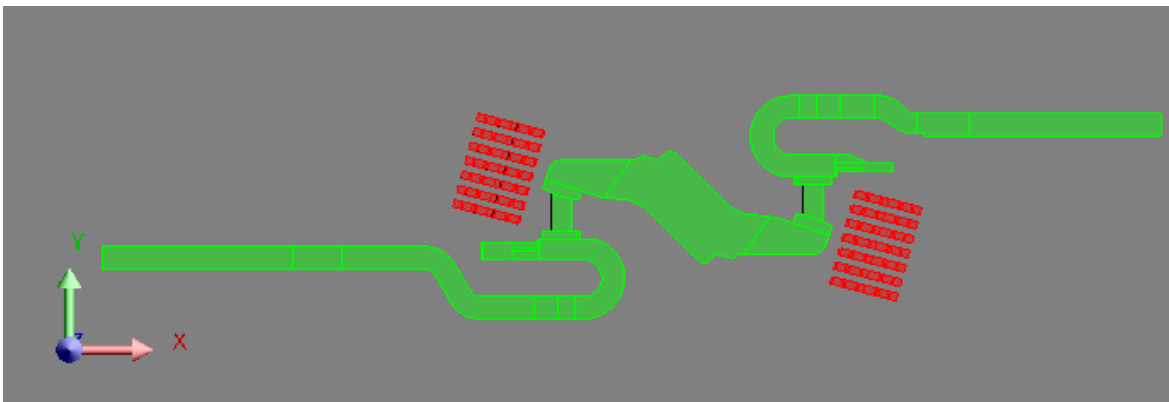


Figure 14. Geometry of the case III.

The same path of the current of the anterior case is shown in this figure, the red elements correspond to the arc chutes, it is conformed by seven plates as the real MCCB module extinction module which is the base model of this simulations. This pieces are created to attract the arc and elongate it to increase the voltage at the arc and extinct it. This is a fundamental component that is presented in almost all types of low voltage circuit breakers. This element will be studied with more detail in the next chapter.

IV.II.IV Case IV: Flat geometry 35 kA including the arc chutes

The flat geometry of the case I is taken in this case but the addition of the arc chutes are made. The realization of this simulation was done with the intention of measuring the

contribution of the chutes to the original model by discounting the effect of the loop, unlike case III where there is the addition of the loop and the arc chute, in this simulation it is taken into account only the appearance of the chutes arc, so is possible to calculate directly the contribution of these. It is also possible to calculate the effect of the union of the loop and of the arc chute as a whole since it is possible that there are contributions of components as a whole that is different from the individual sum of the forces of each element separately.

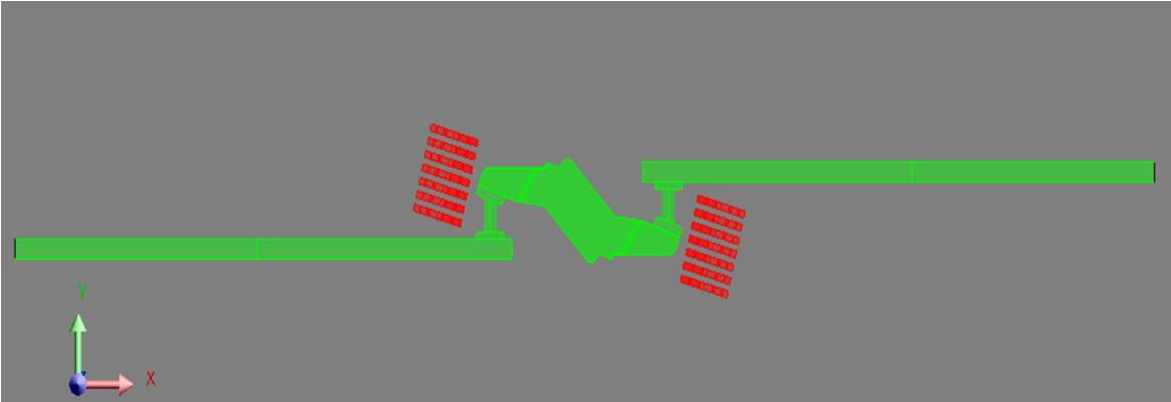


Figure 15. Geometry of the case IV.

As in the other cases, the elements in green represent copper components, the arc chute are shown in red, this arrangement is made up of seven plates, as in case III, this number of plates in the arc chute is fixed and will not be modified in any future simulation.

IV.II.V Case V: Original geometry 35 kA including the arc chutes and shields

In order to verify the interaction between the arc chutes, shields and the original geometry were added these steel components in the simulation, excluding the effect of the cheeks. The MCCB is surrounded by air. The current applied is 35 kA of direct current as all the other cases. The shields are small pieces of steel whose intention is to increase the density of flow in strategic areas of the extinguishing chamber to increase and direct the force in the arc toward the extinguishing chamber.

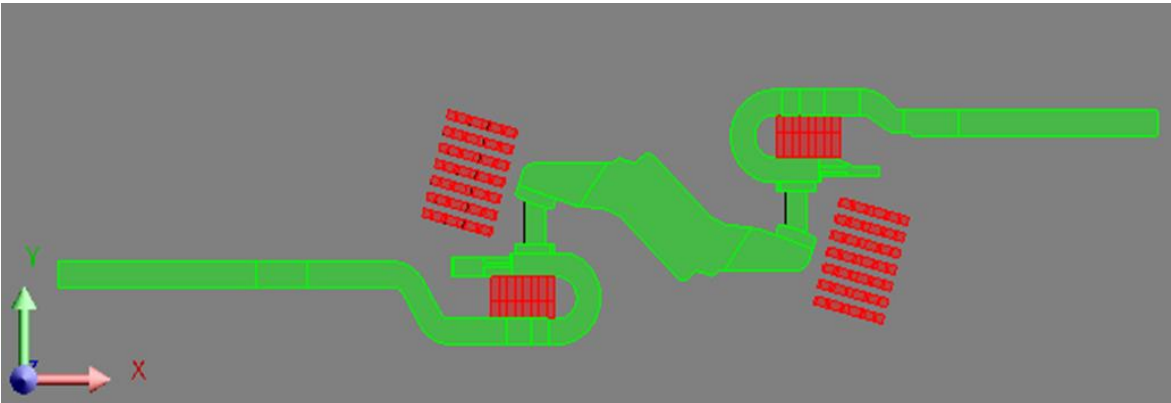


Figure 16. Geometry of the case V.

The shields appear in red in Figure 16, it is located in the middle of the loop, this model has eight blocks that conform a shield. The entire arrangement is called shield, and the MCCB normally has two shields as is shown in the same figure.

The coupling with the loop and the shields in the geometry is designed to significantly increase the Lorentz forces in the electric arc. This approach will be corroborated by the results obtained.

IV.II.VI Case VI: Original geometry 35 kA including the arc chutes and the cheeks

In this case, we added the arc chutes and the cheeks, excluding the effect of the shields, only to verify how are changing the electric variables as the magnetic flux density, the current density and the Lorentz forces. The current applied is 35 kA of direct current. The cheeks are the rectangles in red close to the electric arcs. The main purpose of the addition of these components to the module is to redirect the arc movement to the arc chutes.

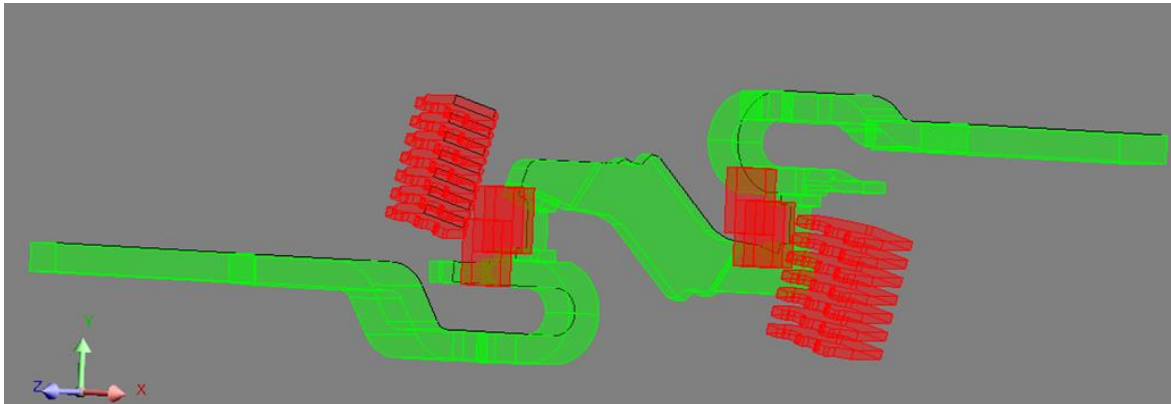


Figure 17. Geometry of the case VI.

There are three cheeks placed in front of each of the arcs, so are six in total for each extinction module. In this case is shown a three-dimensional view because the arrangement of the cheeks is better perceived in this way. The cheeks are placed at a small distance from the arc and also two are aligned and one is placed at a slightly lower height.

IV.II.VII Case VII: Original geometry 35 kA including all steel components: arc chutes, shields, cheeks and arc runners

All steel components are added in this case: arc chutes, shields, cheeks, and arc runners. The current applied is 35 kA of direct current as the anterior models analyzed. It is expected to this simulation present the most great values of the Lorentz forces. The arc runners addition could contribute to the direction of the Lorentz forces, but their main purpose is to conduct electrically the arc to the plates of the arc chute. The material of the arc runner is steel and is expected that this component will be capable of redirect the arc at the first moments acting like a bridge between the contacts and the arc chutes.

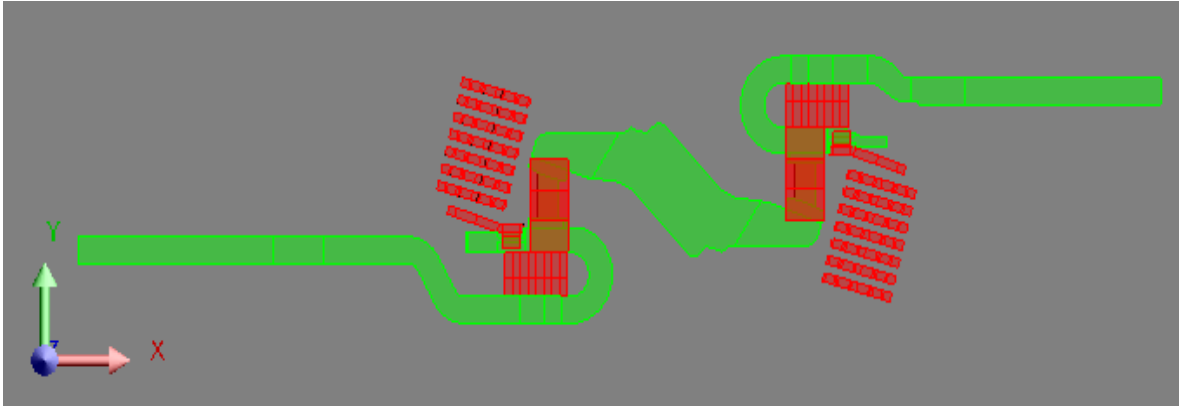


Figure 18. Geometry of the case VII.

The arc runner is shown in this figure as the component located under the arc chutes, next to the cheeks and over the shields (at the components situated in the left zone of the blade). The arc runner located at the right of the blade is situated over the arc chutes, under the shields and, besides the cheeks. (This arrangement is almost symmetrical). The path of the arc normally travels to the contacts to the arc chutes passing through the arc runners. The other components are not touched by the plasma and do not interact directly with the arc, the shields and the cheeks are designed to only interact with the magnetic field of the arc.

IV.II.VIII Case VIII: Original geometry 5 kA excluding the steel components

The geometry analyzed, in this case, is exactly the same as the geometry presented in Figure 13 but the level of the current is changed to 5kA of direct current. This is done to verify the effect of high currents in the magnetic saturation of the material, this is an important factor to consider because as we know, the behavior of a ferromagnetic material could change if high currents are applied and generate a strong magnetic field that exceeds the saturation point of the ferromagnetic materials. Case VIII and Case IX are simulated to be compared each other. It is expected to perceive a nonlinear behavior in this cases. The values in the magnetic field of the arc are expected to be much lower than the cases where is applied the 35 kA of DC, as we know the magnetic field depends of the quadratic of the applied current.

IV.II.VIII Case IX: Original geometry 5 kA including the arc chutes

This case is similar to the case III, where is considered the addition of the arc chutes to the model. The geometry used in this simulation is exactly the same as the shown in Figure 14. As explained in chapter two, ferromagnetic materials change their behavior when the point of saturation of the material is exceeded. The relative permeability decreases to very low levels comparable to that of the paramagnets. That is why we will try to determine in these cases, the effect of the current level on the force perceived by the electric arc and how the magnetic field of the arc chute is modified.

IV.III Results of the qualitative study of the electric arc in an MCCB

All results are grouped in Table 3 where are resumed the data of the electric parameters: Current density (J), magnetic flux density at the electric arc (B), Lorentz force per unit volume (F_{L_v}) and Lorentz force (F_L). In this qualitative study, we can observe the variation between the electric parameters in the different cases are mainly presented in the Lorentz force, the other parameters do not differ too much (Case I to Case VII), except the cases where the electric current is different (Case VIII and Case IX). The components X and Y of the Lorentz forces are shown in the last column of the table, the values of Z components are close to zero ($\sim 10^{-3}$) and are omitted. The force in negative X-axis is at least 17.5 times larger than the force in Y component. The arc chute near to the arc 1 is located in this direction, so the electric arc would deviate to the negative X-axis direction deforming its cylindrical structure. This is a behavior observed in all cases. A detailed analysis of the Lorentz forces is explained at the end of this chapter.

Maximum values of electric parameters				
Cases	J (A/m ²)	B(T)	Lorentz Force Density (N/m ³)	Lorentz Force (N) Arc 1
Case I: Flat 35 kA DC surrounded by air	3.401x10 ⁹	3.209	11.311x10 ⁹	-21.277 î + 1.214 ĵ
Case II: 35 kA DC surrounded by air	3.014x10 ⁹	3.326	9.540x10 ⁹	-55.649 î + 1.523 ĵ
Case III: 35 kA DC Steel 1010 arc chutes included	3.014x10 ⁹	3.389	9.732x10 ⁹	-66.732 î + 1.927 ĵ
Case IV: Flat 35 kA Steel 1010 arc chutes	3.014x10 ⁹	3.249	11.553x10 ⁹	-43.223 î + 2.109 ĵ
Case V: 35 kA Steel 1010 arc chutes and shields	3.014x10 ⁹	3.426	9.835x10 ⁹	-74.625 î + 2.06 ĵ
Case VI: 35kA DC Steel 1010 arc chutes and cheeks	3.014x10 ⁹	3.451	9.956x10 ⁹	-70.665 î + 1.811 ĵ
Case VII: 35 kA DC Steel 1010 arc chutes, cheeks and shields	3.014x10 ⁹	3.458	10.251x10 ⁹	-88.367 î + 2.26 ĵ
Case VIII: 5 kA DC air surrounded	430.550x10 ⁶	0.475	194.700x10 ⁶	-1.136 î + 0.047 ĵ
Case IX: 5 kA DC Steel 1010 arc chutes added	530.55x10 ⁶	1.703	202.096x10 ⁶	-1.589 î + 0.047 ĵ

Table 3. Results of the qualitative study of MCCB design.

There is a tendency to increase the Lorentz Force when the steel components appear but the others parameters do not increase their magnitude in a really appreciable way. The last cases are totally different to the first seven, their values are more adjusted to common values presented in experimental studies as presented by Kesorn Pechrach and Rau [1], [24].

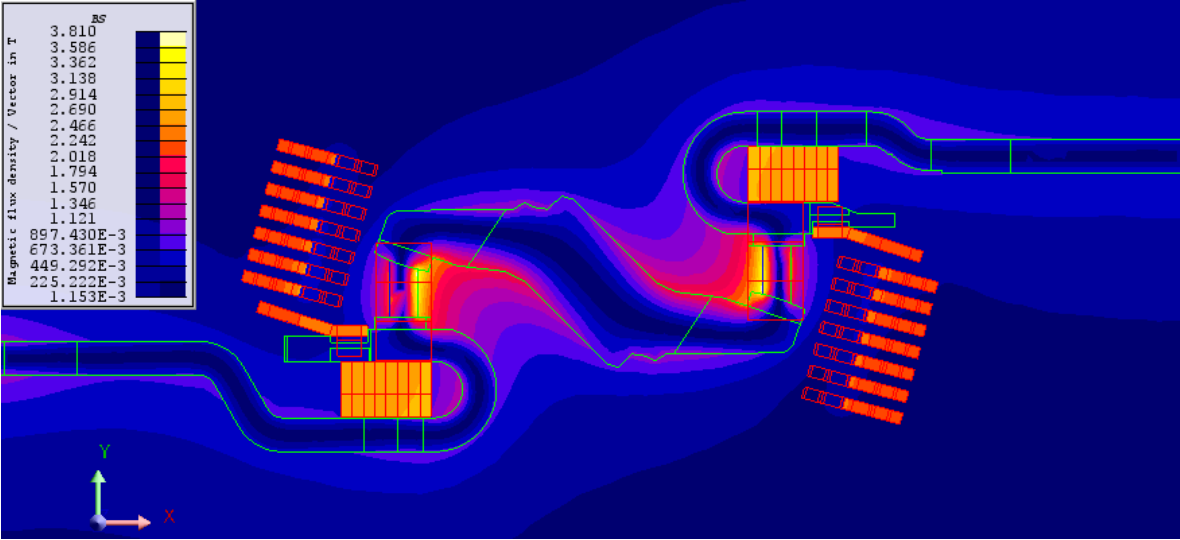


Figure 19. Isovalues of the magnetic field at the electric arc module of extinction.

In the previous Figure 19 the distribution of the magnetic field in the extinction module is perceived, it is important that a greater magnetic flux density is observed in the areas of the shields and the electric arc. It is expected that the electric arc has a very high magnetic flux density value since it is the source of the magnetic field. As explained below, the interaction of all the magnetic components added to the extinction module, such as arc chutes, shields, arc runners and cheeks, allow the Lorentz force that causes movement in the arc, be it grow and also be in the direction of the chutes.

In the previous figure the effect of the cheeks is not perceived because the graph is done on a plane XY at a fixed distance Z, and since the cheeks are in a different z plane, the distribution is not perceived, but its effect It is shown in the following figure.

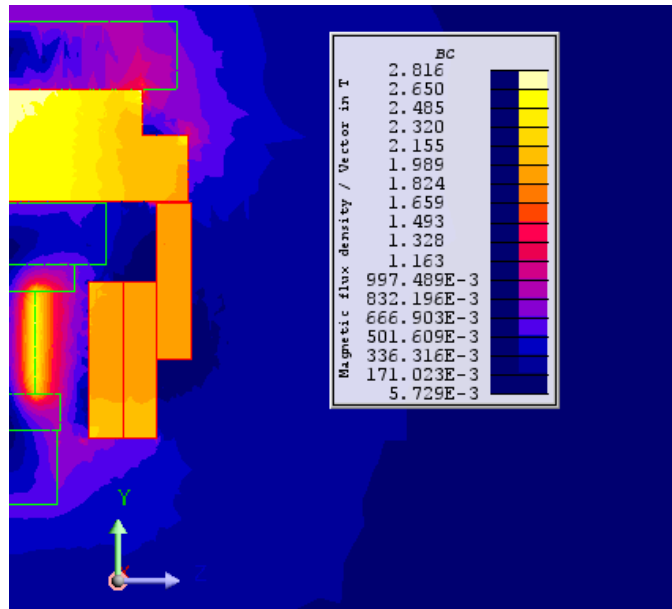


Figure 20. Isovalues of the magnetic flux density at the cheeks.

In Figure 20 is shown the values of the magnetic flux density at case VII, where all steel components are considered, an effect of the cheeks is perceived, the magnetic flux is about the 1.989 T, as we can see. The contour of the magnetic field of the arc is extended to these pieces. The others remarkable components are the shields, they present superior values of magnetic flux density, close to 2.650 T. We can confirm that the use of these elements is to augment the force, and the presence of the cheeks is explained due to the redirection of the arc. The Lorentz's forces intensifications could be explained if we analyze the reorientation of the magnetic flux in each case, as we can see in Figure 21 the alignment in the case VII, where all magnetic components were added, we note an alignment of magnetic field in Z direction, all steel components redirect the field to Z positive axis direction.

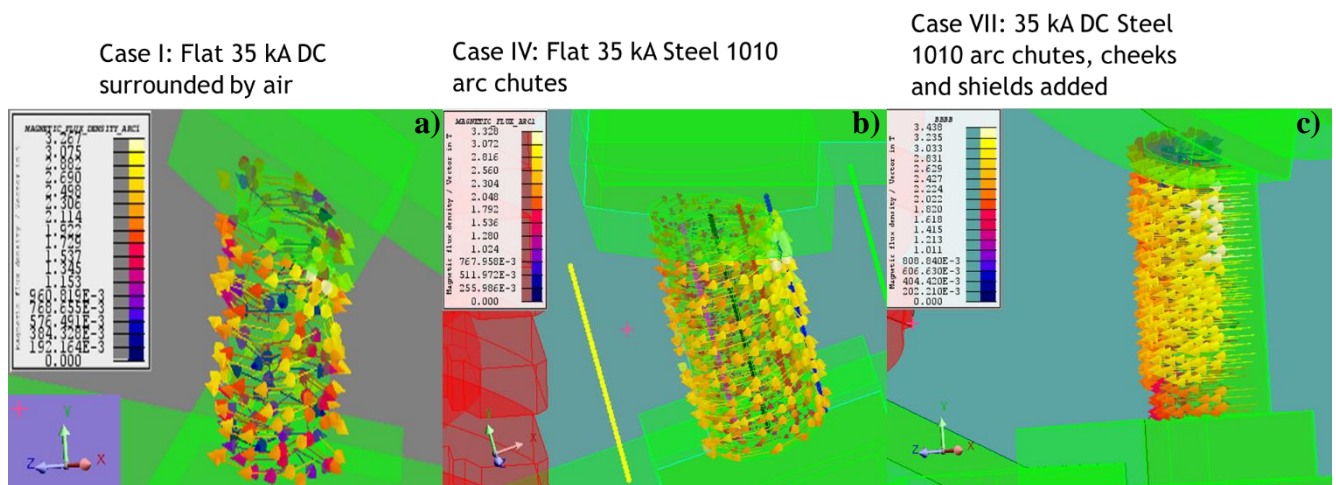


Figure 21. Alignment of magnetic fields at the arc 1.

In the calculation of the Lorentz forces, two variables, the magnetic flux density, and the current density, are mainly involved. The changes in the density of flow are very palpable in Figure 21, in Figure 22 we can see the current density through the electric arc, it is noteworthy that in its input the current circulates in a non-uniform way, but as it moves through of the trajectory of the arc, this tends to be more uniform. It can be seen in Figure 22 that at its entrance the current is distributed more in the upper right, the current density is considerably lower in the left sector but as the current advances, it is redistributed and reaches an approximate average value of $2.0 \times 10^9 \frac{A}{m^2}$.

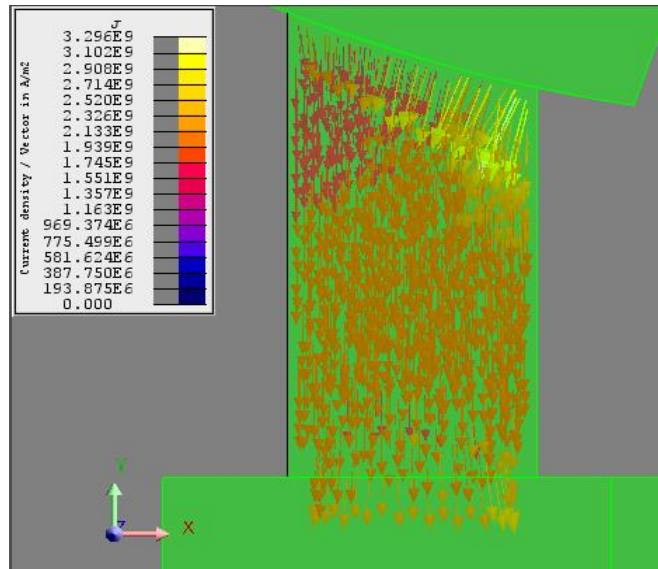


Figure 22. Current density vectors in the electric arc 1.

Five paths are drawn in Figure 23 to demonstrate the alignment and sense the effect of the components in the current density and the magnetic field. The length of the arc is considered with a value of 9.142 mm, this is a reasonable value considering that the maximal space available to elongate the arc is 20 mm.

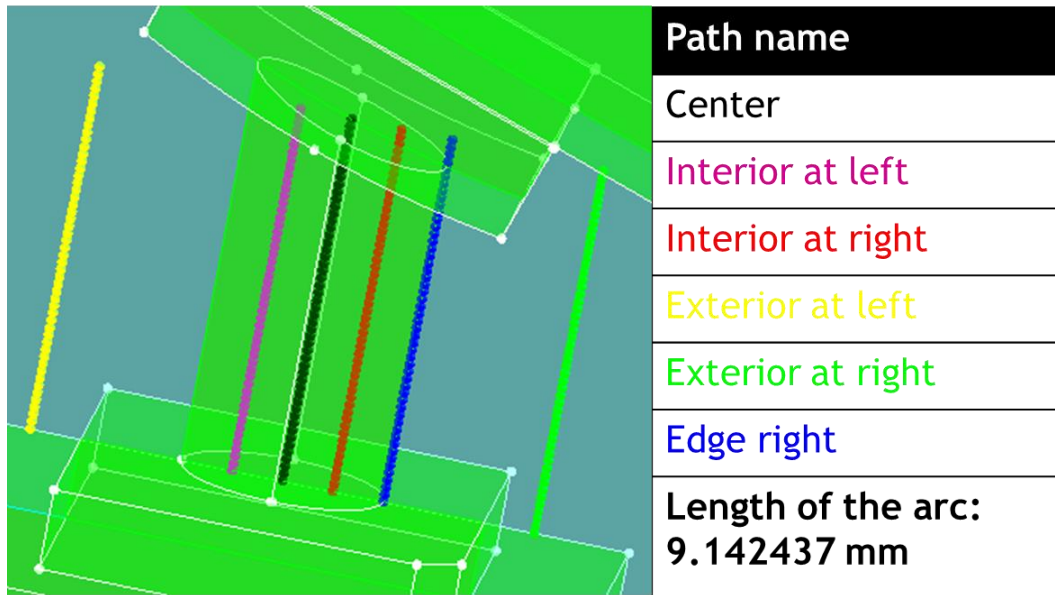


Figure 23. Paths to calculate current density and magnetic fields into and between the arc.

A nomenclature was made to identify easily the results of each path. It is shown in Table 4. The order is important to identify correctly the name of the path, the first tag “F” indicates if the simulations correspond to the flat geometry, an absence of this tag indicates that the model corresponds to the geometry that includes the loop. “A1” is to identify that the results correspond to the arc 1. All results made in this sections corresponds to the arc 1, the arc 2 presents almost the same results (not shown in this section) but varying in sign but not too much in magnitude. The “I” denotes that the path is into the arc. “E” indicates that the path is out the volume of the arc. “L”, “C” and “R” specifies the position of the path at the left, center or right respectively. The last position indicates us if the case corresponds to a model where the arc chutes are added, (Cases III – VI) or a case where the current paths are surrounded only by air (Case I & Case II). The tag “all” denotes only the Case VII, where all steel components are considered.

Nomenclature		
Tag	Name	Position
F	Flat	1st
A1	Arc 1	2nd
I	Interior	3rd
E	Exterior	3rd
L	Left	4th
C	Center	3rd
R	Right	4th
Air	Air	5th
Ach	Arc chutes added	5th
All	All steel components added	5th

Table 4. Nomenclature of graph cases.

The graphs of the magnetic flux in the mentioned paths are shown in the next figures. The magnetic flux density at the arc in main cases is analyzed for components X, Y, and Z. In order to demonstrate the alignment seen in Figure 21, the Figure 24 is showing X and Y components of the magnetic flux in the arc, all simulations present the same behavior, the values of the magnetic field components X and Y are very small to appreciate. A slight increase is noted in cases where the steel components are removed, (only air is surrounding the structure of copper).

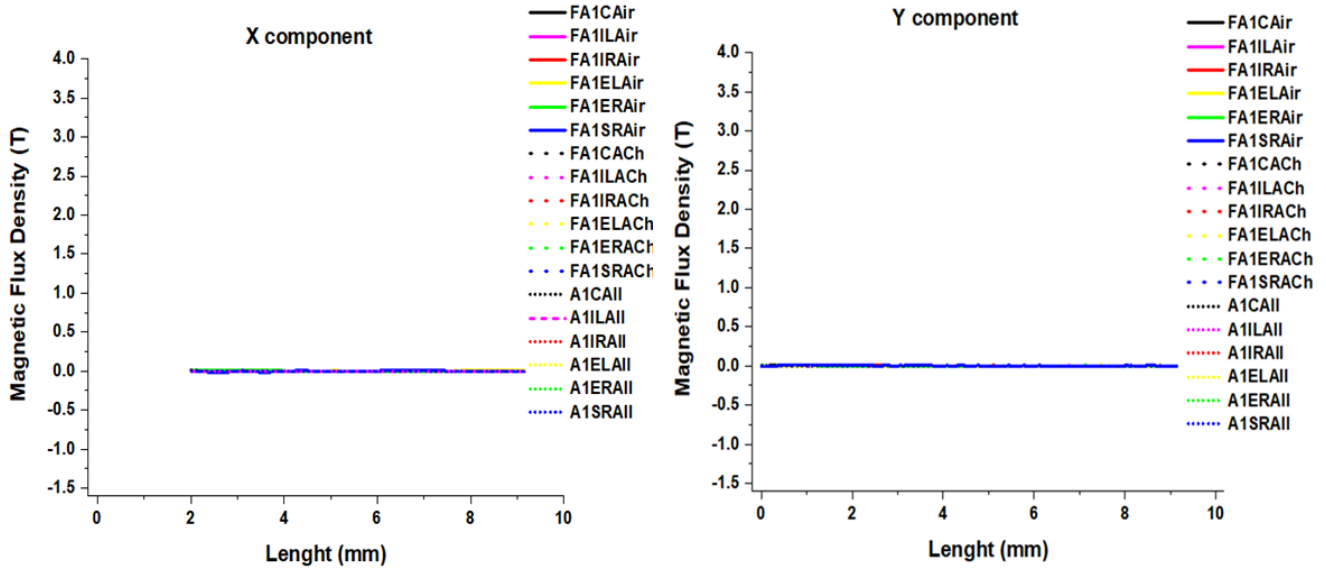


Figure 24. X & Y components from the magnetic flux density at the arc 1.

In Figure 25 is shown the Z component of the magnetic field at the arc 1, in this graph, we note that the greatest contribution to the magnetic field is due to this component, as we could see in Figure 21, the alignment is towards the positive axis of Z. The maximum values of the magnetic flux in the arc are presented at the right edge (blue line) in all cases, the case where we obtain the greatest value is when we add all the steel elements. The maximum values are very large, reaching peak values of 3.31 for the case FA1SRAiro and 3.81 T for the case A1SRAII. If we compare both cases, the first one where we remove all steel elements and the loop is omitted and the last one where all steel elements are presented and the loop is considered, we have an increase close to 14.71 % in the magnetic flux. If we ignore the loop and consider only the effect of the effect of the arc chutes, we obtain an increase of 1.9% in the magnetic flux. In the center of the arc (black line), the smallest values are found. The values at both sides in the interior of the arc are symmetrical as we can see in lines magenta and lines red. The values at the exterior of the arc (lines yellow and green) are symmetrical too, the values are much lower than the edge of the arc as we expected because we are modeling the arc as a small cylinder and the magnetic flux density in a cylinder is given as:

$$B_{Int} = \frac{I\mu_0 r}{2\pi a^2} \quad (2.13) \text{ Magnetic flux density at the interior of a cylinder}$$

$$B_{Ext} = \frac{I\mu_0}{2\pi r} \quad (2.14) \text{ Magnetic flux density at the exterior of a cylinder}$$

These equation described in an approximative way the models; the variation at the interior of the cylinder is changing according to a linear tendency but at the outside the field is changing in a quadratic form respecting to a distance r defined from the center of the arc to the point where is evaluated; if we maintain the same radius we can observe that we have a quasi-invariant system affected only by the elements that surround the current path. In cases where the magnetic elements are added (short dot lines), are found the greatest values in all paths evaluated, as we can see in Figure 25. There is a clear effect of the steel components in

the magnetic field of the arc. The maximum values are very large, reaching peak values of 3.81 T, these values are very large but they are presented only in specific zones in a very short time, if we substitute a current of 35 kA in the equation 2.14, we will obtain a value of 2.8 T, this equation is for an ideal case where we do not have magnetic materials surrounding the cylinder.

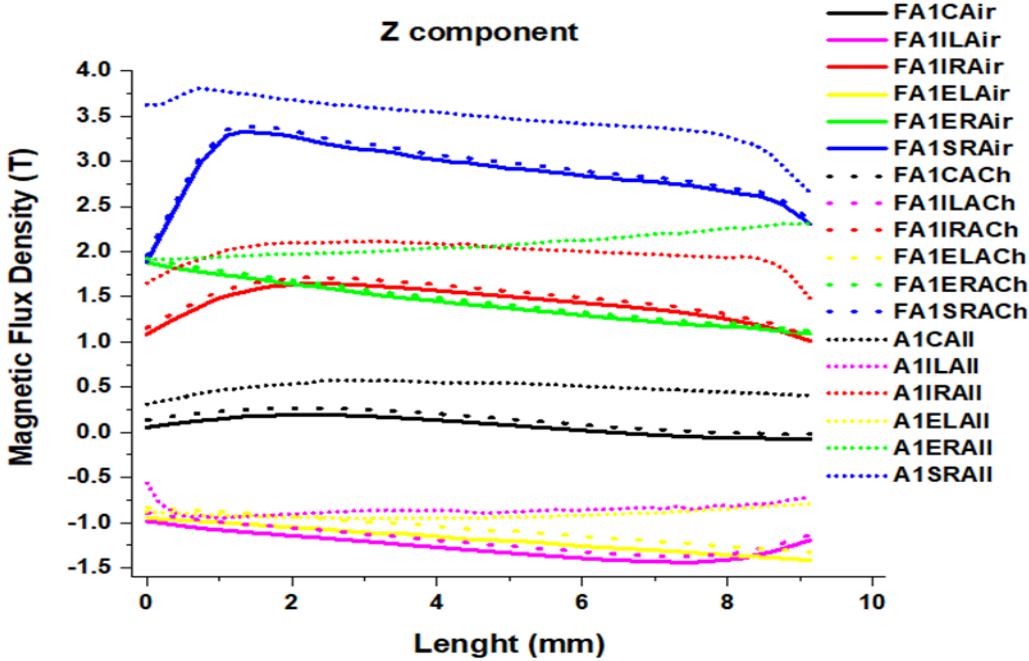


Figure 25. Z component of the magnetic flux density at the arc 1.

The current density at the arc 1 is graphed in figures Figure 26 and Figure 29, there are shown the X & Z components and Y component respectively. The magnitude of X and Z components are much smaller than the Y component. The X & Z current densities are almost zero in the center of the arc, where the Y component is larger. At the beginning of the path, the current density at X is bigger and grows again at the end of the path. The Z components do not grow in almost all cases, the exception is the case A1IRAll, where the influence of all steel components is considered, so the current density is varying in a more appreciable way. Several outliers are presented in Z component in this sample, this can be explained if we consider that all components have an effect on the current density, this is called Hall effect and is considered in Flux solving equations.

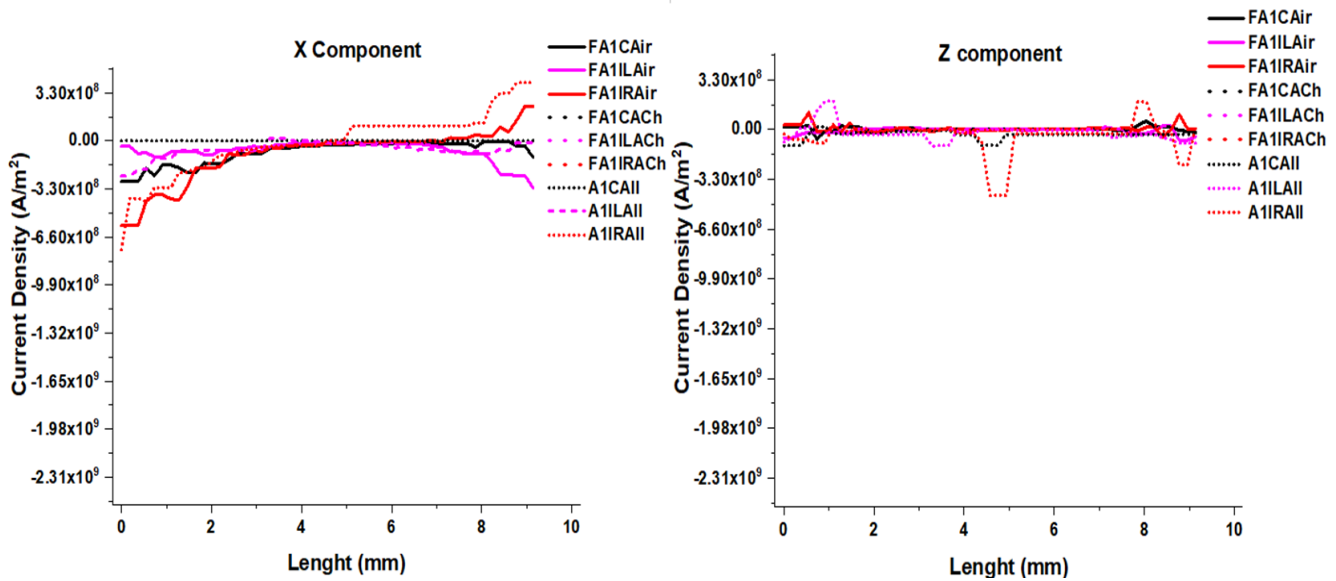


Figure 26. X & Z components of current density at the arc 1.

The graph shown in Figure 27 illustrates us that the current density in almost all cases is uniform at the center but varies at the extremes of the arc, where the X component increase the Y component decrease. The steel components have an effect on Y component more notable than the others, this is attributable to the Hall effect in the current at the electric arc. The average value of the current density of this component is $-1.78 \times 10^9 \text{ A/m}^2$ (excluding the outliers). The case A1IRAI shows again atypical values compared with the other cases. The outliers are located at the end of the path, where the influence of the arc runners and the shields is greater, taking values of $-2.4 \times 10^9 \text{ A/m}^2$.

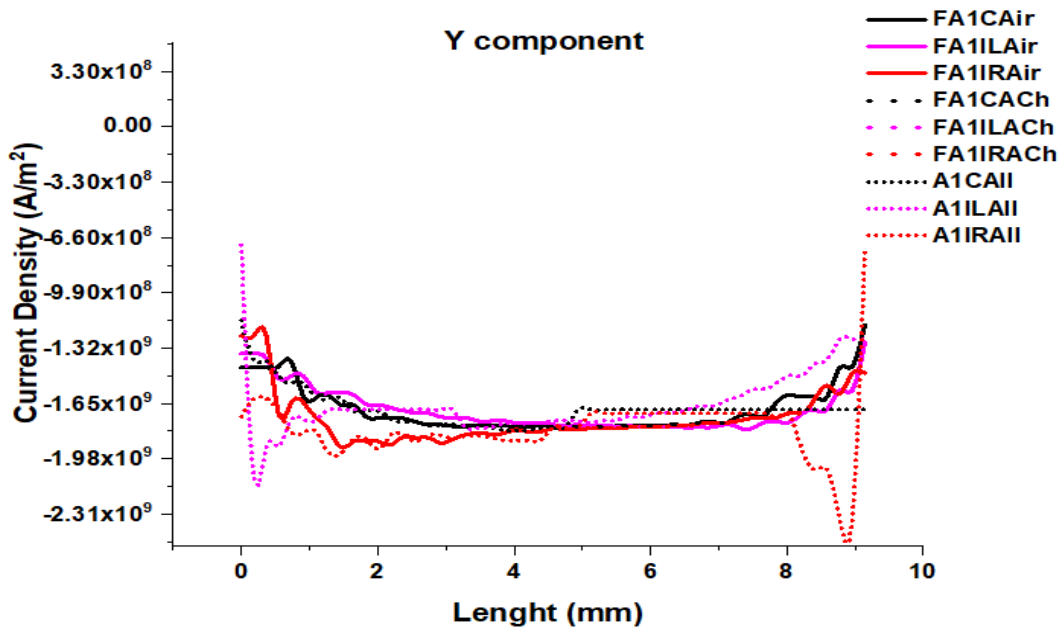


Figure 27. Y component of current density at the arc 1.

The influence of the steel components on the current density is perceptible but the averages values are not very different between them on the left side (magenta lines), if we take only the averages values considering in our calculations the outliers, we can see that the current density is larger in cases where the loop is removed and is substituted with a flat geometry, the average value of these cases is close to $-1.68 \times 10^9 \text{ A/m}^2$. The average values of the geometries where a flat geometry is considered but the arc chutes are included the average values of the current density are close to $-1.74 \times 10^9 \text{ A/m}^2$. In cases where all steel components are considered and the loop is added, we have average values of $-1.66 \times 10^9 \text{ A/m}^2$. If we analyze the right side (red lines) where the atypical values are present, we have that the variation between cases where the loop is removed are almost identical with an average value of the current density of -1.74 A/m^2 , but if we add the loop and all steel components the current density increase to -1.78 A/m^2 . Clearly, the values of the current are larger in the right side of the arc, this is due to the geometry is not symmetric at the beginning of the path as we saw in Figure 22.

Lorentz forces of all cases listen in Table 5. The black squares in the table represent if the element of the column is considered in the simulation; as an example, in the first case none of these elements were considered, in the second one only the loop was added but all steel elements were omitted, we apply this method in all cases to identify them easily.

Case	Loop	Arc chute	Shield	Cheeks	Arc runner	X component of the Lorentz force (N)
I						21.277
II	■					55.649
III	■	■				66.732
IV		■				43.223
V	■	■	■			74.625
VI	■	■		■		70.665
VII	■	■	■	■	■	88.367
VIII	■					1.136
IX	■	■				1.589

Table 5. Lorentz forces of studied cases with a quick description.

The current applied in cases I to VII is fixed in 35 kA of direct current, so we have that if this level of current is applied to the first case we will obtain a force of 22. 277 N due only to the geometry of the blade, the smallest of all cases, when the loop is considered the forces increase more than two times with 55.649 N. We can attribute an augment of 34.372 N in the force due to the addition of the loop in the geometry at this level of current. The third case presents the addition of the arc chute respecting the case II and the force is increased to 66.732 N, so we have an increase of 11.083 N due to the arc chute. The case IV is similar to the case I but adding the arc chute, so in this case, we have a Lorentz force of 43.223, we determine that the influence of the loop is greater than the effect of the arc chute. In case V, where the shields, arc chutes, and the loop are considered the Lorentz force grows to 74.625

N. The attributable force to the shields in this analysis is rounding the 7.893 N. In case VI where the cheeks are added but the shields are omitted, the values gotten are 70.665 N, so we estimate a value of 3.933 N due to the cheeks. In case VII where all components of steel are included in the analysis, considering even the arc runners, we have a Lorentz force calculated in 88.367 N. The augment due to the arc runner and the combination of all steel components is rounding the 9.81 N. If we compare the case I with the case VII, we have an augment of more than four times the initial value of the Lorentz force. The case VIII and the case IX could be compared with each other. The augment in the Lorentz force in these cases due to the addition of the arc chute is about 39% this is explained by the non-linear behavior of the magnetic field due to the effect of magnetization on ferromagnetic materials. After to reach the magnetic saturation we have a linear behavior of the Lorentz forces in the arc. This is explained through a new analysis focused only in the arc chutes design on chapter V.

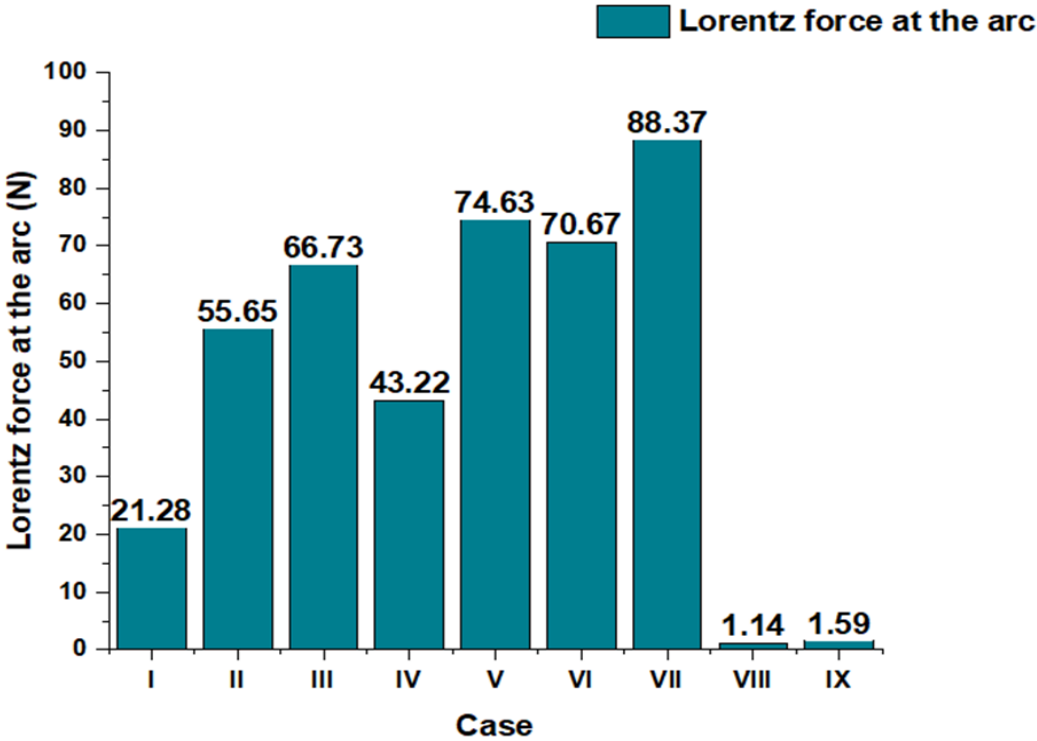


Figure 28. Lorentz force of cases analyzed.

CHAPTER V: Analysis of arc chutes

The arc chute is a series of plates in the path of that arc that split it up into smaller segments (as we have mentioned before), the main purpose is to lower the energy in each arc segment to that it needs less dielectric strength (of air) to extinguish it, in order to not allow it to sustain itself any longer. The arc chute also serves to cool the thermal energy in the arc. Without arc chutes, the breaker would need more space to dissipate the energy and the arcs would deteriorate the contacts and other components considerably faster.

In this chapter, the behavior of the electric arc in the neighborhood of the arc chute is studied, With the aid of FEM, the Lorentz force is calculated for different arc chute plates configurations and a brief analysis of the induced eddy currents is made. The characteristics of the arc chute plates are taken into consideration.

IV.I Plates shape

The shape of the plates is a well-thought design, the most effective design according to the literature [10], [30], is the V-shaped form. This design increases the magnetic flux in certain zones and takes the arc toward to the arc chutes. These characteristics in the design enhance the magnetic field at the plates and increase the attractive force in the electric arc, provoking an increase of the Lorentz force that takes the arc to the chamber of extinction, then, once the arc is divided in several arcs into the arc chutes, the voltage of the arc increases by the resistive effect, the voltage exceeds the capacity of the voltage source and consequently the arc cannot be sustained [30]. The shapes analyzed in this work are shown in Figure 29:



Figure 29. Models of plates with different shapes.

They are named as “plate 1”, “plate 2” and “plate 3”. Magnetic flux density, current density and Lorentz force in the arc were measured in a path. In order to evaluate the effect of a short circuit current in the plates, a simulation was made. The parameters of the applied current of all simulations of arc chutes analysis are listed in the next table:

Current source data:	Formulation
Short circuit current with maximum asymmetry	$i_{sc}(t) = 5000\sqrt{2} \left(-\cos(\omega t) + e^{-\frac{t}{T}} \right)$
Time constant	$T = \frac{X/R}{2\pi f} \approx 0.01019 \text{ s}$
Frequency associated	$f=50 \text{ Hz}$
Ratio X/R	$\left(\frac{X}{R}\right)_{MCCB} = 3.2$

Table 6. Current source parameters.

The inductive reactance was calculated through tables of ratios of X/R in MCCBs [37]. The time constant was obtained considering an X/R factor of 3.8. the frequency associated with the short circuit current function was 50 Hz. This typical frequency is selected to reduce the rounding errors in the Altair Flux[®] software. The maximum current applied resulted in 9720.28 A of this asymmetrical short-circuit current. This maximum value is used to calculate the maximum forces reached.

The assumed trajectory of the electric arc movement is along the y axis shown in Figure 30, the results of the electromagnetic variables were calculated for three distances: 10, 5.25 and 0.5 mm; a straight path was considered, the axis X and Y are shown in Figure 30. To avoid errors related to the mesh, the results were calculated in the same model, the mesh was the same for the three models but the air regions were varied according to the shape of the model becoming air only certain areas. All calculations were made by using a mesh of second order.

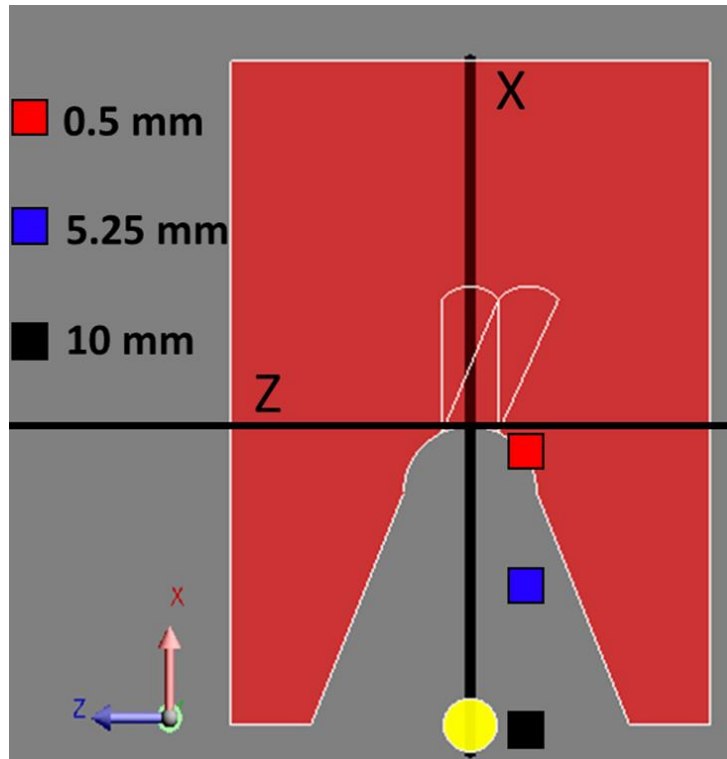


Figure 30. Model to compare shapes in plates.

Due to the symmetry of the geometry, the X and the Z force components are much smaller than Y component, so it is preferable to analyze this component to appreciate the effects of the plate in the arc. The report of the force acting on the electric arc is only in the Y direction.

The magnetic fields reported in this section was calculated fixing the maximum value of the current at 9720.28 A. In Figure 31, in the first instance we can see three peaks, the first one is due to the electric arc at 10 mm of distance, the second one in red is at 5.25 mm and the blue one is at 0.5 mm of distance to the origin. These arc curves have two main values, we can see that the values of the magnetic flux density are not symmetrical at their positive and negative extremes, to explain this we will analyze first the curve in black (10 mm of distance), the minimum value of the magnetic flux density is -1.930 and the maximal value is 1.708, this difference lets the apparition of a net force different to zero, the direction of the Lorentz force is obtained when we made the cross product between the current density \vec{j} and the magnetic flux density \vec{B} . Figure 32 shows the direction of the current in the Z axis, so we obtain as result a Lorentz force in the Y positive direction.

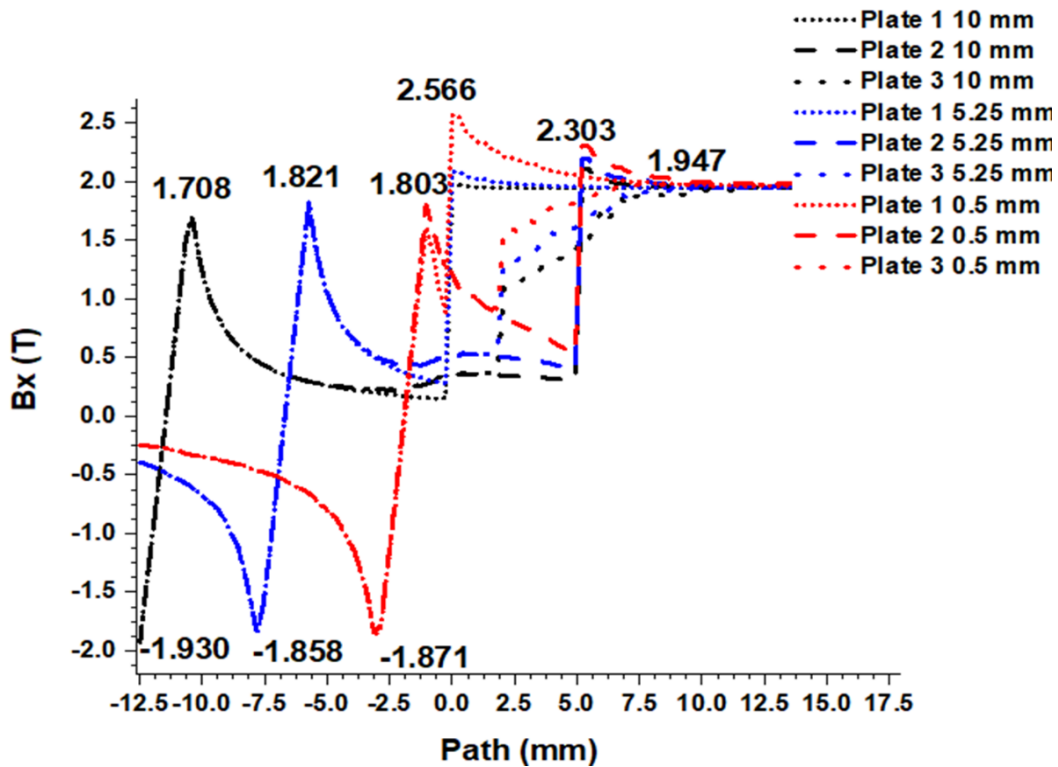


Figure 31. Graph of Magnetic flux density at X direction through the path of Figure 23.

In Figure 32 we can note that the current density in the arc is uniform, we are modeling the arc as cylinder but in a most real model the shape of the arc is varying, but in the first displacements of the arc, a cylinder form is a good approximation, the maximum distance where the arc is not deformed completely and maintains a cylindrical form is close to the 0.5 mm according to [34], [35], [38] so we can have an idea of what is happening in the arc at the moment before of its insertion to the arc chute.

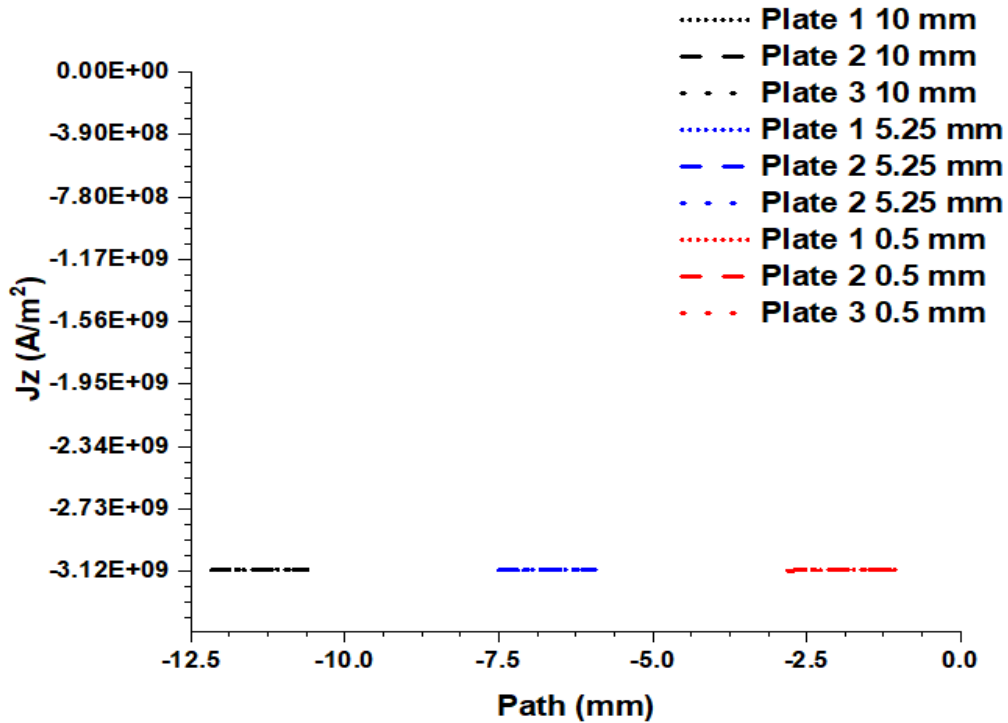


Figure 32. Current densities at the arc.

The Lorentz force resulting in each case are shown in Figure 33 as we can note, the Lorentz force resulting in the plate 1 is higher than the other two cases, particularly when we are closer to the plate, the effect of the grooves reduces the net force at the arc. The effect in the voltage when the arc is inserted to the arc chute is not considered in this simulation, but if we consider only the magnetic force in the arc, the plate one is the best candidate.

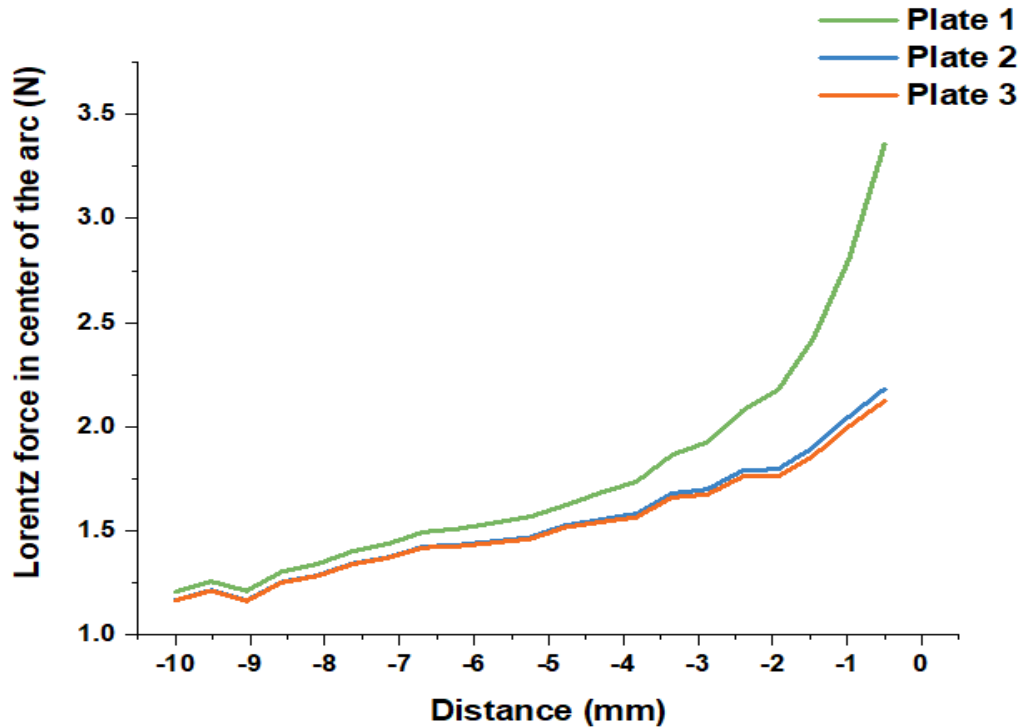


Figure 33. Lorentz force acting in the arc through a straight trajectory in Y direction from 10 mm of distance to 0.5 mm from the origin defined in figure 12 .

IV.II Plates material

The materials in the arc chutes construction is a very important aspect to consider, this because the magnetic properties of the plates play a very important role in the arc extinction process, as we mentioned before, the plates act in the arc attracting it to the chamber extinction. The conditions of the electric current applied are the same than the case explained before, the model geometry is not variated, only the material of the plate region is changed, all parameters and initial conditions were maintained without modifications.

The materials selected were steels with different levels of permeability, conductivity and magnetic saturation, the purpose of this is to determinate how the magnetic properties are related with the magnetic forces in the arc and try to determinate their relevance in the design of the plates. The steels are ferromagnetic materials with high levels of magnetic saturation and they are very common in the industrial world, the first candidate that we chose, shown in Table 7 is called AFK1 760, this is an alloy mainly composed by iron and cobalt, two ferromagnetic materials. This material is used in aerospace industry and electrical applications. The steel 1008 is a mild steel, it is cheaper and very common for structural applications, it does not have special treatments to increase their electrical and thermic properties. The third material listed is M800, is an electrical steel non- oriented, it is widely used to form the laminated cores of transformers, and the stator and rotor of electric motors. The fourth one is another electric steel laminated called China Steel 65CS800, it is specially

designed to avoid eddy currents in its interior layers. The last one is the original material used in the MCCB design described in chapter IV of this proposal thesis.

Three parameters are listed in Table 7 shown the properties of several materials that were considered in the case of study:

Material	μ_{r_i}	B_{sat}	σ	Price
		(T)	(Ωm)	(USD/ton)
AFK1 760	5898	2.4	2.00E-07	9800 – 15800 ^[39]
Steel 1008	1486.691	2.1	1.42E-07	480 – 700 ^[39]
M800	1299	2.097	2.30E-06	620 – 750 ^[39]
China Steel 65CS800	14111	2	2.90E-05	620 – 750 ^[39]
Steel 1010	2023	1.85	1.43E-07	450 – 750 ^[39]

Table 7. Properties of magnetic materials for new designs of plates.

The contours of the magnetic fields of the center of the plate appear in Figure 34, these contours belong to the case where the AFK1 760 is simulated, the black path was used to graph the magnetic field in all cases analyzed for each material. In the contour, we can see the zones where the magnetic flux density has its largest values. In this work are confirmed the results of other investigations [10], [30], the V-shaped arc and the combination of ferromagnetic materials, determine the effectiveness of the design of a plate, in this figure is appreciated the accumulation of the magnetic field in the V-zones, this clearly increase the magnetic force of the arc, provoking the accelerated redirection of the arc to the arc chute.

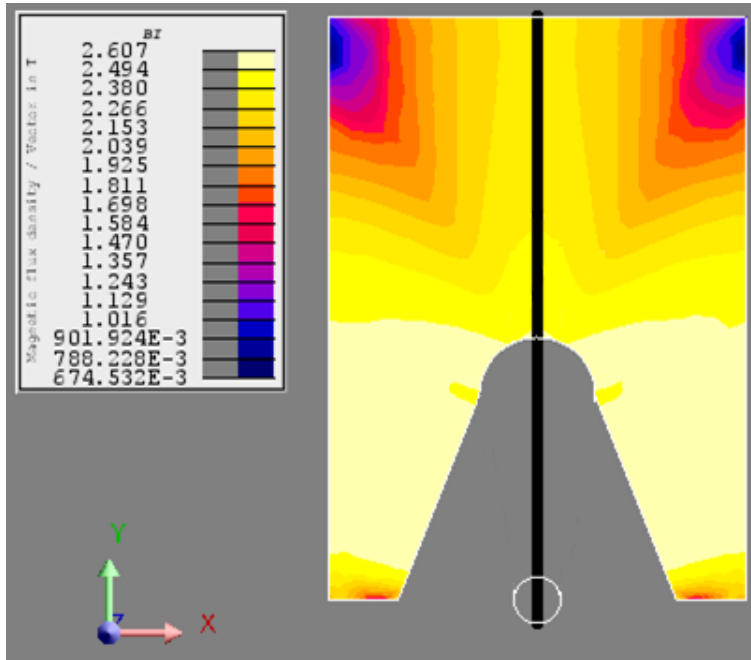


Figure 34. Contours of magnetic flux density at the plate made of AFK1.

In Figure 35 is shown the effect in the magnetic field of the arc and the plates for each material simulated.

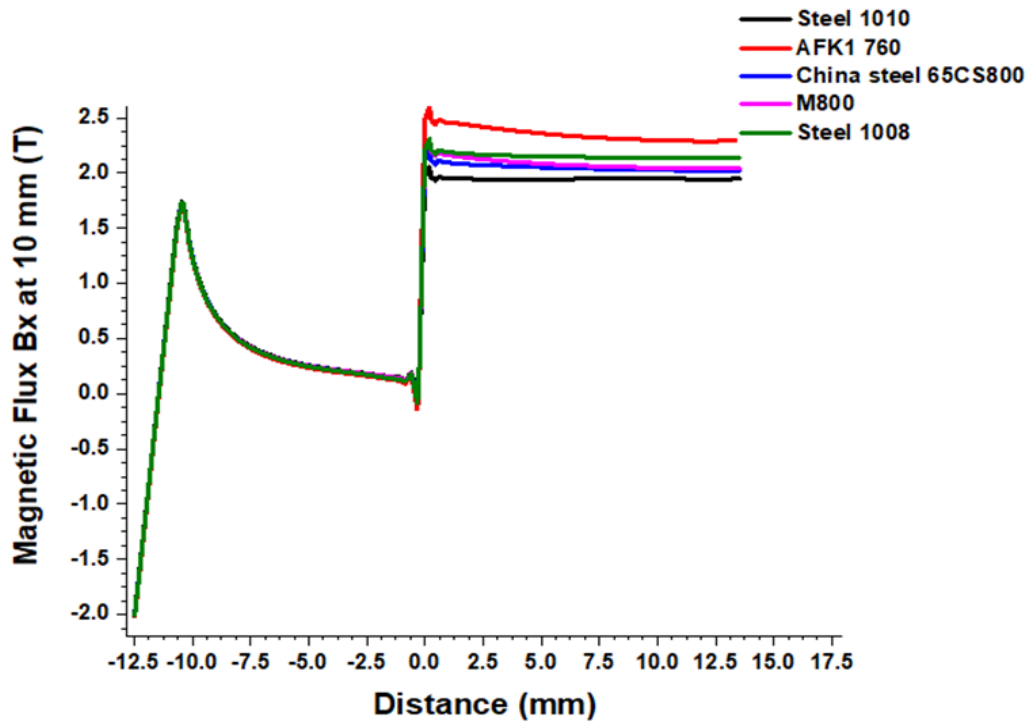


Figure 35. Magnetic fields of the arc varying the material of the plate.

At first glance, there is not a noticeable difference in the magnetic flux density at the arc, but it is notable that the levels of magnetic flux density in the plate formed by the material AFK1 760 are considerably larger than in the other materials. The magnetic saturation level of this material is much higher than mild and electric steels. To analyze the effects of the changes in the current density at the arc and plates is presented the Figure 36. In this case, a change in the current density at the arc is not appreciated, the current density at the arc is uniform, we can establish that the rise of the Lorentz forces is due to the magnetic flux, which is changing according to the trajectory of the arc. The current density is very high reaching values of $3.115 \times 10^9 \text{ A/m}^2$.

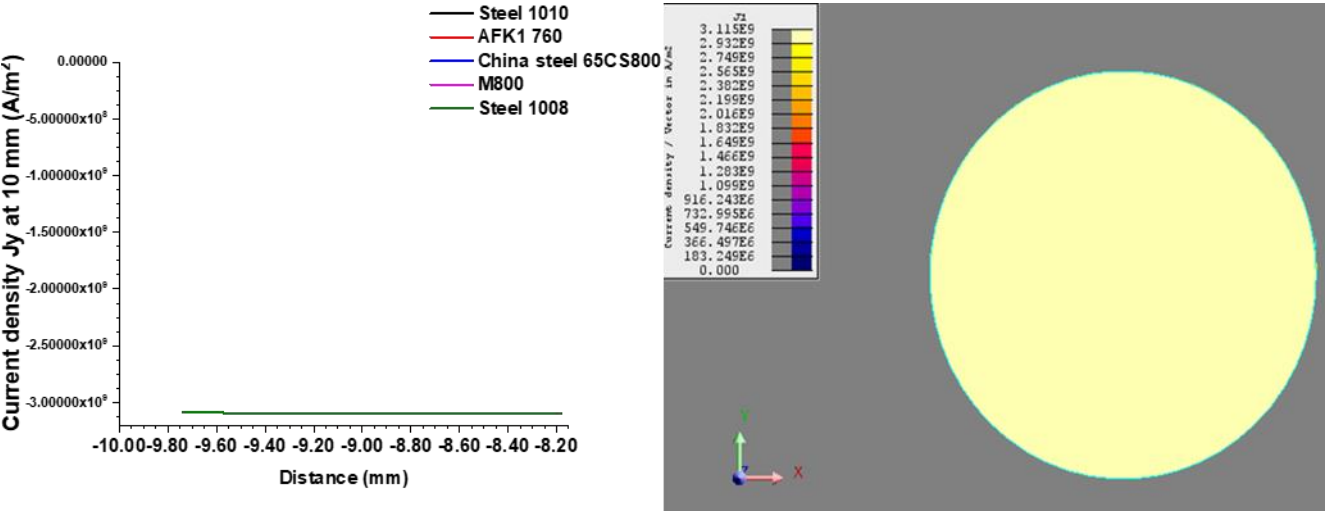


Figure 36. Current density at the arc varying the materials of the plate.

Another aspect to analyze is the presence of the eddy currents in the models, we can graph the vectors and the contours of the plates, they are shown in Figure 37. As it is expected, the eddy currents present current densities much lower than the values of the arc (~ 1000 times smaller). The eddy currents are larger in the surfaces and decrease their values in the middle zone. It is appreciable that the pointy edges present inferior values. This is explained by the circular behavior of the eddy currents. The values of these currents are graphed in Figure 38.

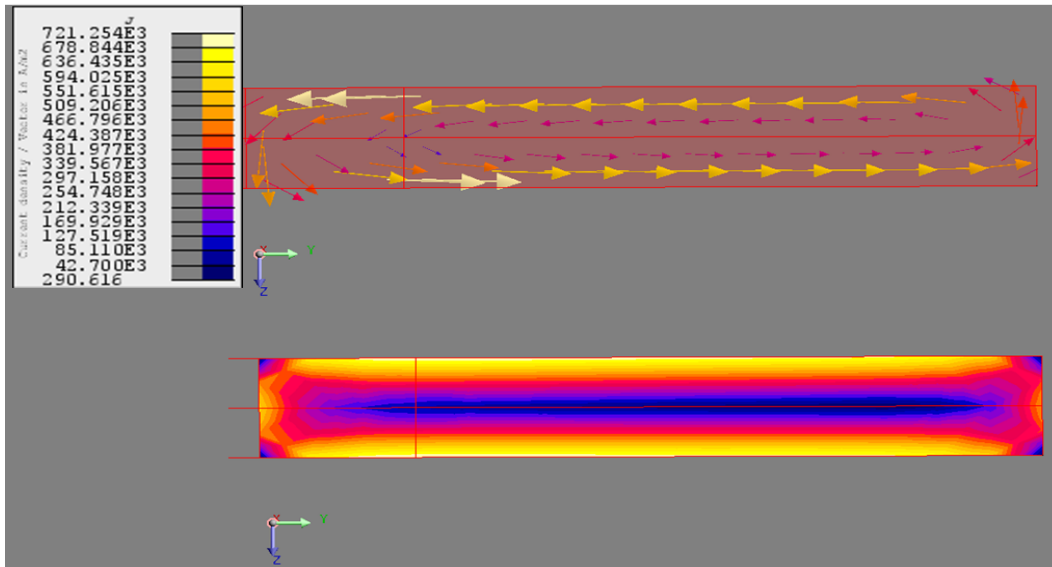


Figure 37. Vectors and contours of eddy currents in the plate.

The path through the currents densities are graphed is shown in Figure 38 (beside the graph), the path is located on the surface of the plate, where the eddy currents are larger.

The values of the electric steels are the smallest of the group, the mild steels are the greatest, this is logical because the resistivity of the electric steel is designed to be greater and minimize the effect of the eddy currents. The mild steels do not have this treatment because their application does not require this special design, for this reason, are cheaper [39].

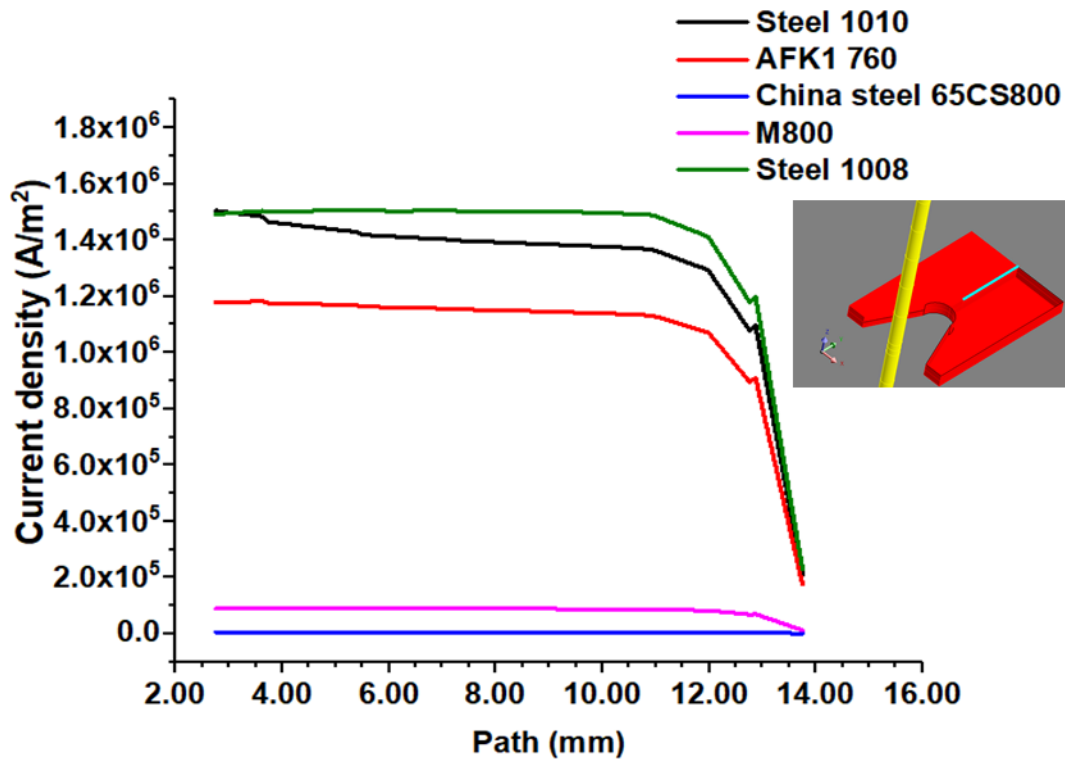


Figure 38. Eddy current density of the materials.

The Lorentz forces are calculated through the trajectory of Figure 30, it is supposed a movement of the arc without varying its cylindrical form, this is cylindrical form is a good approximation for ranges of distances superior to 0.5 mm between the arc and the plates as is seen in MHD model as described in, when the distance is shorter, the form of the arc changes to a U-shaped arc [3], [10], [38]. The AFK1 760 exhibits the greatest force of the group, this is explained by the high level of its high magnetic saturation, as we explicated before, the current density does not increase through the trajectory so the rise in the Lorentz force is due to the augment in the magnetic flux. The electric steel M800 and the mild steel 1008 curves are very similar, this could indicate that the magnetic properties of the materials are more relevant to grow the force than the electric properties of the materials because the electric properties of both materials are radically different but their magnetic properties are almost the same. The conductivity of the materials is not as relevant to the redirection of the arc to the chamber extinction as the magnetic saturation of the materials, at least at the first moments after the arc initiation. All candidates to substitute the material of the plates have superior levels of force than the original material Steel 1010 as is seen in Figure 39. The augment in the AFK1 760 plate is almost 30% higher than the original plate. The second increase in the Lorentz force most considerable is the Steel 1008, this mild steel showed an increment of 14.04%. The participation of eddy currents becomes relevant at the instant just before the arc touches the metal plates, because the existence of these allows a better insertion of the arc towards the plates, so it is important that the conductive properties in the surface.

are

high

enough.

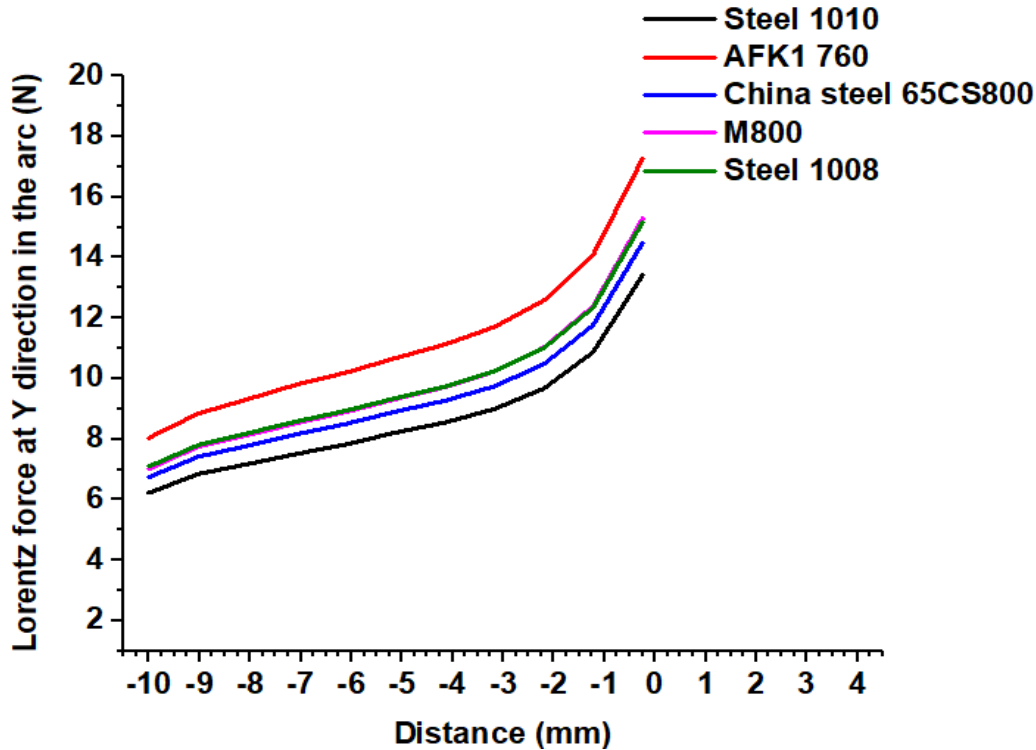


Figure 39. Y component of the Lorentz force of the arc varying with the distance.

IV.III Number of plates in the arc chute

The number of plates is an important aspect to consider in circuit breakers designs because they determine the voltage of the arc and how the number of plates changes the voltage is predicted by empirical equations that are demonstrated through experimental results, an experimental formula has been developed and is shown in several studies[10], [40]:

$$V_d = 2.3 \times 10^3 L_d + 24.5 N_p \quad (3.1) \text{ Arc voltage drop due to the plates}$$

Where:

L_D : Total length of the arc between plates

N_p : Number of plates on which new arc roots are originated

The voltage is not analyzed in this work, the main interest of this section of the chapter is to determine the effect of the number of plates in the Lorentz forces.

Seven cases were simulated, there were the analysis of the Lorentz forces in 1 to 7 plates, a tendency is appreciated in the force and it is shown in Figure 40, the force was calculated in two distance, the columns in black were taken when the arc was at 10 mm of distance, the columns in red correspond to the arc at 0.5 mm of the origin (appreciated in Figure 30). The most important values are when the arc is at 10 mm, this is a typical distance before the arc would be redirected to the chamber extinction, if the Lorentz force is big enough, the arc

would be redirected rapidly to the arc chutes and eventually, be extinguished. In the graph is noted an increase with a linear tendency, an equation similar to the proposed for the voltages is coupled to the Lorentz forces:

$$F_L = 10.05N_p - 2.245 \quad (3.2) \text{ Lorentz force at 10 mm of distance varying with the number of the plates}$$

Where:

F_L : Total force of the arc at 10 mm of the arc chute

N_p : Number of plates

To this equation, the R^2 associated takes a value of 0.9799. We have a similar behavior comparing with the calculation of the voltage varying the number of plates.

The behavior of the Lorentz force at 0.5 mm of distance is completely different, thus the saturation of the plates is reached, the magnetic field cannot augment considerably, so the Lorentz force cannot change either. As we mentioned before, when the arc is closer than 0.5 mm to the plate, has a very important deformation and cannot be approximated as a cylinder.

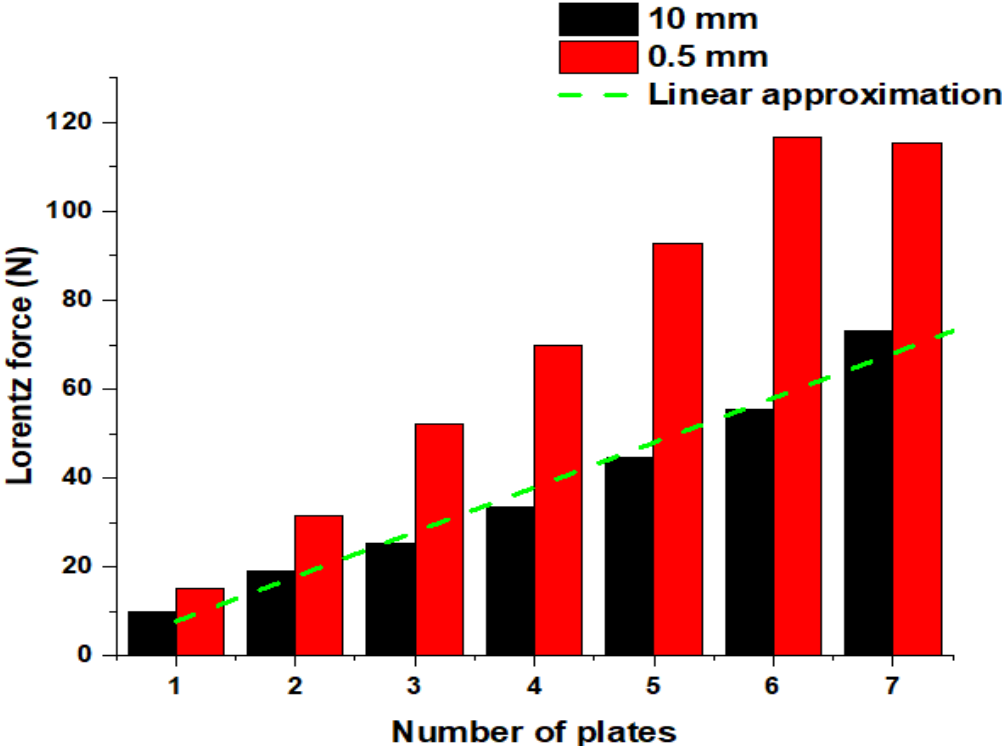


Figure 40. Lorentz force vs number of plates.

IV.IV Distance between plates

The effect of the distance of the plates has a proven effect in the voltage of the arc, this feature is calculated to rise properly the voltage, the distance determines two palpable effects: one is

on the temperature of the plasma and the second one is on the arc voltage; the temperature of the arc decreases when the arc goes through the plates, the plasma resistivity depends on the temperature, if the plasma is hotter the resistivity is lower, but if the plasma is cooled, then the resistivity increases, thus the voltage grows and cannot allow the arc persistence.[1], [3], [6]–[8], [10], [13]. The effect of the distance between plates is not as studied as the effect of voltage, a brief analysis of these magnetic forces at the arc is made in this section of the chapter. The length of the arc is supposed in 35 mm, the number of plates is fixed in five elements, the distances were variated to 1.5 to 3.5 mm with steps of 0.5 mm. The magnetic force at the plates was calculated and is shown in Figure 41. Letter A corresponds to the most external plate at the top of the arc chute. B plate is the second one in descending order. The C plate is corresponded to the center of the arc chute. D and E plates are oppositely symmetrical to the A and B plates but they are located at the bottom of the arc chute.

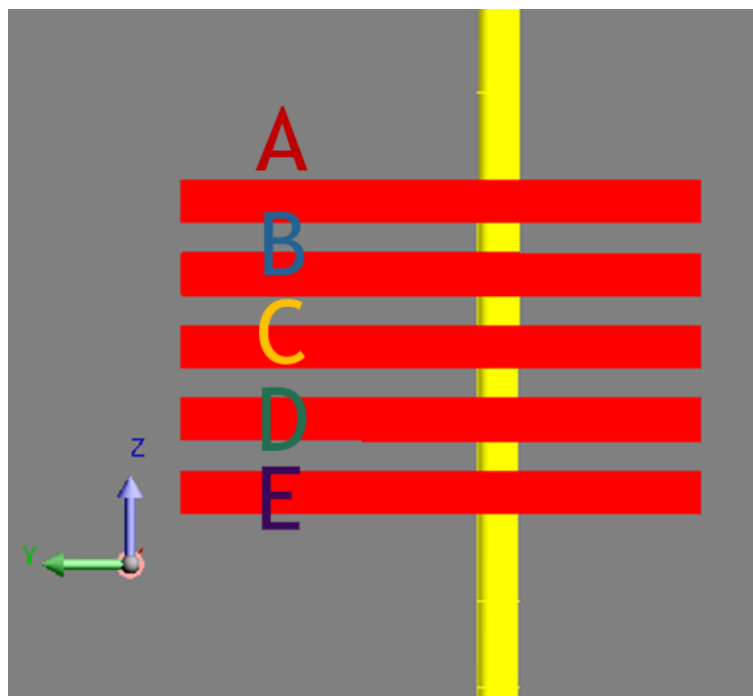


Figure 41. Model proposed to analyze the distance between plates.

The variation of the Lorentz forces with the distance between plates is shown in Figure 42. The minimum and maximum values are displayed on the graph. A tendency is appreciated in this figure, a directly proportional increase between the force and the distance of the plates is perceived. The augment of the forces seems not to be large, this increment on the force is close to 2.86% at the moment when the arc is closer to the plate (line green), this poor increment is explained again by the magnetic saturation, the magnetic field cannot increase consequently the Lorentz force cannot augment either. The line in blue describes when the arc is situated at 10 mm and the distance between plates is variated, the increase is superior but the force is less than a half of the force when the arc is situated to 0.5 mm to the plate . The distance between plates, under this analysis, could not have an important contribution to the Lorentz forces.

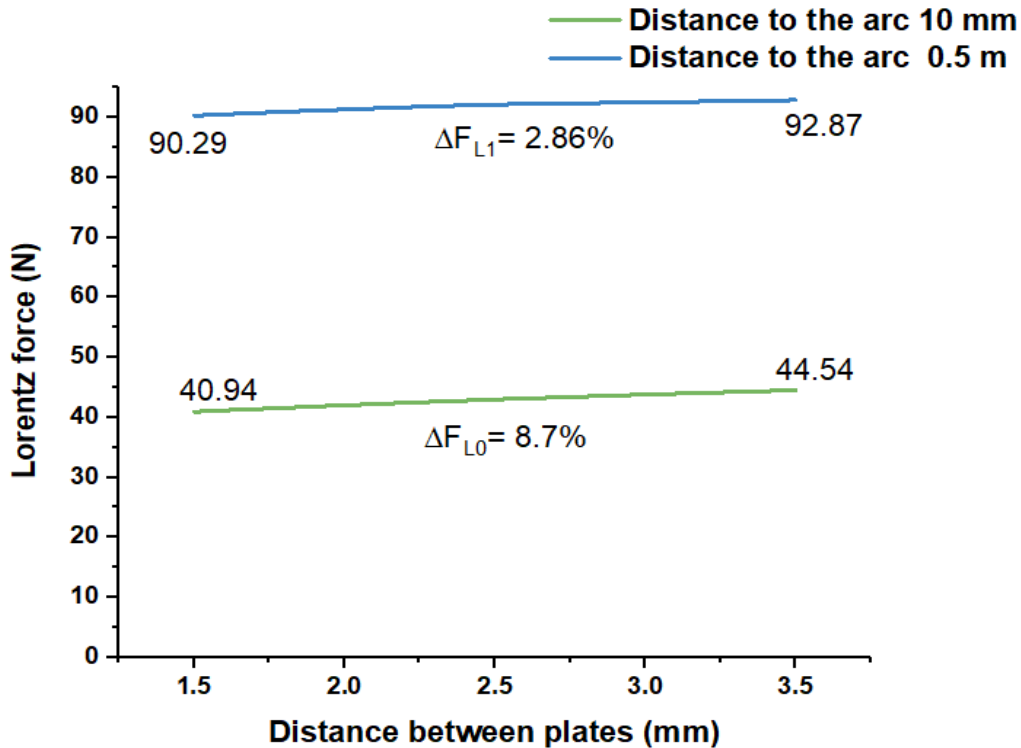


Figure 42. Lorentz forces vs distance between plates.

The magnetic flux densities of each plate were calculated in a similar route that showed in Figure 30. The paths were the same but varying the height according to coincide with the plates. Different magnetic flux densities were obtained and they are shown in Figure 43, the tendency observed indicate us that the magnetic field is lower at the plate located in the center of the arrangement, and the field is higher in the plates at the extremes of the arc chute (plate A and plate E, the behavior is symmetrical as is expected. The plates B and D presents a similar behavior too, the force is superior to the central plate but lower than the outer plates

The effect of the magnetic fields generated by the eddy currents subtract energy to the magnetic field and this is shown in Figure 43, where is appreciated a dropping effect in the magnetic flux density at the center plates. This effect has been studied by other authors under another perspective, the eddy currents facilitate the formation of new arc roots on the plate [34], [35], [40], but at the first moments before the arc reach the arc chute, they diminish the Lorentz forces, this because the resulting magnetic field of the eddy currents is opposite to the magnetic field of the arc, as establish the Lenz law.

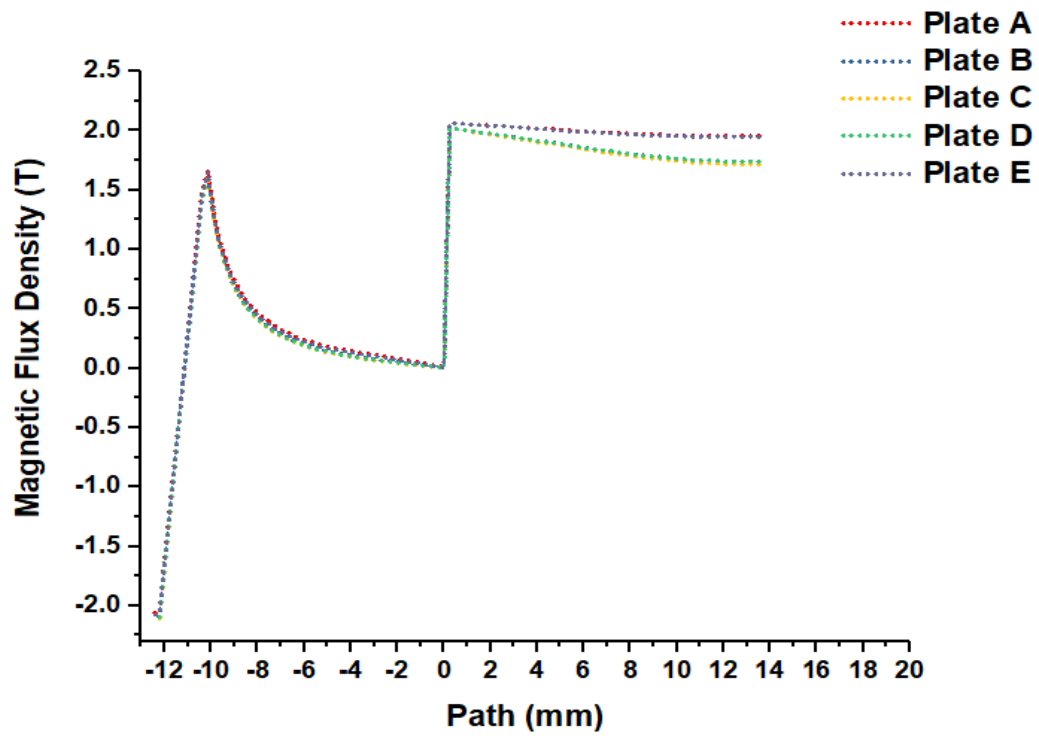


Figure 43. Magnetic fields of an arc chute of five plates.

CHAPTER VI: Conclusions

In the first section of this work, the problem to be studied was determined and identified. A brief description of the project was given. Clear objectives were determined, focusing the work in two main sections: the study of the MCCB and the study of the configurations of the Arc Chutes.

In the second section of this work, the conditions in which plasma can be simulated were outlined, since this is a fluid with implications that go beyond traditional physics and require knowledge of relativistic statistical and mechanical physics for a deep analysis, In this paper the simplifications made by the MHD model are taken into account and it is further simplified trying to reduce the problem to its electromagnetic part, aware of the fact that the experiments yield partial results.

In the third chapter of this work, the limitations of the software used to carry out this thesis are taken into account. Altair Flux is a software with great capabilities for the simulation of electromagnetic phenomena designed for solids and non-fluids, so the approximations made in this work are validated only in specific conditions prior to the moment of the complete extinction of the arc. Maxwell's equations are solved by the use of finite element methods, a very powerful numerical technique developed in recent years, this electromagnetic analysis is not complete because of the thermal variables are neglected but offers a quick view of the arc extinction phenomenon. The computational resources utilized in this type of analysis are considerably lower, the resolution time is much shorter than used to solve MHD with VFM.

In chapter four, the characteristics of the circuit breaker to be analyzed are summarized. Materials are specified and the main components of the MCCB extinction module are modeled. The values of magnetic flux density, current densities and Lorentz forces are also obtained. The contributions of each component to the increase of the magnetic force in the electric arc are also specified. It is concluded in this chapter that each component serves to redirect the arc towards the extinction chamber, the absence of one or more components radically affects the magnitude and direction of the force that causes the arc to be carried to the arc chutes.

Knowing the importance of arc chutes is proposed the fifth chapter of this thesis, an analysis is made on the shape of the plate and how it contributes to the increase or decrease of Lorentz forces, this section determines that the optimal way to increase Lorentz forces when the arc is 10 mm away (typical distance in an MCCB array) has a v-shaped plate without extended slots in the center. Also in this chapter, the importance of the materials in the elaboration of the plates that conform the arc chute is studied in depth, five materials with remarkable magnetic properties were proposed and the best candidate was chosen, being the AFK1 760. In addition it was determined that a factor of importance to determine the force that causes the movement in the arc is the magnetic saturation of the material. The AFK1 760 reaches a very high saturation point, located at 2.4 T. This material although increases the strength of

Lorentz almost 30%. Because this material is very expensive it is concluded that the most viable material to replace the steel 1010 is steel 1008, a material that is very similar in structural properties and is commonly used in the construction of support structures and although its structural properties are similar to those of steel 1010. The magnetic properties are superior, since unlike steel 1010 which has a magnetic saturation level of 1.85 -1.9 T, steel 1008 reaches a saturation level of 2.1 T.

The number of plates in the arc chute array is also analyzed and it was determined that there is an approximately linear correlation between the number of plates and the force felt by the arc at 10 mm separation distance with an applied short-circuit current of 5 kA. The saturation effect of the material is also perceived, since at distances of 0.5 mm the increase in force is much smaller and the linear tendency is broken. This brief analysis can give us a simple way to calculate the magnetic force in the arc in an approximate way in similar circumstances, and for this study we also determined the minimum distance in which the arc can be modeled as a cylinder, based on MHD works and models, which tend to do better approximations than purely electromagnetic analyzes. Finally, when analyzing how the distance between plates alters the Lorentz forces in the arc, it was determined that the distance between them does not produce very large changes in force, but it could be detected how eddy currents reduce the magnetic field in the arc producing a deceleration in its journey towards the arc chutes.

CHAPTER VII: Future work

As future work, it is proposed to make the combination of the two chapters, modifying geometries and materials in the MCCB model, analyzing similarly to how it was done with the arc chute other elements of the extinction module, such as shields, checks or the arc runners.

The analyzes carried out in chapter four can be improved considering design angles and other specifications that were simplified in these geometries.

Analyze how similar the MHD simulations and the FEM simulations are, since although the MHD simulations present more real results they also have a very considerable computational cost and in some cases the approaches using FEM could be sufficient, so comparing both could give us an idea of how accurate the FEM can be.

The maximum test to the models proposed in this thesis would be the implementation of experimental tests for the contrast of results, for this it is necessary that the simulations are reconditioned to the experiment, adjusting materials, forms and appropriate distances. A great contribution to this work would be the performance of experimental tests that could validate the results obtained through simulation.

Appendix A:

Features of Altair Flux[®] at simulations

The first step to develop a simulation in the software is to import a geometry in the *Modeler context* section of Altair Flux[®], the models of the qualitative study of the MCCB were created in a solid modeling computer-aided design (CAD) software. The other cases were built using the geometry section of Flux.

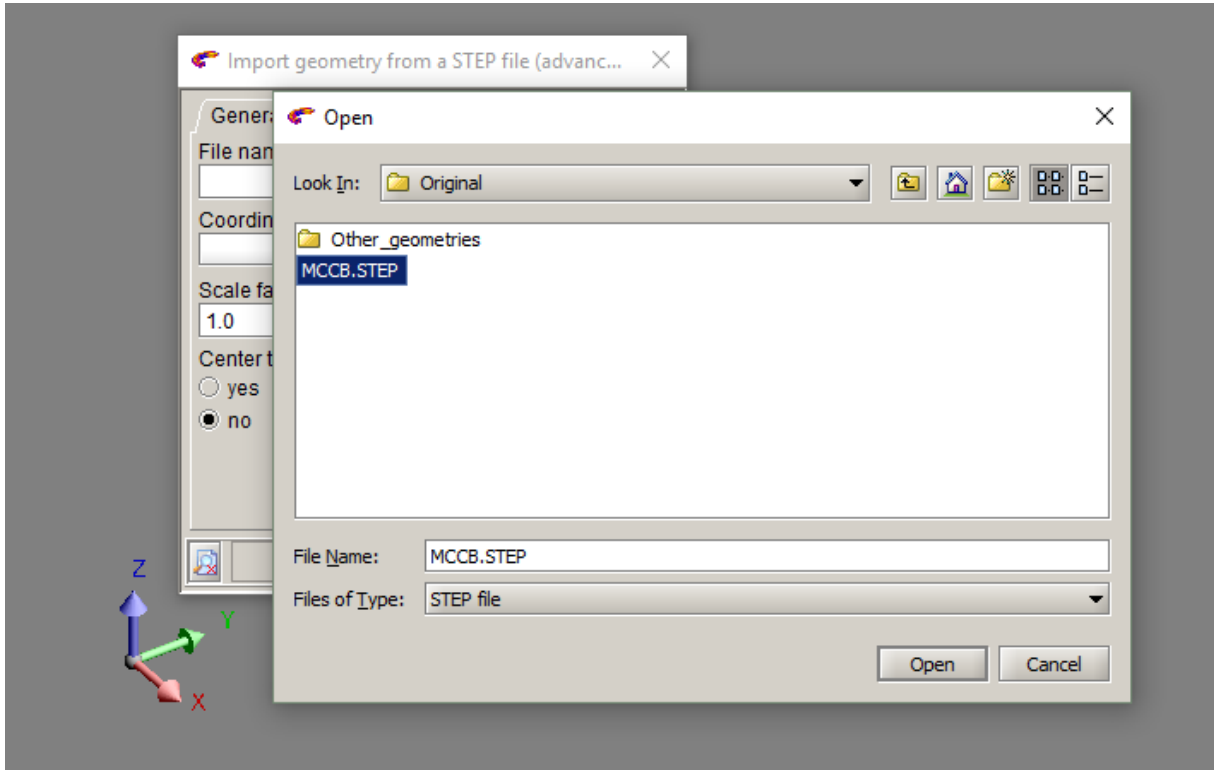


Figure A- 1. Import geometry from modeler context in Altair Flux[®]

The next step was to create the air that surround the MCCB, we made a box using points which are at 1557.5 mm of the imported geometry. Follow this, the geometry is verified, using the *Check geometry* tool.

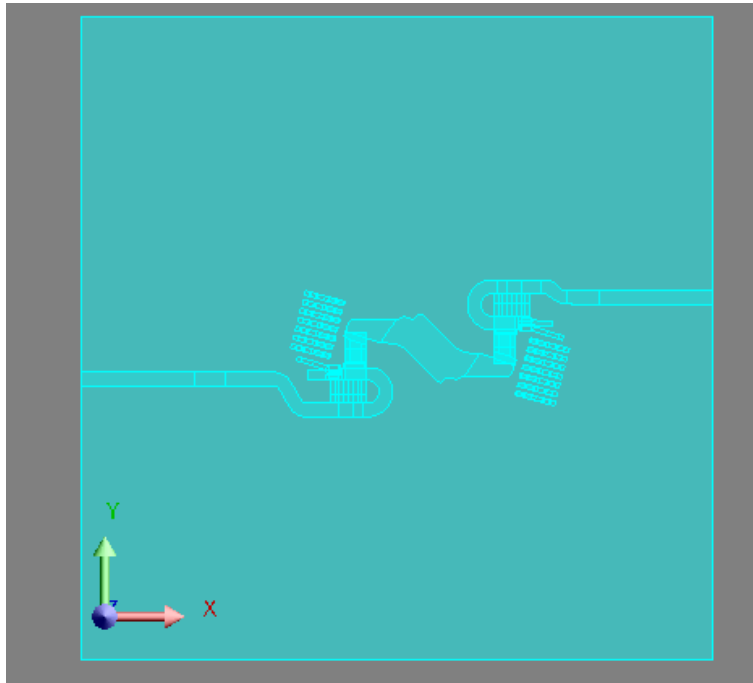


Figure A- 2. Geometry imported from the model with air surrounded the MCCB

The next step is to create the mesh of the model, to do this *mesh points* are created with the tool of mesh in the *Mesh context*. The data of the mesh point is listed in the next table.

Mesh point name	Size of the element on the mesh (mm)
MP0P6	0.6
MP1P9	1.9
MP7	7
MP50	50

The mesh is created through the mesh generator as we can see in the figure

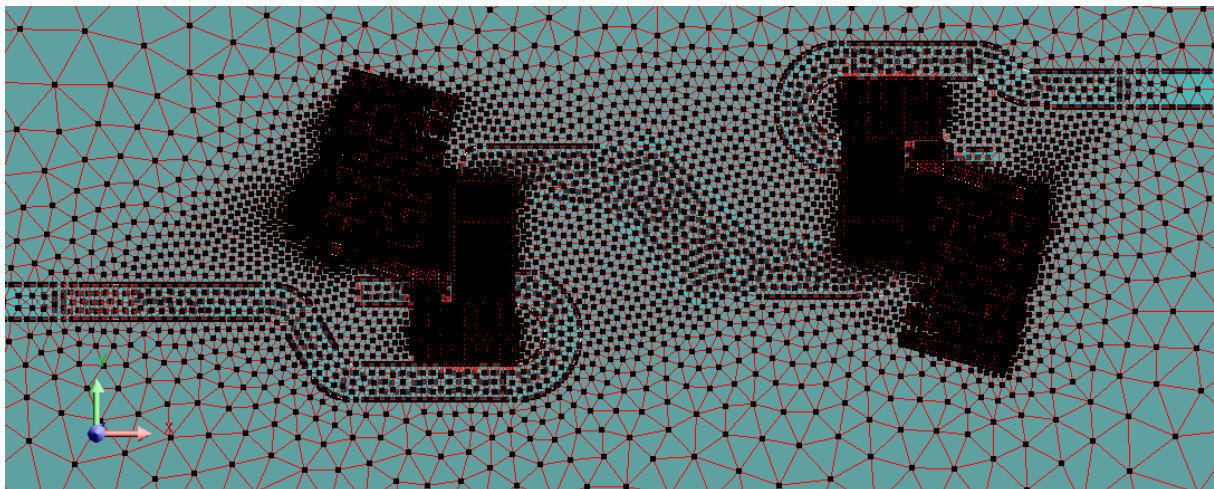


Figure A- 3. Mesh of model of the MCCB extinction module.

Mesh data:

Volume elements:

- Number of elements not evaluated: 0 %
- Number of excellent quality elements: 59.88 %
- Number of good quality elements: 30.25 %
- Number of average quality elements: 7.77 %
- Number of poor quality elements : 2.1 %
- Number of nodes: 262169
- Number of line elements: 10179
- Number of surface elements: 145983
- Number of volume elements: 995851

Mesh order: 1st order.

Once we made the meshing process, the physical context needs to be configured. We select the application that will help us to solve correctly the problem studied, in this case the application selected was *Transient Magnetic 3D* because we are modeling a solid conductor, our study is clearly an static phenomenon but in Flux this application is properly if we modify some features, a special configuration is made to our model because we are injecting a DC current of 35 kA, to avoid the effect of the eddy currents a special macro is activated, so we need to choose the configuration that appear in Figure A- 4.

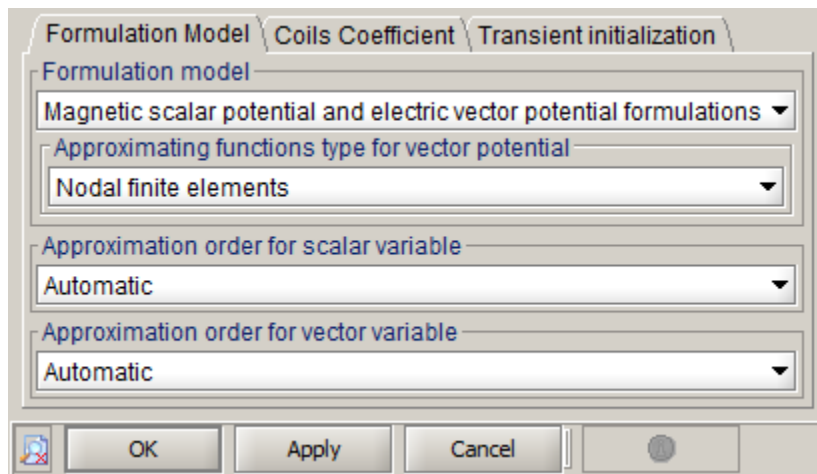


Figure A- 4. Configuration of the formulation model in Transient Magnetic 3D application.

The first step in the *Physics* mode is to create the equivalent circuit in the *circuit dedicated context*.

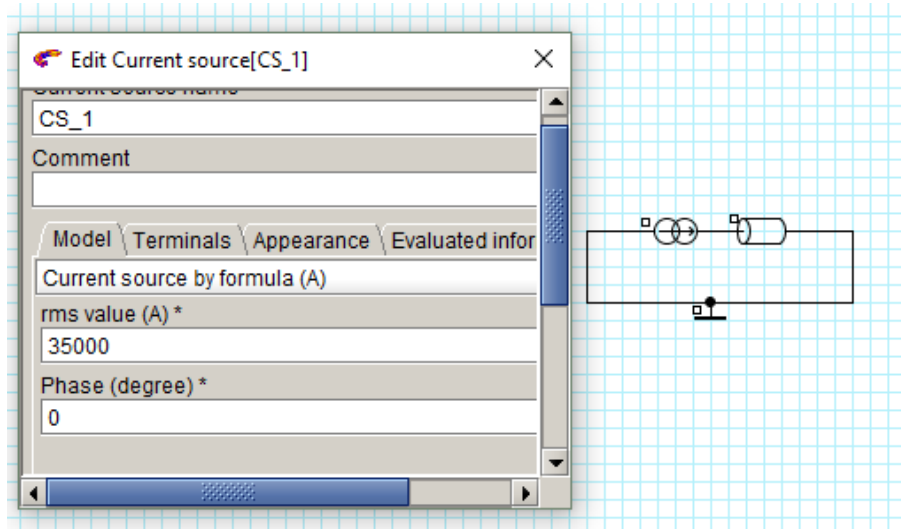


Figure A- 5. Current applied to the model in the circuit dedicated context.

The materials database will give us the properties of the materials used in the construction of the MCCB. The database of Flux is opened by selection the materials option and clicking the option *import from material manager*. This is shown in figure

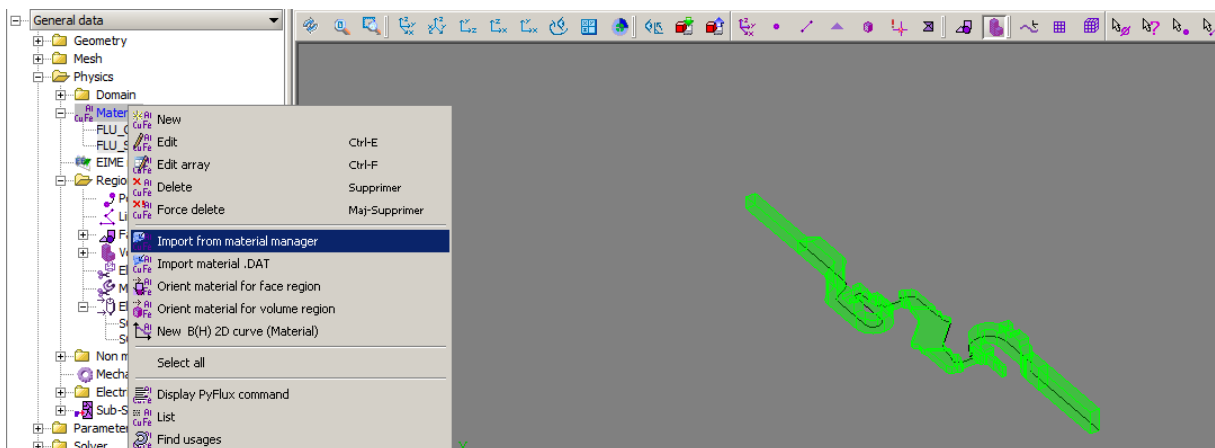


Figure A- 6. Importing material from material manager.

The materials are located in the box of the left, the materials assigned were copper and steel 1010, so we drag these elements to the right side in the *Flux projects* section, as we can see in Figure A- 7.

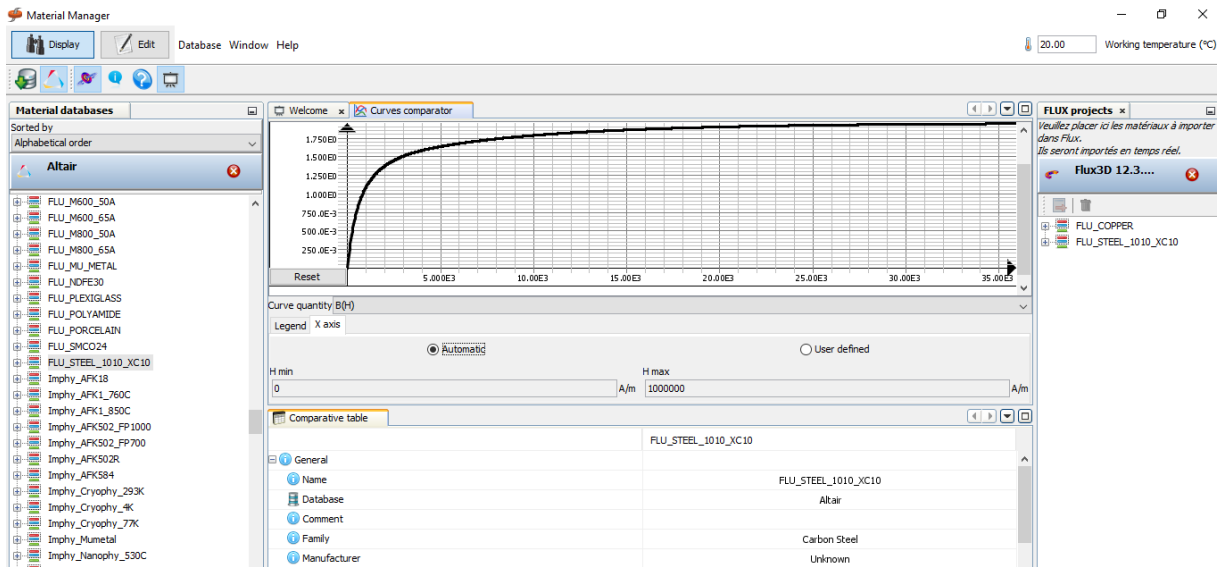


Figure A- 7. Material manager from Altair Flux®.

The following step after this assignation, is to create the *volume regions*, in this option are designed the properties of the materials for each volume of the geometry. In our case, we create a region for each component. The material selected were copper and steel 1010, the copper zones appear in green and the steel components appear in red in Figure A- 8.

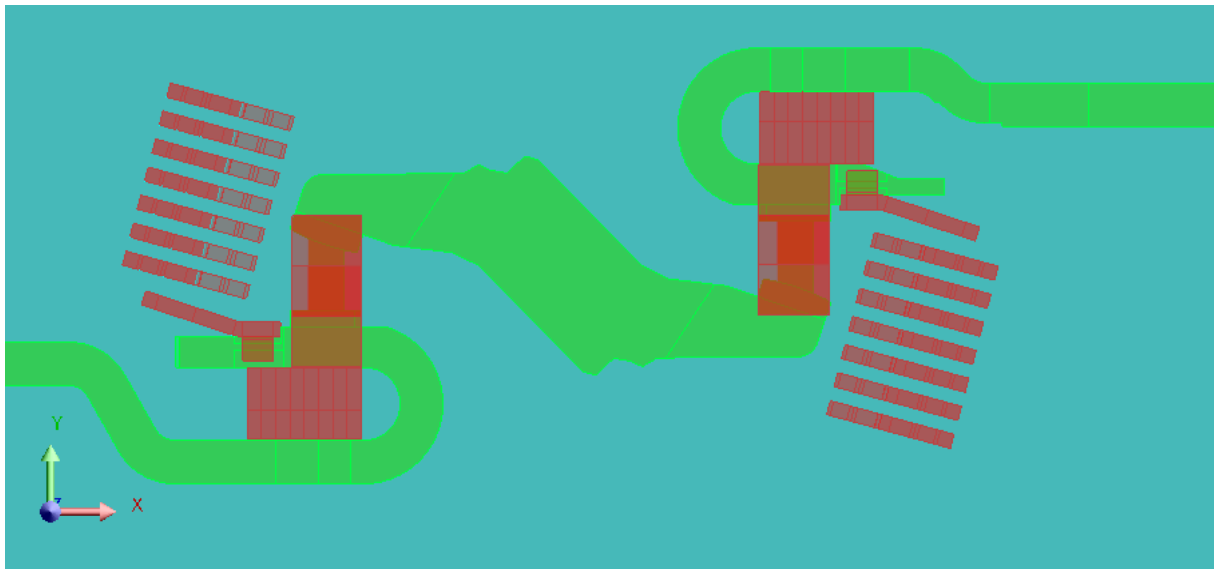


Figure A- 8 Volume regions of the MCCB extinction module.

After the assignation of each volume, the next step is to assign the terminals to solid conductors. A face of the geometry is chosen to define the input current and other is assigned to establish the face where the current will get out.

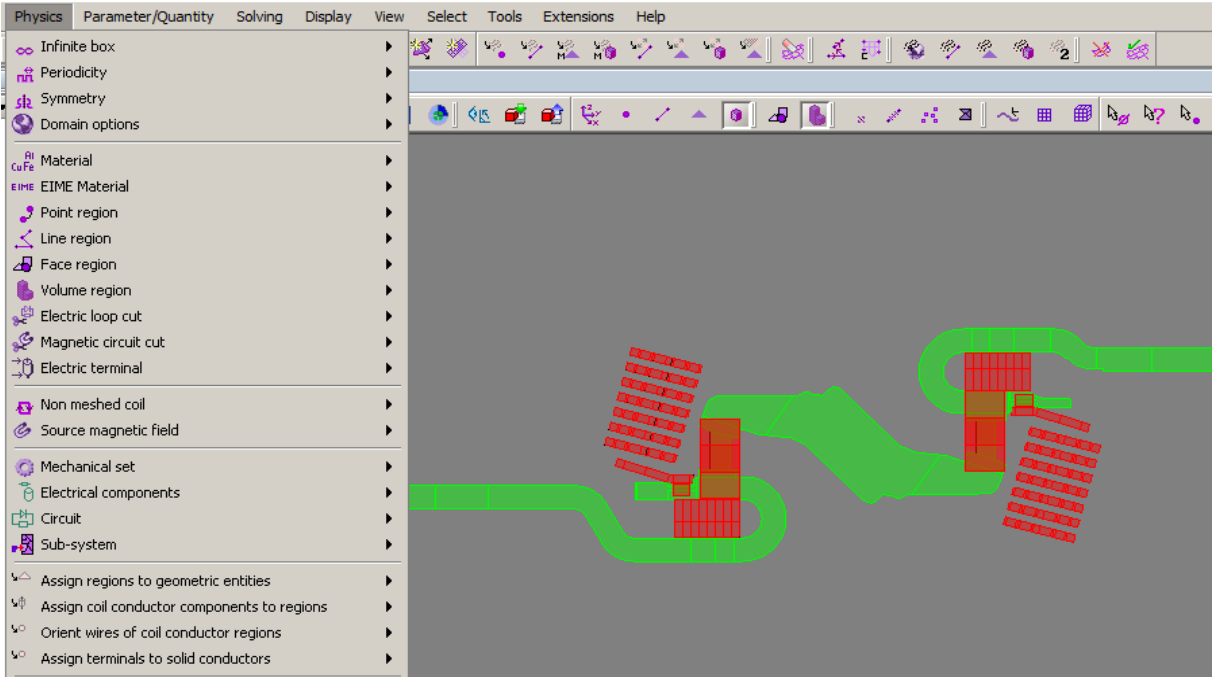


Figure A- 9. Assignment terminals to solid conductors.

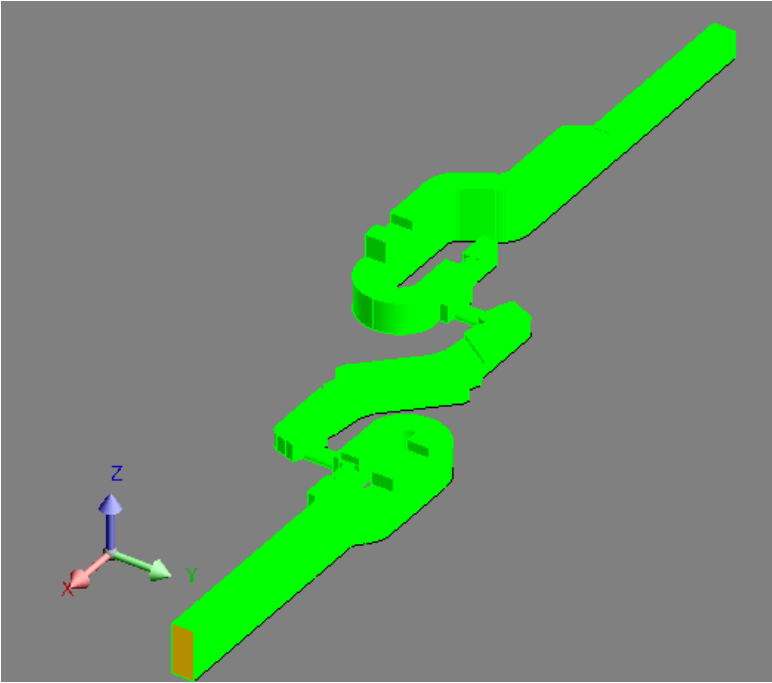


Figure A- 10. Face assigned to the input current.

The last step in the physics context is to add and activate the macros needed to avoid the effect of the eddy currents in the DC model. We can make this going to Extensions click in Loads and selecting the Macros_Flux3D_Physics/SolidConductorNoEddyCurrent/SolidConductorNoEddyCurrentCreate.PFM. We made this steps for all the macros saved in the folder “SolidConductorNoEddyCurrent”. Finally, we click on the first icon: and select the volume regions that are solid conductors, in our case, we select all excluding the air region. The last step before running the simulation is to create a scenario. We made this in the Scenario section and select New scenario, as we are modeling a static phenomenon we give only one step to one second as we can see in Figure A- 11.

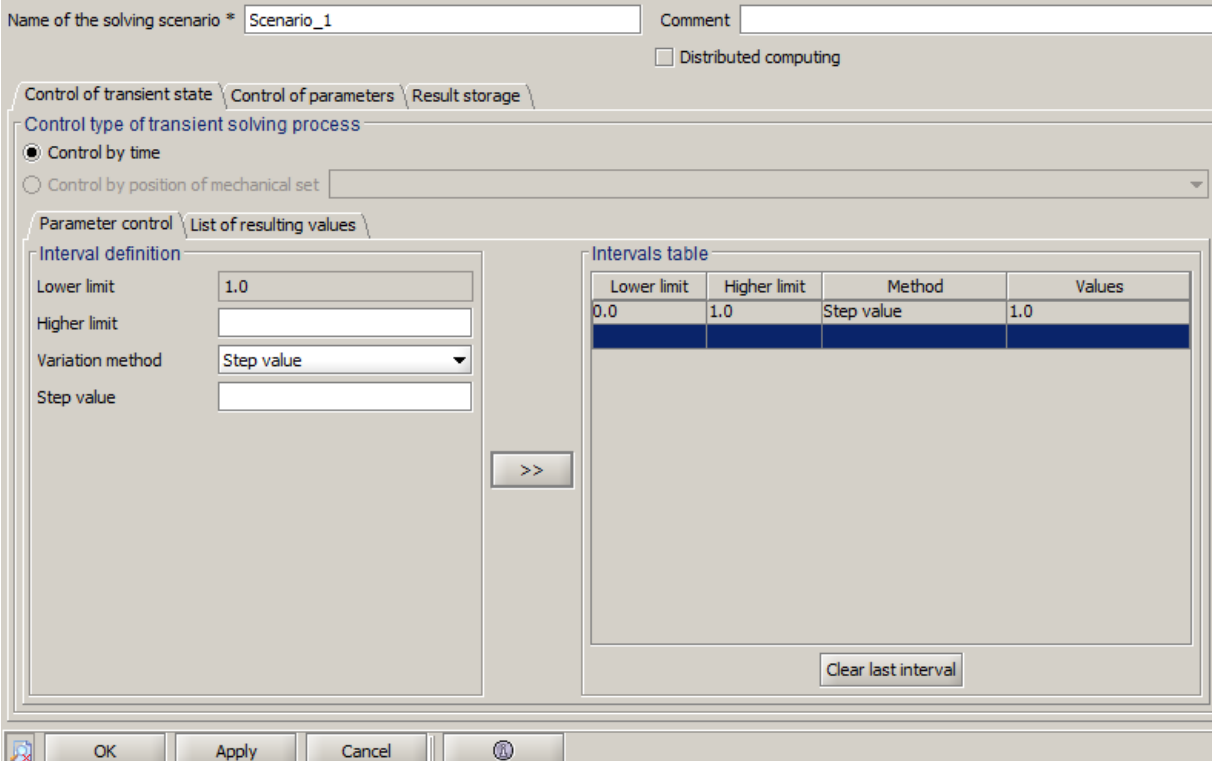


Figure A- 11. Scenario to solve the MCCB extinction module model.

We can verify if the model is ready to solve, and then click to solve button. The post-processing analysis depends on our objectives and what want to analyze. In our case, we are graphing the magnetic flux density and the current density vectors. In the Postprocessing section, we can create Spatial groups, Cut planes and Grids to study and visualize the effect of these parameters in the model. To analyze the data in more detail, we can create Paths and Sensors. We can calculate several predefined quantities as “Losses by Joule’s effect” or magnetic forces and magnetic energies. Other quantities can be calculated by integrals in lines, surfaces or volumes.

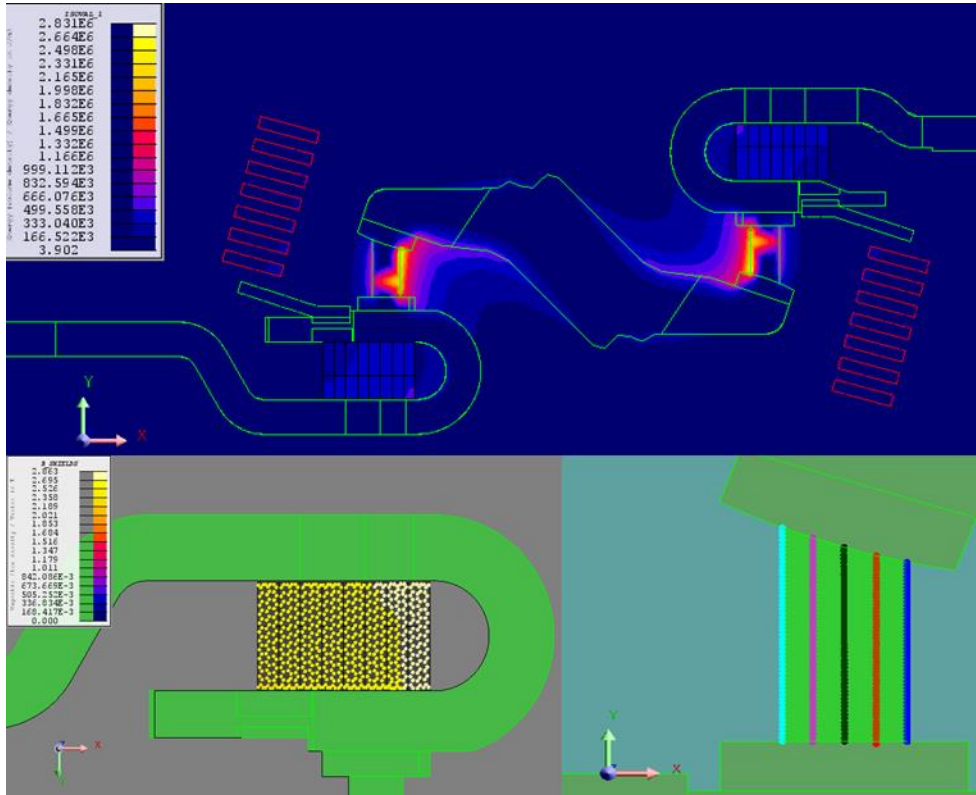


Figure A- 12. Post-processing analysis in Altair Flux. (Isovalues, arrows vectors and paths).

Appendix B:

Mesh data of the models

Analysis of the MCCB module extinction

Cases I – IX

Mesh data:

- Number of elements not evaluated: 0 %
- Number of excellent quality elements: 59.88 %
- Number of good quality elements: 30.25 %
- Number of average quality elements: 7.77 %
- Number of poor quality elements : 2.1 %
- Number of nodes: 262169
- Number of line elements: 10179
- Number of surface elements: 145983
- Number of volume elements: 995851

Mesh order: 1st order.

Analysis of the arc chutes:

Shape analysis

Mesh data:

- Number of elements not evaluated: 14.47%
- Number of excellent quality elements: 44.56 %
- Number of good quality elements: 34.31 %
- Number of average quality elements: 6.27 %
- Number of poor quality elements: 0.39 %
- Number of nodes: 294749
- Number of line elements: 1853
- Number of surface elements: 31062
- Number of volume elements: 187798

Mesh order: 2nd order

Material analysis

- Number of elements not evaluated : 14.47 %
- Number of excellent quality elements : 44.56 %
- Number of good quality elements : 34.31 %
- Number of average quality elements : 6.27 %

- Number of poor quality elements : 0.39 %
- Number of nodes : 294749
- Number of line elements : 1853
- Number of surface elements : 31062
- Number of volume elements : 187798

Mesh order : 2nd order

Number of plates analysis

7 plates

Mesh data:

- Number of elements not evaluated : 0 %
- Number of excellent quality elements : 47.69 %
- Number of good quality elements : 41.27 %
- Number of average quality elements : 10.06 %
- Number of poor quality elements : 0.98 %
- Number of nodes : 463346
- Number of line elements : 5006
- Number of surface elements : 58335
- Number of volume elements : 336483

Mesh order : 2nd order

6 plates

- Number of elements not evaluated : 0 %
- Number of excellent quality elements : 53.92 %
- Number of good quality elements : 39.13 %
- Number of average quality elements : 6.63 %
- Number of poor quality elements : 0.33 %

- Number of nodes : 190464
- Number of line elements : 3362
- Number of surface elements : 28216
- Number of volume elements : 136431

Mesh order : 2nd order

5 – 3 – 2 plates

- Number of elements not evaluated : 0 %

- Number of excellent quality elements : 47.35 %
- Number of good quality elements : 41.72 %
- Number of average quality elements : 10.18 %
- Number of poor quality elements : 0.75 %
- Number of nodes : 366654
- Number of line elements : 3786
- Number of surface elements : 46107
- Number of volume elements : 265536

Mesh order : 2nd order

Distance between plate analysis

- Number of elements not evaluated : 0 %
- Number of excellent quality elements : 47.35 %
- Number of good quality elements : 41.72 %
- Number of average quality elements : 10.18 %
- Number of poor quality elements : 0.75 %
- Number of nodes : 366654
- Number of line elements : 3786
- Number of surface elements : 46107
- Number of volume elements : 265536

Mesh order : 2nd order

Appendix C: Features of the MCCB analyzed

Table 2: Interrupting Rating

	UL® / CSA® / NOM®					IEC 647-2 Icu/lcs					
	240 Vac	480 Vac	600 Vac	250 Vdc ¹	500 Vdc ²	220/240 Vac	380/440/415 Vac	500/525 Vac	690 Vac	250 Vdc ¹	500 Vdc ³
D	25 kA	18 kA	14 kA	20 kA	—	25/25 kA	18/18 kA	14/14 kA	—	20 kA	20 kA
G	65 kA	35 kA	18 kA	20 kA	20 kA	65/65 kA	35/35 kA	18/18 kA	—	20 kA	20 kA
J	100 kA	65 kA	25 kA	20 kA	—	100/100 kA	65/65 kA	25/25 kA	—	20 kA	20 kA
L	125 kA	100 kA	50 kA	20 kA	50 kA	125/125 kA	100/100 kA	50/50 kA	—	20 kA	20 kA
R	200 kA	200 kA	100 kA	—	—	150 kA	125 kA	75 kA	20 kA	—	—

¹ 250 Vdc ratings only available with PowerPact H or J circuit breakers with thermal-magnetic trip units (not including MCP).

² UL 500 Vdc ratings only available with PowerPact H-, J-, and L-frame circuit breakers with thermal-magnetic trip units (not including MCP).

³ IEC 500 Vdc rating only available on PowerPact J-frame circuit breakers.

Table-C 1. Interrupting Rating of the Schneider Electric MCCBs [36].

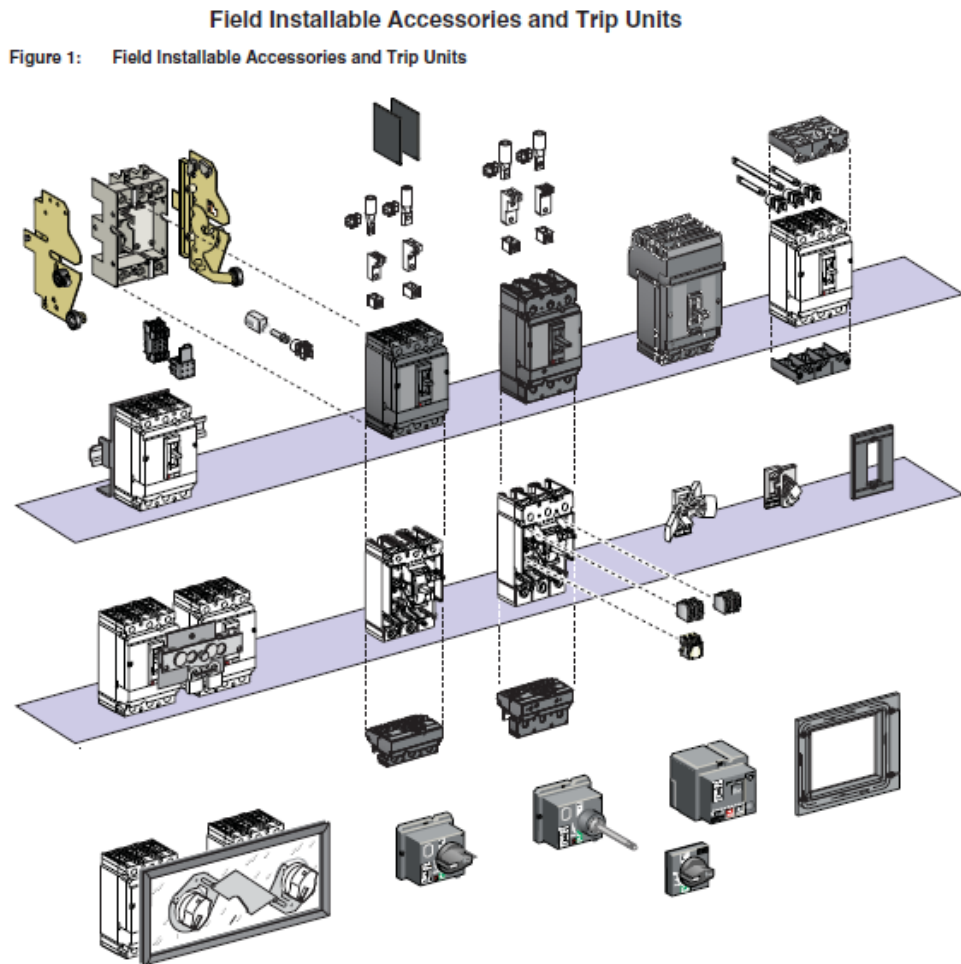


Figure-C 1.L-frame assembly [36].

Table 8: Codes and Standards (Domestic)

PowerPact H-, J-, and L-Frame Circuit Breakers	H-, J-, and L-Frame Switches	PowerPact H-, J-, and L-Frame Motor Circuit Protectors
UL 489 ¹ IEC 60947-2 CSA C22.2 No. 5 ² Federal Specification W-C-375B/GEN NEMA AB1 NMX J-266 CCC CE Marking	UL 489 ³ IEC 60947-3 CSA C22.2 No. 5 ⁴ Federal Specification W-C-375B/GEN NEMA AB1 NMX J-266 CE Marking	UL 508 IEC 60947-2 CSA C22.2 No. 14 NEMA AB1 CCC CE Marking

¹ PowerPact H- and J-frame circuit breakers are in UL File E10027. PowerPact L-frame circuit breakers are in UL File E63335.

² PowerPact H- and J-frame circuit breakers are in CSA File LR40970. PowerPact L-frame circuit breakers are in CSA File 69561.

³ PowerPact H- and J-frame switches are in UL File E87159.

⁴ PowerPact H- and J-frame switches are in CSA File LR32390.

Table-C 2.Code and Standards accomplished by Circuit Breakers of Schneider Electric [36].

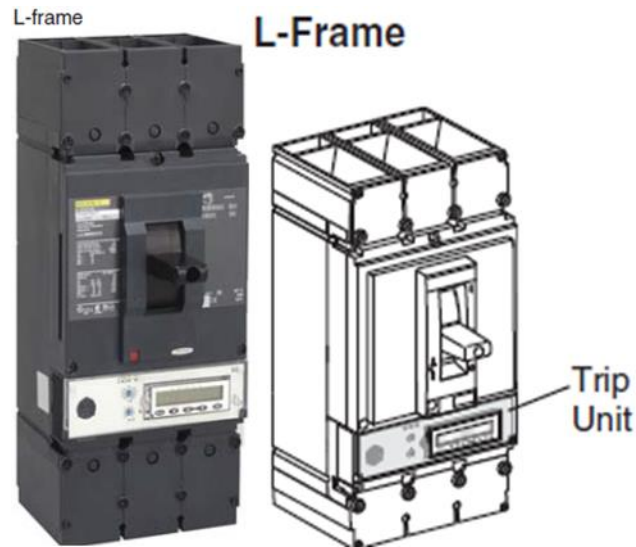


Figure-C 2. L-frame model with the trip unit annexed[36].

Figure 85: L-Frame 300–450 A (LG and LL) 500 Vdc Thermal-Magnetic Trip

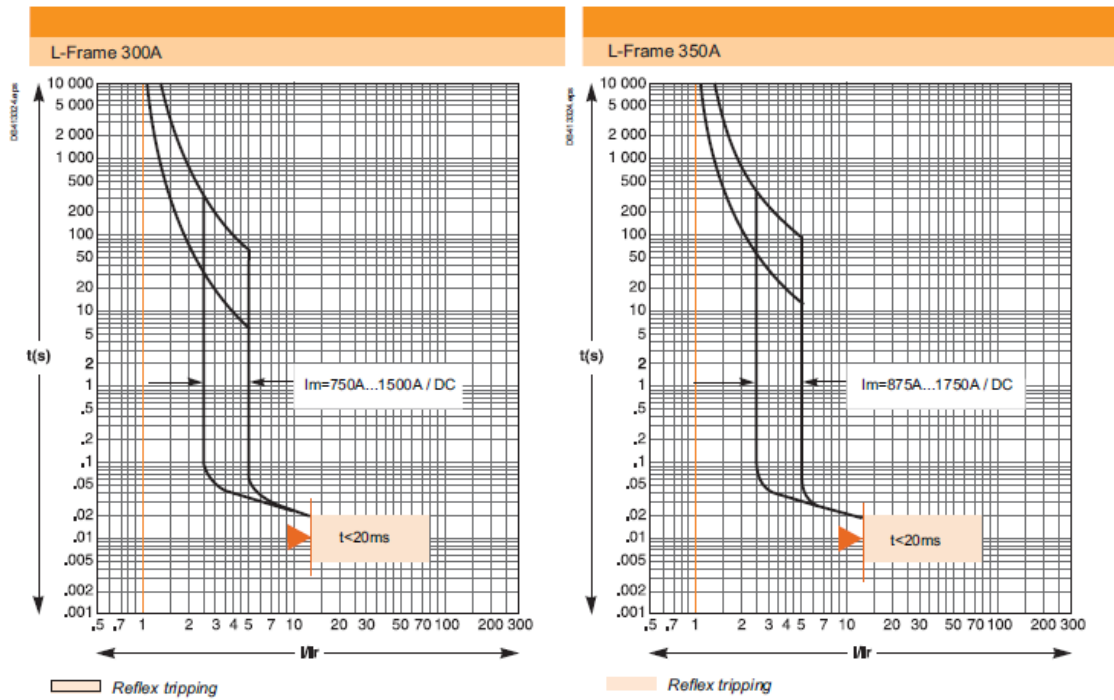


Figure-C 3. Example of L-frame 300-450 A Thermal Unit Trip curves time vs I/I_r [36].

Figure 87: L-Frame 900–1200 A (LG and LL) 500 Vdc Thermal-Magnetic Trip

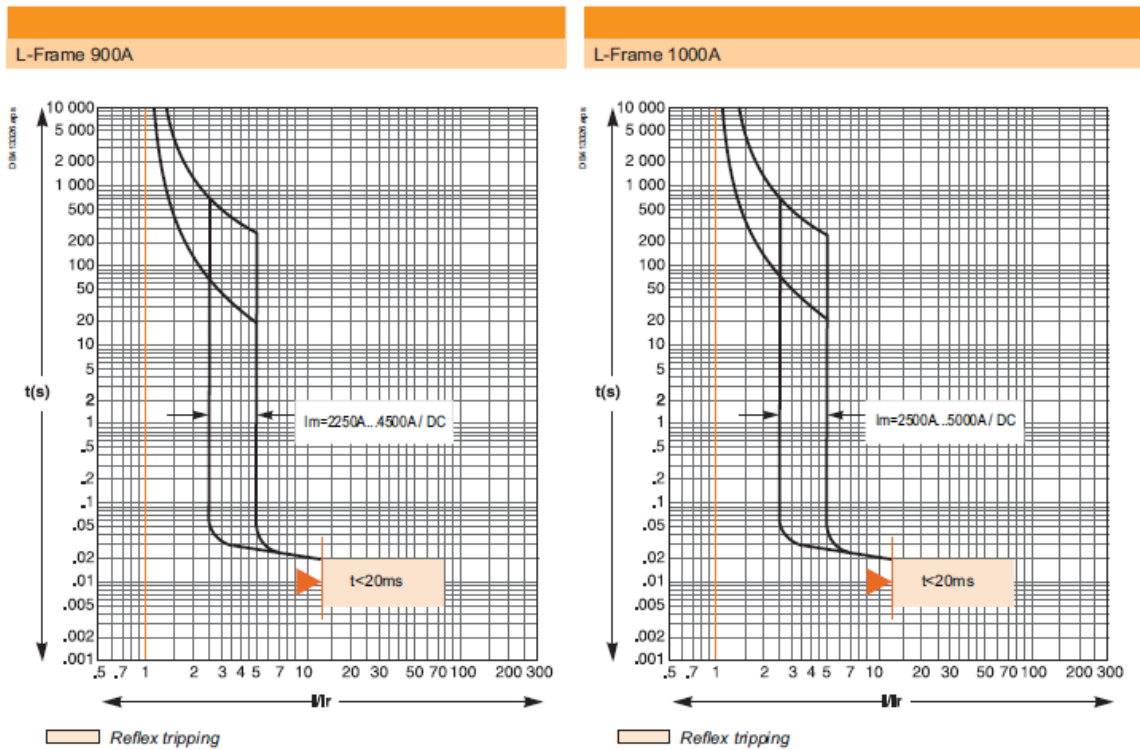


Figure-C 4 Example of L-frame 900-1200 A Thermal Unit Trip curves time vs I/I_r [36].

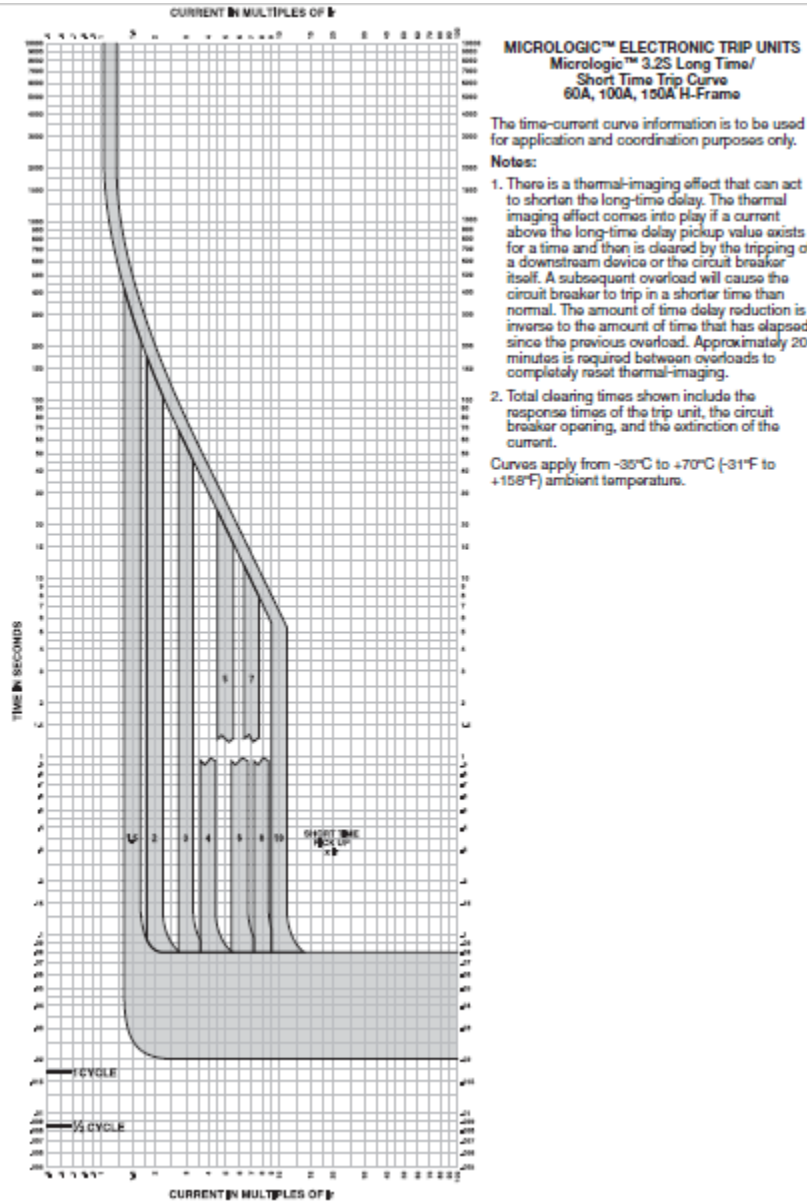


Figure-C 5. Short time trip curve of a L-frame MCCB [36].

Bibliography

- [1] K. Pechrach, *Arc Control in Circuit Breakers Low Contact Velocity*. VDM Publishing House Ltd., 2009.
- [2] E. M. Belbel and M. Lauraire, "Behaviour of Switching Arc in Low Voltage Limiter Circuit Breaker," *IEEE Trans. components, hybrids Manuf. Technol.*, vol. CHMT 8, no. 1, p. 4, 1985.
- [3] L. Rendot, "Modélisation magneto-hydrodynamique par la méthode des volumes finis : Application aux plasmas de coupure Loïc Rondot To cite this version : HAL Id : tel-00544359 Modélisation magneto-hydrodynamique par la méthode des volumes finis : Application aux plasm," Institut polytechnique de Grenoble, 2010.
- [4] Q. Wang, X. Li, S. Member, D. Chen, and S. Member, "Analysis of the Interruption Process of Selective Miniature Circuit Breaker With Permanent Magnet Release," *IEEE Trans. Components, Packag. Manuf. Technol.*, vol. 4, no. 7, pp. 1177–1183, 2014.
- [5] A. Piel, *Plasma physics : an introduction to laboratory, space, and fusion plasmas*. Berlin London: Springer, 2010.
- [6] A. A. Fridman and A. K. Lawrence, *Plasma physics and engineering*. Boca Raton, FL: CRC Press, 2011.
- [7] L. Wang, K. Qin, L. Hu, X. Zhang, and S. Jia, "Numerical Simulation of Vacuum Arc Behavior Considering Action of Adjacent Phases in Vacuum Circuit Breakers," *IEEE Trans. Plasma Sci.*, vol. 45, no. 5, pp. 859–867, 2017.
- [8] S. Shkol'nik, "Anode phenomena in arc discharges ;," *Plasma Sources Sci. Technol.*, vol. 20, no. 013001, 2011.
- [9] M. Abbaoui and B. Cheminat, "Determination of the Characteristics of an Electric Arc Plasma Contaminated by Vapors From Insulators jpl," *IEEE Trans. Plasma Sci.*, vol. 19, no. I, 1991.
- [10] A. Iturregi Aio, "Modelization and analysis of the electric arc in low voltage," Universidad Del País Vasco Euskal Herriko Unibertsitatea, 2013.
- [11] A. K. Kagoné, Z. Koalaga, and F. Zougmore, "Calculation of air-water vapor mixtures thermal plasmas transport coefficients," in *Conference, I. O. P., Materials*, 2012, p. 9.
- [12] Y. Tanaka, Y. Takeuchi, T. Sakuyama, Y. Uesugi, S. Okabe, and S. Kaneko, "Numerical and experimental investigations on thermal interaction between thermal plasma and solid polymer powders using induction thermal plasma technique," *J. Phys. D Appl. Phys.*, vol. 41, no. 025203, p. 15, 2008.
- [13] X. Li, D. Chen, Y. Wu, and R. Dai, "A comparison of the effects of different mixture plasma properties on arc motion," *J. Phys. D. Appl. Phys.*, vol. 40, no. 6982, 2007.
- [14] D. L. Shmelev, S. A. Barenholts, and M. M. Tsventoukh, "Numerical Simulation of Plasma Near the Cathode Spot of Vacuum Arc," *IEEE Trans. Magn.*, vol. 45, no. 11,

pp. 3046–3053, 2017.

- [15] J. Li, D. Ingham, L. Ma, N. Wang, and M. Pourkashanian, “Numerical Simulation of the Chemical Combination and Dissociation Reactions of Neutral Particles in a Rarefied Plasma Arc Jet,” *IEEE Trans. Plasma Sci.*, vol. 45, no. 3, pp. 461–471, 2017.
- [16] Y. Liu, D. Chen, H. Yuan, L. Ji, and Z. Ma, “Research of Dynamic Optimization for the Cam Design Structure of MCCB,” *IEEE Trans. Packag. Manuf. Technol.*, vol. 6, no. 3, pp. 390–399, 2016.
- [17] X. Li, D. Chen, S. Member, H. Liu, Y. Chen, and Z. Li, “Imaging and Spectrum Diagnostics of Air Arc Plasma Characteristics,” *IEEE Trans. Plasma Sci.*, vol. 32, no. 6, pp. 2243–2249, 2004.
- [18] X. Zhou, X. Cui, M. Chen, and G. Zhai, “Evaporation Erosion of Contacts Under Static Arc by Gas Dynamics and Molten Pool Simulation,” *IEEE Trans. Plasma Sci.*, vol. 43, no. 12, pp. 4149–4160, 2015.
- [19] K. Bo, X. Zhou, and G. Zhai, “Investigation on Arc Dwell and Restriking Characteristics in DC High-Power Relay,” *IEEE Trans. Plasma Sci.*, vol. 45, no. 6, pp. 1032–1042, 2017.
- [20] M. Higginson and D. B. Durocher, “Proper application & maintenance of molded case breakers to assure safe and reliable operation,” *IEEE Conf. Rec. Annu. Pulp Pap. Ind. Tech. Conf.*, pp. 90–101, 2009.
- [21] G. Bizjak and P. Zunko, “Circuit breaker model for digital simulation based on mayr’s and cassie’s differential arc equations,” *IEEE Trans. Power Deliv.*, vol. 10, no. 3, pp. 1310–1315, 1995.
- [22] J. Freidberg, *Plasma Physics and Fusion Energy*. Cambridge University Press, 2007.
- [23] C. Power, I. Industry, and A. Society, *IEEE Recommended Practice for Protection and Coordination of Industrial and Commercial Power Systems*. 2001.
- [24] S. Rau, S. Member, and W. Lee, “DC Arc Model Based on 3-D DC Arc Simulation,” *IEEE Trans. Ind. Appl.*, vol. 52, no. 6, pp. 5255–5261, 2016.
- [25] H. Wu, X. Li, D. Stade, and H. Schau, “Arc Fault Model for Low-Voltage AC Systems,” *IEEE Trans. Power Deliv.*, vol. 20, no. 2, pp. 1204–1205, 2005.
- [26] L. Chan, “Molded Case Circuit Breaker (MCCB) Basic Knowledge.” [Online]. Available: <https://www.linkedin.com/pulse/molded-case-circuit-breaker-mccb-basic-knowledge-lily-chan/>.
- [27] F. W. Kussy and J. L. Warren, *Design Fundamentals for Low-Voltage Distribution and Control*, 1st ed. CRC Pr I Llc, 1987.
- [28] J. Ro, H. Bak, and H. Jung, “Characteristic analysis and design of a novel lorentz force driving actuator for a molded case circuit breaker,” *IET Electr. Power Appl.*, vol. 9, no. 1, pp. 1–9, 2015.
- [29] X. Li, D. Chen, S. Member, Y. Wang, Q. Wang, and Y. Geng, “Analysis of the

- Interruption Process of Molded Case Circuit Breakers,” *IEEE Trans. Packag. Technol.*, vol. 30, no. 3, pp. 375–382, 2007.
- [30] P. G. Slade, *Electrical Contacts: Principles and Applications*, Second edi. CRC Press, 2014.
- [31] D. R. Askeland, P. P. Fulay, and W. J. Wright, *The Science and Engineering of Materials*, SI. CENAGE Learning, 2011.
- [32] MatWeb, “MatWeb: Online Materials Information Resource,” 1996. [Online]. Available: www.matweb.com.
- [33] Cedrat, “User guide Flux® 12.1 Volume 3 Physical applications: magnetic, electric, thermal, ...,” vol. 3. Cedrat, pp. 79–135, 2015.
- [34] S. Ito and Y. Takato, “Numerical Analysis of Electromagnetic Forces in Low Voltage AC Circuit Breakers Using 3-D Finite Element Method Taking into Account Eddy Currents,” *IEEE Trans. Magn.*, vol. 34, no. 5, pp. 838–846, 1998.
- [35] Y. Kawase and H. Mori, “3-D Finite Element Analysis of Magnetic Blowout Forces Acting on the Arc in Molded Case Circuit Breakers,” *IEEE Trans. Magn.*, vol. 33, no. 2, pp. 2053–2056, 1997.
- [36] S. Electric, “PowerPact H-, J-, and L-Frame Circuit Breakers Catalog 0611CT1001 R02/16.” 2015.
- [37] J. Merrel, “The Importance of the X / R Ratio in Low-Voltage Short Circuit Studies,” *Power Stud.*, pp. 1–6, 1999.
- [38] J. C. Bautista Cruz, “Characterization of arc extinction in direct current residential circuit breakers,” Instituto Tecnológico de Estudios Superiores de Monterrey, 2018.
- [39] L. Dalian Jingtai Industry Trade Co., “Alibaba,” *Minerals & Metallurgy*, 2018. [Online]. Available: www.alibaba.com.
- [40] K. Nakayama, Y. Yokomizu, T. Matsumura, E. Kanamori, and K. Kuwamura, “Mechanism of Voltage Rise of High-Current Arc at Atmospheric Pressure Due to Deion Plates,” *Electr. Eng. Japan (English Transl. Denki Gakkai Ronbunshi)*, vol. 145, no. 3, pp. 17–25, 2003.

